Endoplasmic reticulum stress causes insulin resistance by inhibiting delivery of newly synthesised insulin receptors to the cell surface

Revised Version

Max Brown[1-3], Samantha Dainty[1-3], Natalie Strudwick[1-3], Adina D. Mihai[1-3], Jamie N. Watson[1-3], Robina Dendooven[1-3], Adrienne W. Paton[4], James C. Paton[4], and Martin Schröder[1-3]

1) Durham University, Department of Biosciences, Durham DH1 3LE, United Kingdom.

2) Biophysical Sciences Institute, Durham University, Durham DH1 3LE, United Kingdom.

3) North East England Stem Cell Institute (NESCI), Life Bioscience Centre, International Centre for Life, Central Parkway, Newcastle Upon Tyne, NE1 4EP, UK.

4) Research Centre for Infectious Diseases, Department of Molecular and Biomedical Science, University of Adelaide, Adelaide, SA 5005, Australia.

Address for correspondence: Martin Schröder, Durham University, Department of Biosciences, Durham DH1 3LE, United Kingdom.

phone: +44 (0) 191-334-1316

FAX: +44 (0) 191-334-9104

email: martin.schroeder@durham.ac.uk

Running Title: ER stress depletes insulin receptors

Keywords: endoplasmic reticulum stress, insulin receptor, insulin resistance, receptor trafficking, signal transduction, unfolded protein response

ABSTRACT

Accumulation of unfolded proteins in the endoplasmic reticulum (ER) causes ER stress and activates a signalling network known as the unfolded protein response (UPR). Here we characterise how ER stress and the UPR inhibit insulin signalling. We find that ER stress inhibits insulin signalling by depleting the cell surface population of the insulin receptor. ER stress inhibits proteolytic maturation of insulin proreceptors by interfering with transport of newly synthesised insulin proreceptors from the ER to the plasma membrane. Activation of AKT, a major target of the insulin signalling pathway, by a cytosolic, membrane-bound chimera between the AP20187-inducible F_V2E dimerisation domain and the cytosolic protein tyrosine kinase domain of the insulin receptor was not affected by ER stress. Hence, signalling events in the UPR, such as activation of the JNK MAP kinases or the pseudokinase TRB3 by the ER stress sensors IRE1α and PERK, do not contribute to inhibition of signal transduction in the insulin signalling pathway. Indeed, pharmacologic inhibition and genetic ablation of JNKs, as well as silencing of expression of TRB3, did not restore insulin sensitivity or rescue processing of newly synthesised insulin receptors in ER-stressed cells.

HIGHLIGHT SUMMARY

ER stress inhibits activation of AKT by insulin by depleting insulin receptors and interferes with delivery of newly synthesised insulin receptors to the cell surface. Bypass of the secretory pathway in synthesis of the cytosolic protein tyrosine kinase domain of the insulin receptor negates the effects of ER stress on activation of AKT by insulin.

INTRODUCTION

In mammalian cells, most secreted proteins and proteins residing in the plasma membrane or the secretory pathway are transported into the ER while their polypeptide chains are being assembled by translating ribosomes (Walter and Lingappa, 1986). In the ER, newly synthesised proteins fold into their native three-dimensional structures, undergo multiple post-translational modifications including asparagine (N)-linked glycosylation (Hubbard and Ivatt,

1981; Kornfeld and Kornfeld, 1985) and the formation of disulphide bonds (Fewell et al., 2001). Interaction of newly synthesised proteins with several chaperone systems facilitates their productive folding, but also serves as a quality control mechanism to retain newly synthesised proteins in the ER until they have completed their folding and maturation processes (Hebert and Molinari, 2007). Consequently, unfolded or only partially folded proteins are prevented from exiting the ER until they have completed their folding process or are targeted to degradation mechanisms if they fail to fold productively, such ER-associated degradation (ERAD) (Meusser et al., 2005) or ER-phagy (Bernales et al., 2006).

The accumulation of unfolded and partially folded proteins in the ER activates a signalling network termed the unfolded protein response (UPR) (Schröder and Kaufman, 2005; Walter and Ron, 2011). Three ER transmembrane proteins, the membrane-bound transcription factor ATF6 (Yoshida et al., 2000, 2001b), the protein kinase PERK (Shi et al., 1998; Harding et al., 1999; Shi et al., 1999), and the protein kinase-endoribonuclease (RNase) IRE1α (Tirasophon et al., 1998) initiate signalling in the UPR. After cleavage from the endomembrane system ATF6 translocates to the nucleus and activates transcription of genes encoding ER-resident molecular chaperones and components of the ER-associated protein degradation machinery (Ye et al., 2000; Wu et al., 2007; Yamamoto et al., 2007). PERK transiently attenuates general translation in ER-stressed cells by phosphorylating the α subunit of eIF2 (Shi et al., 1998; Harding et al., 1999). Phosphorylation of eIF2α also promotes translation of mRNAs with several short upstream open reading frames leading to induction of the transcription factor CHOP (Harding et al., 2000) and the pseudokinase TRB3 (Ohoka et al., 2005).

IRE1α is a bifunctional protein kinase-RNase (Tirasophon et al., 1998; Tirasophon et al., 2000). The IRE1α RNase activity initiates splicing of *XBP1* mRNA which encodes a bZIP transcription factor (Shen et al., 2001; Yoshida et al., 2001a; Calfon et al., 2002; Lee et al., 2002). Spliced XBP1 ($XBP1^{s}$) is a more potent transcriptional activator than unspliced XBP1 ($XBP1^{u}$) for genes encoding ER resident molecular chaperones, phospholipid biosynthetic enzymes, and proteins involved in ER-associated protein degradation (Shen et al., 2001;

Yoshida et al., 2001a; Calfon et al., 2002; Lee et al., 2002). In addition, relaxed specificity of the RNase activity mediates decay of many mRNAs encoding proteins targeted to the secretory pathway (Hollien and Weissman, 2006; Hollien et al., 2009; Gaddam et al., 2013). Through association with the E3 ubiquitin ligase TRAF2 IRE1α activates the JNK family of mitogen-activated protein kinases (Urano et al., 2000).

Insulin signaling is initiated by binding of insulin to the insulin receptor, activation of the protein tyrosine kinase domain and tyrosine autophosphorylation of the insulin receptor, and extensive tyrosine phosphorylation of insulin receptor substrate (IRS) proteins [reviewed in (Saltiel and Kahn, 2001)], including phosphorylation of Y612, Y632, Y896, Y941, Y1173, and Y1229 in human IRS1 (Shoelson et al., 1992; Sun et al., 1993; Rocchi et al., 1995; Xu et al., 1995; Esposito et al., 2001; Hers et al., 2002). Phosphorylated Y612, Y632, and Y941 are binding sites for the Src homology 2 (SH2) domain of the p85α subunit of phosphatidylinositol (PI) 3-kinase (PI3K) (Sun et al., 1993; Rocchi et al., 1995; Esposito et al., 2001). After formation of PI-3,4-bis- and PI-3,4,5-trisphosphate by PI3K, phosphoinositide-dependent kinases (PDKs) and isoforms of the protein serine/threonine kinase AKT are recruited to the plasma membrane. Colocalization of PDKs and AKT to the plasma membrane facilitates phosphorylation of AKT on T308 by PDK1 (Alessi et al., 1996), and on S473 by mTORC2 (Sarbassov et al., 2005; Guertin et al., 2006; Jacinto et al., 2006), PAK1 (Mao et al., 2008), and ILK (McDonald et al., 2008) leading to activation of AKT. Activated AKT facilitates glucose transport, protein and glycogen synthesis, and inhibits gluconeogenesis. Recruitment of GRB2 to IRS1 phosphorylated at Y896 via its SH2 domain (Sun et al., 1993; Myers et al., 1994) activates mitogen-activated protein kinases, such as p42/p44, and contributes to generating a mitogenic signal in insulin-stimulated cells (Valverde et al., 2001).

Inhibition of signal transduction in the insulin signalling pathway is the cause for insulin resistance when cells fail to respond normally to insulin. Insulin resistance can be caused by a decrease in insulin receptors or defects in signal transduction downstream of the insulin receptor. Activation of JNKs and TRB3 by the UPR has been implicated in the inhibition of

insulin signalling downstream of the insulin receptor (Özcan et al., 2004; Koh et al., 2006; Koh et al., 2013). JNKs inhibit tyrosine phosphorylation of IRS1 by the insulin receptor by phosphorylating S307 in murine IRS1 and S312 in human IRS1 (Aguirre et al., 2000; Aguirre et al., 2002). Consequently, phosphorylation and activation of AKT by insulin is inhibited by JNKs (Lee et al., 2003; Nguyen et al., 2005; Emanuelli et al., 2008). TRB3 interacts with and inhibits phosphorylation of AKT (Du et al., 2003) and also interacts with IRS1 and inhibits its phosphorylation at Y612 by the insulin receptor (Koh et al., 2013).

JNKs become rapidly and transiently activated in ER-stressed cells to promote an adaptive response to ER stress (Brown et al., 2016). The motivation for this study was to characterise whether this rapid, initial JNK activation in the first 10 - 120 min of the ER stress response causes insulin resistance. However, we find no evidence for inhibition of insulin-stimulated AKT phosphorylation or IRS1 tyrosine phosphorylation in cells exposed to ER stress for up to ~8-12 h despite activation of JNKs and induction of TRB3. Only ER stress lasting for more than ~8-12 h inhibited insulin-stimulated AKT phosphorylation, but did so independent of JNKs and TRB3, and correlated with depletion of β chains of the mature insulin receptor, accumulation of unprocessed α-β precursors of the insulin receptor in the ER, and depletion of GFP-tagged insulin receptors from the plasma membrane. Moreover, phosphorylation of AKT at S473 in response to activation of a cytosolic, membrane-bound chimera between the AP20187-inducible F_V2E dimerisation domain (Clackson et al., 1998; Yang et al., 2000) and the protein tyrosine kinase domain of the insulin receptor is not affected by ER stress lasting for 24 h. We propose that inhibition of trafficking of newly synthesised insulin receptors to the plasma membrane suffices and is necessary to inhibit activation of AKT by insulin in ER-stressed cells by depleting the plasma membrane population of the insulin receptor.

RESULTS

ER stress for up to 8 h does not inhibit insulin-stimulated AKT activation. We used *in vitro* differentiated C_2C_{12} myotubes, 3T3-F442A preadipocytes, and Hep G2 hepatoma cells to

characterise the effects of ER stress on insulin signalling, because these cell types are cell culture models of the main tissues and organs contributing to glucose homeostasis, muscle, adipose tissue, and the liver (Saltiel and Kahn, 2001). We first characterised whether ER stress induced with different ER stressors for up to 8 h inhibits signal transduction downstream of the insulin receptor by monitoring insulin-stimulated phosphorylation of AKT at T308 and S473 in *in vitro* differentiated C_2C_{12} myotubes. C_2C_{12} myotubes were serum-starved for 18 h, treated with ER stressors for the last 1 to 8 h of serum starvation and then stimulated with 100 nM insulin for 15 min in the continued presence of ER stressors. 100 nM insulin was chosen, because inhibition of insulin signalling downstream of the receptor manifests independent of insulin concentration (Olefsky and Kolterman, 1981). To exclude drug specific effects on insulin signalling, we used three different ER stressors, the SERCA pump inhibitor thapsigargin (Thastrup et al., 1990), the N-glycosylation inhibitor tunicamycin (Kuo and Lampen, 1976; Lehle and Tanner, 1976), and the protease SubAB, which cleaves and inactivates the ER resident HSP70 class molecular chaperone BiP/GRP78 (Paton et al., 2006). We also titrated the concentrations of both thapsigargin and tunicamycin in the culture medium over a 10- or 100-fold concentration range, respectively. AKT phosphorylation was chosen as readout, because its dynamic range is larger than the dynamic ranges of many physiological responses to insulin such as translocation of GLUT4 to the plasma membrane (Hoehn et al., 2008), uptake of 2-deoxyglucose (Whitehead et al., 2001), or glucose oxidation (Kono and Barham, 1971). Induction of ER stress with 0.1-1.0 μM thapsigargin, 0.1-10 μg/ml tunicamycin, or SubAB for up to ~8 h in C_2C_{12} myotubes, however, did not decrease insulin-stimulated phosphorylation of AKT at T308 (Figure 1, A and B) or S473 (Figure 1, A and C).

To confirm that treatment of serum-starved C_2C_{12} cells with ER stressors induces ER stress, we monitored *XBP1* splicing using reverse transcriptase PCR. The IRE1α-initiated *XBP1* splicing reaction removes a 26 nt intron from *XBP1* mRNA. Therefore, the appearance of a shorter reverse transcriptase PCR product on 2% (w/v) agarose gels indicates activation of the RNase activity of IRE1α. Upon exposure of serum-starved C_2C_{12} cells to 0.3 μM thapsigargin, 1 μg/ml tunicamycin, or 1 μg/ml SubAB a shorter reverse transcriptase PCR

158 product appeared (Figure 1, D), which represents spliced *XBP1* mRNA. Strong induction of
159 *TRB3* mRNA after induction of ER stress for 4 or 8 h was also detected (Figure 1, E and F),
160 which suggests that serum-starved C_2C_{12} cells experience ER stress when challenged with
161 thapsigargin, tunicamycin or SubAB. Furthermore, serum starvation did not decrease *XBP1*
162 splicing in cells exposed to 1 μM thapsigargin for 1 h (Figure S1, A), which argues against
163 the possibility that induction of ER stress is blunted by decreased protein synthesis rates in
164 serum-starved cells. Thapsigargin-, tunicamycin-, or SubAB-induced ER stress for up to 12 h
165 also did not inhibit insulin-stimulated AKT activation in 3T3-F442A adipocytes or Hep G2
166 hepatoma cells, or over a period of 4 h in Fao rat hepatoma cells cultured in RPMI 1640 or
167 Coon's modification of Ham's F12 medium (data not shown).

168 JNKs are activated as early as 10 min after induction of ER stress in C_2C_{12} myotubes and
169 3T3-F442A adipocytes, and after 30 min in Hep G2 cells (Brown et al., 2016), which raises
170 the possibility that ER stress may inhibit the insulin signalling pathway around these times in
171 the ER stress response. However, 30 min of thapsigargin-induced ER stress did not decrease
172 insulin-stimulated phosphorylation of AKT on S473 in 3T3-F442A adipocytes, C_2C_{12}
173 myotubes, or Hep G2 cells (Figure S1, B and C). Induction of ER stress for 30 min with
174 tunicamycin or SubAB also did not decrease insulin-induced phosphorylation of AKT (Figure
175 S1, B and C). These results suggest that activation of JNKs by ER stress does not inhibit
176 signal transduction in the insulin signalling pathway. To characterise whether lower, more
177 physiologic insulin concentrations (Cryer and Polonsky, 1998; Unger and Foster, 1998)
178 unmask effects of ER stress on insulin-stimulated AKT phosphorylation, we stimulated cells
179 with 10 nM insulin for 15 min. ER stress induced with 0.3 μM thapsigargin, 1 μg/ml
180 tunicamycin or SubAB for 30 min up to 8 h had no effect on phosphorylation of AKT on
181 S473 in 3T3-F442A, C_2C_{12}, or Hep G2 cells stimulated with 10 nM insulin for 15 min (Figure
182 2). In summary, these data establish that short periods of ER stress lasting for up to ~8 h, in
183 which JNKs are activated (Brown et al., 2016) and *TRB3* is induced (Figure 1, E and F), do
184 not inhibit insulin-dependent AKT phosphorylation in 3T3-F442A, C_2C_{12}, Fao, and Hep G2
185 cells.

ER stress for up to 30 min does not inhibit IRS1 tyrosine phosphorylation. Phosphorylation of AKT is downstream of tyrosine phosphorylation of IRS1 by the activated insulin receptor in the insulin signalling pathway (Backer et al., 1992; Franke et al., 1995). The absence of effects of heterozygosity for IRS1 in lean mice on control of blood glucose levels (Shirakami et al., 2002) and the lack of effects of partial shRNA-mediated knockdown of IRS1 in skeletal muscle on local glucose clearance (Cleasby et al., 2007) suggest that IRS1 is available in excess over the amounts needed for full activation of downstream events in the insulin signalling pathway. To address the possibility that decreases in IRS1 tyrosine phosphorylation in ER-stressed cells are not reflected at the level of AKT phosphorylation, we directly examined the effects of ER stress on IRS1 tyrosine phosphorylation. First, we characterised whether within the initial 30 min time window after induction of ER stress, in which ER stress activates JNKs in 3T3-F442A, C_2C_{12}, and Hep G2 cells (Brown et al., 2016), a decrease in tyrosine phosphorylation of specific, well-characterised insulin-responsive tyrosine phosphorylation sites, such as Y608 (mouse)/Y612 (human; from here on abbreviated as Y608/612), Y628/632, Y891/896, and Y935/941 (Shoelson et al., 1992; Sun et al., 1993; Xu et al., 1995; Hers et al., 2002), could be observed. We could extract intact IRS1 from 3T3-F442A, C_2C_{12}, and Hep G2 cells only under strongly denaturing conditions such as 8 M urea, 2.5% (w/v) SDS, or 7 M urea, 2 M thiourea, 2.5% (w/v) SDS, or 8 M guanidinium hydrochloride, 1% (v/v) Triton X-100, or 4 M guanidinium thiocyanate, 1% (v/v) Triton X-100, or 10-20% (w/v) trichloroacetic acid (TCA, data not shown). In addition, detection of full-length IRS1 by Western blotting required electrotransfer onto PVDF membranes at pH ~10 in the presence of SDS as described in “Materials and Methods”. Under these conditions, Western blots displaying one band at ~180 kDa, the migration position of IRS1 in SDS-PAGE (Sun et al., 1991), were obtained with all four single tyrosine phosphorylation site antibodies and anti-IRS1 antibodies (Figures 3, S2, and S3). Antibodies against phosphorylated tyrosine phosphorylation sites gave much stronger signals on samples isolated from insulin-treated cells at ~180 kDa (Figures 3, S2, and S3). Induction of ER stress with 1 μM thapsigargin for up to 30 min or with 0.1 μg/ml, 1 μg/ml, or 10 μg/ml tunicamycin for 30

min did not affect phosphorylation of Y608/612, Y628/632, Y891/896, or Y935/941 when cells were stimulated with 10 or 100 nM insulin for 5 min (Figures 3, S2, and S3). An ~3-fold increase in IRS1 levels upon insulin stimulation in 3T3-F442A cells (Figure S2) and an ~2-fold increase in C_2C_{12} myotubes and Hep G2 cells (Figures 3 and S3) were also not affected by thapsigargin or tunicamycin.

Human IRS1 has 32 tyrosyl residues, while murine IRS1 has 34. Phosphorylation of at least 19 tyrosines in human IRS1 and 13 tyrosines in murine IRS1 has been shown experimentally (Hornbeck et al., 2015). An additional eight tyrosines in human IRS1 and nine tyrosines in murine IRS1 feature at least one acidic amino acid in the six immediately upstream amino acids. Upstream acidic amino acids can be a feature of tyrosine phosphorylation sites (Neil et al., 1981; Smart et al., 1981; Baldwin et al., 1982; Hunter, 1982; Patschinsky et al., 1982; Pike et al., 1982; Baldwin et al., 1983) and are, for example, enriched in the experimentally confirmed tyrosine phosphorylation sites of human and murine IRS1 (human IRS1, upstream positions -1 to -3, χ^2 p value < 0.05; murine IRS1, upstream positions -1 to -6, χ^2 p value < 0.01). Given the large number of confirmed and putative tyrosine phosphorylation sites in IRS1, it is possible that individually surveying a subset of tyrosine phosphorylation sites may not uncover effects of ER stress on tyrosine phosphorylation of IRS1. To address this concern, we immunoprecipitated IRS1 from cell lysates prepared from unstressed cells, or cells that were exposed to 1 μM thapsigargin or 10 μg/ml tunicamycin for 30 min and then stimulated with 10 or 100 nM insulin for 5 min in the continued presence of thapsigargin or tunicamycin, and Western blotted the immunoprecipitates with a pan-phosphotyrosine antibody (clone 4G10® Platinum), and an anti-IRS1 antibody (Figure 4). We observed a strong increase in tyrosine phosphorylation after stimulation with either 10 or 100 nM insulin for 5 min, but neither thapsigargin nor tunicamycin had any effect on the level of tyrosine phosphorylation of IRS1 (Figure 4). In summary, these data show that ER stress lasting for up to 30 min does not affect insulin-stimulated IRS1 tyrosine phosphorylation.

ER stress does not elicit serine 307/312 phosphorylation of IRS1. JNKs inhibit tyrosine phosphorylation of IRS1 by the activated insulin receptor by phosphorylating IRS1 at S307/312 (Aguirre et al., 2000; Aguirre et al., 2002). Unaltered tyrosine phosphorylation of IRS1 in ER-stressed cells (Figures 3, 4, S2, and S3) suggested that JNKs, despite being activated by ER stress (Brown et al., 2016), do not phosphorylate IRS1 at S307/312 or that phosphorylation of IRS1 at S307/312 by JNKs does not inhibit tyrosine phosphorylation of IRS1 by the insulin receptor in ER-stressed cells. To distinguish between these possibilities, we measured IRS1 S307/312 phosphorylation in serum-starved cells and standardised the phospho-S307/S312 IRS1 signal to the signal for total IRS1 (Figure 5). We included treatment with 5 μg/ml anisomycin for 30 – 60 min, which has been reported to elicit phosphorylation of IRS1 at S307/312 (Aguirre et al., 2000; Aguirre et al., 2002; Werner et al., 2004), as a positive control, because we obtained only faint signals with the anti-pS307/S312 antibody with cell lysates prepared from cells exposed to 1 μM thapsigargin for up to 2 h (Figure 5). In 3T3-F442A and Hep G2 cells, anisomycin retarded migration of IRS1 in 7.5% SDS-PAGE gels (Figure 5, A and E). This suggests that IRS1 becomes phosphorylated at additional sites than those reported in the literature in response to anisomycin, S302/307 (Werner et al., 2004), S307/312 (Aguirre et al., 2000; Aguirre et al., 2002; Werner et al., 2004), and possibly S632/636 and S635/639 (Hiratani et al., 2005), to explain the shift in migration position. Retardation of IRS1 in SDS-PAGE was not seen in thapsigargin-treated cells (Figure 5). These data argue that ER stress induced with thapsigargin does not elicit S307/312 phosphorylation of IRS1 and that phosphorylation of IRS1 at other sites remains below the threshold necessary to affect retardation of IRS1 in SDS-PAGE.

ER stress for ≥ 12 h inhibits insulin-stimulated AKT phosphorylation. Several studies have reported that ER stress lasting for 12 h or longer causes insulin resistance (Zhou et al., 2009; Avery et al., 2010; Xu et al., 2010; Tang et al., 2011; Hassan et al., 2012; Jung et al., 2013; Panzhinskiy et al., 2013). Such long periods of ER stress may cause insulin resistance by depleting the plasma membrane population of the insulin receptor, because the insulin receptor has a half-life of 7-13 h (Reed and Lane, 1980; Kasuga et al., 1981; Reed et al.,

1981a; Reed et al., 1981b; Capeau et al., 1985; Savoie et al., 1986; Grako et al., 1992). For this reason, we characterised whether ER stress for ≥ 12 h decreases insulin-stimulated phosphorylation of AKT. 12 h after induction of ER stress, insulin-stimulated S473 phosphorylation of AKT was decreased in C_2C_{12} cells exposed to 10 μg/ml of tunicamycin (Figure 6, A and B). 18 h after induction of ER stress, several ER stressors and markedly lower tunicamycin concentrations decreased insulin-stimulated AKT phosphorylation at S473 (Figure 6, A and B). After 24 h of ER stress, all ER stress-inducing conditions decreased insulin-stimulated AKT phosphorylation at S473 in C_2C_{12} cells. 24 h of ER stress induced with thapsigargin, tunicamycin, or SubAB decreased cell numbers (Figure S4, A and B), but did not affect the activity of mitochondrial redox chains in the remaining cells (Figure S4, C), suggesting that remaining cells were viable and that loss of viability cannot explain the decrease in S473 phosphorylation of AKT. We made similar observations in Hep G2 and 3T3-F442A cells. In Hep G2 cells, induction of ER stress for 18 h did not affect insulin-stimulated phosphorylation of AKT, except when cells were exposed to 10 μg/ml tunicamycin (Figure S5, A and B). After 24 h of ER stress a ten-fold lower tunicamycin concentration also reduced insulin-stimulated AKT phosphorylation, and after 36 h all ER stress inducing conditions decreased insulin-stimulated AKT phosphorylation (Figure S5, A and B). 36 h of ER stress decreased the number of Hep G2 cells remaining in culture dishes (Figure S4, D and E), but did not affect the viability of the cells remaining in culture dishes (Figure S4, F). In 3T3-F442A cells, insulin-stimulated S473 phosphorylation of AKT started to decline after 12 h of ER stress and continued to decline over the next 12 h (data not shown). These data confirm that periods of ER stress that exceed the half-life of the insulin receptor decrease insulin-stimulated AKT phosphorylation.

Decreased insulin-stimulated AKT phosphorylation correlates with depletion of the β chain of the mature insulin receptor in ER-stressed cells. The hypothesis, that ER stress for > 12 h decreases insulin-stimulated S473 phosphorylation of AKT by depleting the insulin receptor at the plasma membrane, predicts a decrease of mature β chains of the insulin receptor over the duration of ER stress. The insulin receptor is synthesised as a proreceptor of ~190 kDa or

297 ~210 kDa due to alternative glycosylation (Hwang and Frost, 1999). Cleavage of the
298 proreceptor into mature α and β chains of ~135 kDa and ~95 kDa in the *trans*-Golgi network
299 by several proprotein convertases (Robertson et al., 1993; Bravo et al., 1994) yields the
300 mature insulin receptor. Western blotting of cell lysates with an antibody against the β chain
301 of the insulin receptor revealed bands representing the proreceptor at ~190 kDa and ~210 kDa
302 and the β chain at ~95 kDa (Figures 6A and S5A). C_2C_{12} cells stressed with 10 μg/ml
303 tunicamycin displayed a decrease in insulin receptor β chains 12 h after induction of ER stress
304 that is around the same time at which this condition decreases insulin-stimulated AKT S473
305 phosphorylation. After 18 and 24 h of ER stress, lower concentrations of ER stress and other
306 ER stressors such as thapsigargin or SubAB also decreased insulin receptor β chains (Figure
307 6, A and B). The decrease in insulin receptor β chains correlated with the decrease in insulin-
308 stimulated AKT phosphorylation (Figure 6, C). Exposure of Hep G2 cells to 18 h of ER stress
309 did not affect the abundance of β chains of the mature insulin receptor (Figure S5, A). By
310 contrast, after 24 h or 36 h of ER stress a decline in β chain abundance coincided with
311 decreased phosphorylation of AKT on S473 by insulin (Figure S5, A and B). The decrease in
312 S473 phosphorylation of AKT correlated with the decrease in β chain abundance in ER-
313 stressed Hep G2 cells (Figure S5, C) and 36 h of ER stress significantly increased
314 unprocessed α-β proreceptors in Hep G2 cells (Figure S5, D). We also observed a correlation
315 between a decrease in insulin receptor β chains and decreased, insulin-stimulated AKT
316 phosphorylation in 3T3-F442A cells (data not shown). Insulin by itself, however, did not
317 affect the abundance of β chains of the insulin receptor in any cell line (Figures 6A-B and
318 S5A-B, and data not shown). In summary, these data establish that in ER-stressed cells a
319 decrease in insulin-stimulated AKT phosphorylation correlates with a decrease in mature
320 insulin receptors.

321 Next, we characterised whether the depletion of β chains in ER-stressed cells is sufficient
322 to decrease insulin-stimulated AKT phosphorylation by silencing expression of the insulin
323 receptor gene in C_2C_{12} myoblasts by using three small interfering (si) RNAs and comparing
324 insulin-stimulated AKT S473 phosphorylation to cells transfected with a siRNA against

eGFP. All three siRNAs decreased insulin receptor mRNA steady-state levels by 50-70% (Figure 6, D) and mature β chains to a similar extent (Figure 6, E). Concomitant with the decrease in insulin receptor levels, insulin-stimulated AKT S473 phosphorylation was decreased by 50-80% (Figure 6, E). These experiments suggest that an ~50% decrease in insulin receptor levels suffices to decrease insulin-stimulated AKT S473 phosphorylation to a similar degree. In summary, these data suggest that depletion of β chains of the mature insulin receptor suffices to decrease insulin-stimulated AKT phosphorylation in ER-stressed cells.

Inhibition of protein synthesis and synthesis of α-β proreceptors cannot fully explain decreased insulin-stimulated S473 phosphorylation of AKT in ER stress lasting for 24 h. ER stress may decrease mature insulin receptors by decreasing transcription of the insulin receptor gene (Örd and Örd, 2003; Jang et al., 2010), degrading the insulin receptor mRNA via the RIDD activity of IRE1α (Hollien and Weissman, 2006; Hollien et al., 2009), inhibiting translation of the insulin receptor mRNA, by interfering with folding and maturation of newly synthesised insulin receptors in the ER and transport of newly synthesised insulin receptors to the plasma membrane, or increasing the turnover of insulin receptors at the cell surface. Therefore, we decided to determine which of these processes contribute to lower levels of mature insulin receptors in ER-stressed cells.

Reverse transcriptase-quantitative PCR (qPCR) showed that steady-state levels of the insulin receptor mRNA increase ~6 fold in ER-stressed C_2C_{12} cells (Figure 7, A), thus making it unlikely that transcriptional effects or RIDD activity of IRE1α can explain loss of insulin receptor β chains in ER-stressed cells.

To explore whether a translational arrest can explain the loss of β chains, we labelled newly synthesised proteins for 30 min with a mix of [^{35}S]-L-methionine and [^{35}S]-L-cysteine and measured incorporation of [^{35}S]-L-methionine/[^{35}S]-L-cysteine into protein by scintillation counting of TCA precipitates (Figure 7, B-D) or after separating equal amounts of proteins on SDS-PAGE gels by storage phosphor imaging (Figure 7, E). Storage phosphor signals were normalised to the intensity of Coomassie Brilliant Blue R-250 staining of the gels to account for small variations in loading of SDS-PAGE gels. Overall, scintillation

counting of TCA precipitates and storage phosphor imaging of gels gave very similar results (Figure 7, B-E). In C_2C_{12} and Hep G2 cells, 0.1 μM thapsigargin decreased protein synthesis rates measured by scintillation counting to 52 ± 4% and 66 ± 4% of untreated cells, respectively, or 55 ± 3% and 79 ± 2% when measured by storage phosphor imaging. In contrast, treatment with 0.1 μg/ml tunicamycin for 24 h did not affect protein synthesis rates (Figure 7, C-E). Surprisingly, both thapsigargin and tunicamycin increased protein synthesis rates in 3T3-F442A cells 1.97 ± 0.04 and 1.61 ± 0.03-fold when measured by storage phosphor imaging, and 2.1 ± 0.1 and 2.1 ± 0.2-fold when measured by scintillation counting. These effects of both thapsigargin and tunicamycin on protein synthesis rates in 3T3-F442A cells were seen in four independent experiments. To investigate if decreased protein synthesis in thapsigargin-treated C_2C_{12} and Hep G2 cells may be caused by increased phosphorylation of eIF2α at S51, we examined phosphorylation of eIF2α at S51 by Western blotting. While treatment with 0.1 μM thapsigargin for 30 min led to a dramatic increase in phosphorylation of eIF2α in all three cell types, neither treatment with 0.1 μM thapsigargin or 0.1 μg/ml tunicamycin for 24 h affected phosphorylation of eIF2α at S51 (Figure 7, F). Therefore, the inhibitory effect of 24 h of thapsigargin treatment of C_2C_{12} and Hep G2 cells on protein synthesis rates is independent of phosphorylation of eIF2α at S51.

To directly establish whether ER stress affects synthesis of new insulin receptors, we measured synthesis rates of the α-β proreceptor by incorporation of [^{35}S]-L-methionine/[^{35}S]-L-cysteine into newly synthesised proteins and immunoprecipitation of the insulin receptor with an antibody against the β chain of the mature insulin receptor. Immunoprecipitates were resolved by SDS-PAGE after boiling for 5 min in 10% (w/v) SDS and 2.5% (v/v) β-mercaptoethanol (see 'Materials and Methods' for details). Initial experiments showed very faint bands for both the α-β proreceptor and β chain in cell lysates prepared from C_2C_{12} cells labelled for 8 h with ~70% [^{35}S]-L-methionine/~25% [^{35}S]-L-cysteine (data not shown). Much stronger signals obtained with lysates prepared from Hep G2 and especially 3T3-F442A cells labelled for 8 h allowed us to identify several bands that were not observed in a control immunoprecipitation with normal rabbit IgG (Figure 7, G). The running positions of these

bands in SDS-PAGE identified two of these bands as the α-β proreceptor and the β chain of the mature insulin receptor (Figure 7, G). When cells were labelled for 1 h with [^{35}S]-L-methionine/[^{35}S]-L-cysteine, the band representing the β chain of the mature insulin receptor was no longer detected (Figure 7, G). Quantification of storage phosphor signals revealed that in 3T3-F442A cells ≤ 2.6 ± 0.4 % and in Hep G2 cells ≤ 9.0 ± 0.1% of α-β proreceptors were processed to mature insulin receptors in the 1 h label. These values likely represent an upper limit of α-β proreceptor processing in the 1 h label, because of the contribution of other comigrating, [^{35}S]-L-methionine/[^{35}S]-L-cysteine-labelled proteins to the storage phosphor signal at the migration position of the β chain. Hence, the amount of α-β proreceptors synthesised in the 1 h labelling period is representative of the synthesis rate of the α-β proreceptor.

Consistent with total protein synthesis rates, 3T3-F442A cells treated for 24 h with 0.1 μM thapsigargin showed a 2.33 ± 0.04-fold increase in α-β proreceptor synthesis, while treatment of 3T3-F442A cells with 0.1 μg/ml tunicamycin or Hep G2 cells with either 0.1 μM thapsigargin or 0.1 μg/ml tunicamycin for 24 h did not affect α-β proreceptor synthesis (Figure 7, G and H). When cells were treated with tunicamycin, α-β proreceptors migrated faster in SDS-PAGE due to their decreased molecular weights caused by inhibition of N-glycosylation by tunicamycin (Figure 7, G). In summary, these experiments reveal that conditions exist in which ER stress for >12 h decreases insulin-stimulated S473 phosphorylation of AKT without decreasing general protein synthesis or synthesis of the insulin proreceptor, for example exposure of C_2C_{12} cells for 24 h to 0.1 μg/ml tunicamycin (Figures 6 and 7), and 24-36 h exposure of Hep G2 cells to low concentrations of thapsigargin or tunicamycin (Figures S5 and 7).

ER stress does not increase the rate of insulin receptor turnover at the cell surface. Another possibility for how ER stress may deplete β chains of the mature insulin receptor is that increased proteolytic activity associated with the secretory pathway, either lysosomal proteolytic activity (Chiang et al., 2012; Imanikia et al., 2019) or proteasomal activity associated with the ER (Casagrande et al., 2000; Friedlander et al., 2000; Termine et al.,

2009; Ron et al., 2011; Chiang et al., 2012), results in increased turnover of mature insulin receptors in ER-stressed cells. To address this possibility, we determined the half-life of the insulin receptor at the cell surface in unstressed cells, and cells in which ER stress was induced with 0.3 μM thapsigargin, 1 μg/ml tunicamycin, or 1 μg/ml SubAB. We biotinylated surface exposed proteins with the membrane-impermeable biotinylation reagent sulphosuccinimidyl-6-(biotinamido)hexanoate, and then continued to culture cells in the presence or absence of ER stressors for up to 72 h. At several times after biotinylation of cell surface proteins, we analysed proteins isolated with streptavidin-agarose beads by SDS-PAGE and Western blotting. The stability of the streptavidin-biotin interaction in 6 M urea (Kurzban et al., 1991) allowed us to wash streptavidin-agarose beads twice with 6 M urea, 1% (v/v) Triton X-100 to remove non-biotinylated proteins. Western blotting of proteins isolated on streptavidin-agarose beads for the abundant intracellular protein GAPDH revealed that GAPDH was not retained on streptavidin agarose beads (Figure 8), showing that intracellular proteins were not biotinylated and that GAPDH was not retained on the beads via nonspecific interactions. Streptavidin-agarose beads also did not purify any insulin receptors from cells that were not exposed to the biotinylation reagent (Figure 8, A, C, and E, lanes labelled '-'), showing that insulin receptors were only retained on streptavidin-agarose beads when they were biotinylated and, hence, surface exposed. When the supernate of a pull-down reaction with streptavidin-agarose beads was used in a second pull-down reaction with a new aliquot of streptavidin-agarose beads (Figure 8, A, C, and E, lanes labelled '0' and marked with an arrowhead), no or only faint bands were obtained for the β chain of the insulin receptor, showing that the yield of the first pull-down reaction consistently was > 96%. In all cell lines and under all conditions the abundance of insulin receptors that bound to streptavidin-agarose beads decreased over time, indicating that initially surface exposed and biotinylated insulin receptor molecules were degraded. In all cases the decay of biotinylated insulin receptors followed a monoexponential relationship (Figure 8). This allowed us to calculate half-lives for the insulin receptor at the cell surface from the slopes of linearised relationships and to compare half-lives between unstressed cells and cells exposed to ER stressors (Figure 8). The

calculated half-lives are similar to previously reported half-lives of total cellular insulin receptors (Reed and Lane, 1980; Kasuga et al., 1981; Krupp and Lane, 1981; Reed et al., 1981a; Reed et al., 1981b; Grako et al., 1992) and insulin receptors at the cell surface (Rosen et al., 1979; Kasuga et al., 1981; Savoie et al., 1986). In C_2C_{12} and Hep G2 cells, induction of ER stress with 0.3 μM thapsigargin, 1 μg/ml tunicamycin, or 1 μg/ml SubAB did not alter the half-life of the insulin receptor at the cell surface (Figure 8, D and F). By contrast, ER stress increased the half-life of insulin receptors at the surface of 3T3-F442A cells (Figure 8, B). Therefore, increased turnover and degradation of cell surface-exposed insulin receptors cannot explain the loss of insulin receptors leading to a decrease in insulin-stimulated S473 phosphorylation of AKT in ER stressed cells.

Unprocessed α-β proreceptors accumulate in the ER of ER-stressed cells. Since effects on transcription, translation, or degradation of insulin receptors cannot fully explain loss of mature insulin receptors in ER-stressed cells, we characterised whether transport of newly synthesised insulin receptors to the plasma membrane is inhibited by ER stress. Consistent with this hypothesis is that while mature β chains decrease in ER-stressed cells, the levels of α-β proreceptors increase relative to the levels of the β chains (Figures 9A and S5D). This suggests that α-β proreceptors accumulate in an early compartment of the secretory pathway such as the ER or *cis*-Golgi, because cleavage of the proreceptor into α- and β chains occurs in the *trans*-Golgi network (Robertson et al., 1993; Bravo et al., 1994). To provide additional evidence that proreceptors accumulate in the ER or *cis*-Golgi, we digested protein extracts from un- and ER-stressed C_2C_{12} cells with Endo H. Endo H releases high mannose and some hybrid type N-linked oligosaccharides from glycoproteins by cleaving between the two *N*-acetylglucosamine units (Maley et al., 1989). High mannose oligosaccharides are characteristic of proteins that have not been processed by enzymes in the Golgi complex. Endo H-digested α-β proreceptors migrated at the same position in SDS-PAGE as fully deglycosylated proreceptors synthesised in tunicamycin-treated cells (Figure 9, B and D) or obtained with PNGase F (Maley et al., 1989) (Figure 9, B-D), suggesting that none of the *N*-glycans on the majority of α-β proreceptors were exposed to processing enzymes of the Golgi

complex. By contrast, mature α and β chains carry both Endo H sensitive and Endo H-resistant *N*-linked oligosaccharides [(Heidenreich and Brandenburg, 1986; Hwang and Frost, 1999) and Figure 9, D]. These data are consistent with the conclusion that α-β proreceptors accumulate in the ER or *cis*-Golgi of ER-stressed cells.

To directly establish whether insulin receptors deplete at the plasma membrane and accumulate in intracellular compartments, we compared the localisation of *C*-terminally GFP-tagged insulin receptors expressed in HEK 293 cells treated for 18 h with 0.1 μg/ml tunicamycin or 1 μg/ml SubAB to untreated HEK 293 cells. HEK 293 cells were chosen for these experiments because they can be easily transfected, in contrast to Hep G2 cells, do not grow in clumps, and adhered better to culture vessels when treated with ER stressors than C_2C_{12} cells. ER stress lasting for 18 h depletes insulin receptor β chains in HEK 293 cells (Figure 9, E) and slightly decreases cell numbers (Figure 9, F). In unstressed cells, the GFP-tagged insulin receptor predominantly localised to the plasma membrane (Figure 9, G), which is supported by the high Pearson's correlation coefficient, r_{obs}, for the GFP fluorescence and the fluorescence of the CellMask Deep Red plasma membrane stain (Figure 9, H). By contrast, ER-stressed HEK 293 cells displayed intracellular GFP fluorescence and decreased colocalisation of GFP and CellMask Deep Red fluorescence (Figure 9, G and H). These observations are consistent with the conclusion that ER stress depletes the population of insulin receptors at the plasma membrane by interfering with trafficking of newly synthesised insulin receptors from the ER to the plasma membrane.

AKT activation by a cytosolic F_V2E-insulin receptor chimera is not affected by ER stress. To establish whether inhibition of transport of insulin receptors in the secretory pathway is necessary for ER stress to cause insulin resistance, we bypassed the secretory pathway in synthesis of functional insulin receptor protein tyrosine kinase domains by creating a chimera in which the signal peptide, extracellular and transmembrane domains of the insulin receptor have been replaced by an *N*-terminal myristoylation signal and the F_V2E domain (Figure 10, A). The myristoylation signal mediates *N*-terminal myristoylation of the protein and its anchoring to intracellular membranes (Maurer-Stroh et al., 2002a, b). The F_V2E domain

493 contains two binding sites for the bivalent macrolide AP20187 and binds AP20187 with
494 subnanomolar affinities (Clackson et al., 1998; Yang et al., 2000). Binding of AP20187 to the
495 F_V2E domain induces dimerisation of the chimeric protein. Dimerisation of the F_V2E-insulin
496 receptor chimera with AP20187 in stably transfected Flp-In T-Rex 293 cells increased
497 phosphorylation of the chimera at tyrosine 610, which is equivalent to tyrosine 1355 in the
498 long isoform of the human insulin receptor, showing that the chimera possesses tyrosine
499 autophosphorylation activity (Figure 10, B). Because AKT S473 phosphorylation was
500 unresponsive to serum starvation in Flp-In T-Rex 293 cells (data not shown), we transiently
501 transfected the chimera into C_2C_{12} myoblasts. In C_2C_{12} cells, AP20187 stimulated AKT S473
502 phosphorylation ~4.5 fold (Figure 10, C and D). Thus, activation of the F_V2E-insulin receptor
503 chimera recapitulates several events in insulin signalling. In transiently transfected C_2C_{12} cells
504 ER stress induced for 24 h with thapsigargin, tunicamycin, or SubAB reduced endogenous β
505 chains by ~40% (Figure 10, C) but did not affect activation of AKT by the chimera (Figure
506 10, C and D). Furthermore, ER stress induced with thapsigargin, tunicamycin, or SubAB
507 increased the abundance of unprocessed endogenous α-β proreceptors (Figure 10, E) and
508 induced *TRB3* (Figure 10, F). Hence, activation of AKT by the cytosolic, AP20187-
509 stimulated insulin receptor chimera is not affected by ER stress despite induction of *TRB3*,
510 depletion of β chains of the mature, endogenous insulin receptor, and accumulation of
511 unprocessed endogenous α-β proreceptors.

512 *Pharmacologic inhibition of JNKs does not rescue insulin-stimulated S473 phosphorylation*
513 *of AKT in ER-stressed cells.* Previous work has suggested that activation of both the family of
514 JNK MAP kinases and TRB3 by ER stress leads to a decrease in insulin-stimulated AKT
515 phosphorylation in ER-stressed cells (Özcan et al., 2004; Koh et al., 2006; Koh et al., 2013).
516 The lack of effects of 24 h of ER stress on the F_V2E-insulin receptor chimera (Figure 10)
517 prompted us to characterise whether the decrease in insulin-stimulated AKT phosphorylation
518 in cells experiencing ER stress for >12 h manifests independent of activation of JNKs or
519 TRB3. We first characterised JNK activation in C_2C_{12} and Hep G2 cells exposed to ER stress
520 for 12 – 36 h using phosphorylation of JNKs at T183 and Y185 in their T-loops as a marker

for their activation (Lawler et al., 1998; Fleming et al., 2000). No signals for JNKs phosphorylated at T183 and Y185 were obtained for C_2C_{12} cells exposed to 0.1 – 1.0 μM thapsigargin, 0.1 – 10 μg/ml tunicamycin, or 1 μg/ml SubAB for 12, 18, or 24 h or Hep G2 cells exposed to 0.1 – 10 μg/ml tunicamycin or 1 μg/ml SubAB for 18, 24, or 36 h in Western blots, despite detecting very strong signals in cells irradiated with UV light (400 J/m^2, λ = 254 nm; Figure 11, A and data not shown). Thus, if JNKs are activated in these conditions, the levels of JNK species phosphorylated at T183 and Y185 are below levels that can be detected by Western blotting. By contrast, exposure of Hep G2 cells to 0.1 – 1.0 μM thapsigargin for 18 – 36 h revealed activation of JNKs (Figure 11, A). Additional bands detected with the anti-phospho-T183-phospho-Y185-JNK antibody that migrate below the migration position of the 46 and 54 kDa isoforms of JNKs may represent phosphorylated species of other MAP kinases, such as p38, p42, and p44 (Figure 11, A), suggesting that exposure to thapsigargin for ≥18 h may activate several MAP kinases in Hep G2 cells.

To evaluate whether the JNK activation brought about by thapsigargin in Hep G2 cells contributes to the loss of insulin-stimulated S473 phosphorylation of AKT, we employed two selective JNK inhibitors, *N*-(4-amino-5-cyano-6-ethoxypyridin-2-yl)-2-(2,5-dimethoxyphenyl)acetamide (JNKi VIII) and (*E*)-3-(4-(dimethylamino)but-2-enamido)-*N*-(3-methyl-4-((4-(pyridin-3-yl)pyrimidin-2-yl)amino)phenyl)benzamide (JNKi XVI). Both inhibitors inhibited phosphorylation of the JNK substrate c-Jun in Hep G2 cells stimulated with UV or 5 μg/ml anisomycin for 30 min with submicromolar EC_{50} values that are comparable to previously reported EC_{50} values for inhibition of c-Jun phosphorylation in TNF-α treated Hep G2 or HeLa cells (Szczepankiewicz et al., 2006; Zhang et al., 2012) (Figure S6). Both inhibitors also inhibited c-Jun phosphorylation at S63 in Hep G2 cells exposed to 0.1 – 1.0 μM thapsigargin for 36 h (Figure 11, B). Thapsigargin increased steady-state levels of c-Jun (Figure 11, B), which is consistent with c-Jun autoregulating its own expression (Angel et al., 1988). 8 μM of JNKi XVI decreased the increase in c-Jun levels, while the same concentration of JNKi VIII had no effect on the increase in c-Jun levels in thapsigargin-treated Hep G2 cells (Figure 11, B), which correlates with the stronger inhibition

549 of c-Jun S63 phosphorylation elicited by thapsigargin by JNKi XVI. Both JNK inhibitors,
550 however, did not reverse inhibition of phosphorylation of S473 of AKT in Hep G2 cells that
551 were exposed to 0.1 – 1.0 μM thapsigargin for 36 h, and then stimulated with 10 or 100 nM
552 insulin for 15 min in the continued presence of thapsigargin (Figure 11, C-E). Both JNK
553 inhibitors decreased the insulin-stimulated phosphorylation of AKT at S473 (Figure 11, C and
554 D). Normalisation of S473 phosphorylation of AKT to the sample not exposed to thapsigargin
555 within each group (no JNKi, treatment with JNKi VIII or XVI) reinforced the conclusion that
556 both inhibitors do not reverse the inhibitory effect of thapsigargin on insulin-stimulated S473
557 phosphorylation of AKT (Figure 11, E). Consistent with this observation and the proposed
558 role for depletion of insulin receptors in ER-stressed cells as the cause for inhibition of
559 insulin-stimulated S473 phosphorylation of AKT, both JNK inhibitors also did not rescue
560 levels of β chains of the mature insulin receptor or α-β proreceptor processing in Hep G2 cells
561 exposed to 0.1 – 1.0 μM thapsigargin for 36 h (Figure 11, F).
562 *Genetic ablation of JNK1 and JNK2 does not protect mouse embryonic fibroblasts (MEFs)*
563 *from inhibition of insulin-stimulated AKT phosphorylation by ER stress.* To confirm the
564 results obtained with pharmacologic inhibitors of JNKs we compared the effects of 24 h of
565 ER stress on insulin-stimulated S473 phosphorylation of AKT in wild type (WT) MEFs and
566 MEFs deficient in the JNK1 and JNK2 isoforms of the JNK kinases. These $jnk1^{-/-}$ $jnk2^{-/-}$
567 MEFs lack detectable JNK activity because these cells do not express the neuronal isoform of
568 the JNKs, JNK3 (Tournier et al., 2000). Exposure of WT and $jnk1^{-/-}$ $jnk2^{-/-}$ MEFs to
569 thapsigargin, tunicamycin or SubAB for 24 h to elicit ER stress decreased insulin-stimulated
570 AKT phosphorylation in both cell types to the same degree (Figure 12, A-C), despite a 6.1 ±
571 0.6 increase in phosphorylation of JNKs in ER-stressed WT MEFs ($p < 0.0001$ in an ordinary
572 one-way ANOVA, Figure 12, D and E). ER stress also caused similar increases in the
573 abundance of unprocessed α-β insulin proreceptors in WT and $jnk1^{-/-}$ $jnk2^{-/-}$ MEFs (Figure 12,
574 F), which suggests that activation of the JNK kinases in the ER stress response does not affect
575 the protein folding capacity of the stressed ER.

siRNA-mediated silencing of expression of TRB does not protect from inhibition of insulin-stimulated AKT phosphorylation by ER stress. To characterise whether TRB3 contributes to the decrease in insulin-stimulated AKT phosphorylation in cells that experience ER stress for 24 h, we used two siRNAs to knock-down expression of *TRB3*. 48 h after transfection of C_2C_{12} myoblasts, both siRNAs decreased *TRB3* mRNA and protein levels to a similar degree (Figure 13, A and B). However, the knock-down of *TRB3* mRNA and protein levels did not affect insulin-stimulated phosphorylation of AKT (Figure 13, C and D) or the accumulation of unprocessed α-β insulin proreceptors (Figure 13, E) in cells exposed to thapsigargin, tunicamycin, or SubAB to elicit ER stress. These data argue that TRB3 does not contribute to decreased insulin-stimulated AKT phosphorylation or restoration of the protein folding capacity of cells that experience ER stress for 24 h. Taken together, the dispensability for JNKs and TRB3, as well as the absence of effects of ER stress on activation of AKT by the F_V2E-insulin receptor chimera, argue that ER stress decreases insulin-stimulated AKT phosphorylation independent of signal transduction events.

DISCUSSION

The data presented here establish that ER stress interferes with insulin-stimulated phosphorylation of AKT by inhibiting the processing of newly synthesised insulin receptors in the secretory pathway, which will deplete the cell surface population of the receptor over time (Figure 14, A). Several lines of evidence support this conclusion. ER stress extending over several half-lives of the insulin receptor at the plasma membrane inhibits insulin-stimulated AKT phosphorylation (Figures 6 and S5). Periods of ER stress shorter than the half-life of 6-12 h for the insulin receptor at the plasma membrane in ER-stressed cells (Figure 8) do not affect S473 phosphorylation of AKT by insulin (Figures 1, 2, and S1) or IRS1 tyrosine phosphorylation (Figures 3, 4, S2, and S3). The inhibition of insulin-stimulated AKT phosphorylation in ER-stressed cells coincides with a decrease in the abundance of mature insulin receptors (Figures 6A-C and S5A-C). Colocalisation experiments revealed that while GFP-tagged insulin receptors localise to the plasma membrane of unstressed cells, this

603 localisation of insulin receptors to the plasma membrane decreases in ER-stressed cells
604 (Figures 9, G and H). At the same time GFP-tagged insulin receptors accumulate within the
605 cell (Figure 9, G). Unprocessed α-β proreceptors, whose N-glycans remained sensitive to
606 Endo H (Figure 9, B), accumulate in ER-stressed cells (Figures 9A and S5D), suggesting that
607 unprocessed α-β proreceptors do not reach the *trans*-Golgi where they are processed to
608 mature receptors (Robertson et al., 1993; Bravo et al., 1994). siRNA-mediated knock-down of
609 expression of the insulin receptor confirmed that a ~50% decrease in insulin receptor levels
610 suffices to cause a similar decrease in insulin-stimulated AKT phosphorylation (Figure 6, E).
611 Finally, the absence of effects of ER stress on phosphorylation by the activated chimera of the
612 F_V2E domain and protein tyrosine kinase domain of the insulin receptor (Figure 10) showed
613 that processing of insulin receptors in the secretory pathway is necessary for ER stress to
614 inhibit insulin signalling. These experiments also suggested that signalling events in the UPR,
615 such as activation of JNKs or TRB3, do not affect insulin signalling downstream of the
616 insulin receptor. Pharmacologic inhibition and genetic ablation of JNKs (Figures 11 and 12)
617 and siRNA-mediated silencing of TRB3 (Figure 13) confirmed these conclusions.

618 In previous research tunicamycin was nearly exclusively used to inhibit trafficking of
619 newly synthesised insulin receptors (Keefer and De Meyts, 1981; Reed et al., 1981b; Ronnett
620 and Lane, 1981; Boyd and Raizada, 1983; Ercolani et al., 1984; Kadle et al., 1984; Ronnett et
621 al., 1984; Capeau et al., 1985; Goldstein and Kahn, 1988), which led to the conclusion that
622 the underlying cause for the trafficking defect is the lack of N-glycosylation of newly
623 synthesised insulin receptors. We show that two other ER stressors, thapsigargin and SubAB,
624 also inhibit processing of α-β proreceptors to mature receptors (Figures 9A and S5A)
625 suggesting that newly synthesised α-β proreceptors do not reach the *trans*-Golgi to be cleaved
626 into mature α- and β-chains. This conclusion is supported by the observation that all N-
627 glycans of α-β proreceptors in cells treated with thapsigargin or SubAB remain sensitive to
628 Endo H (Figure 9, B). The migration of α-β proreceptors synthesised in the presence of
629 thapsigargin or SubAB in SDS-PAGE suggests that these proreceptors are N-glycosylated to
630 the same extent as proreceptors synthesised by unstressed cells (Figures 6A, 7G, 9B, and

631 S5A), suggesting that both thapsigargin and SubAB do not inhibit N-glycosylation of newly
632 synthesised insulin receptors. Therefore, events other than lack of N-glycosylation can inhibit
633 transport of newly synthesised insulin receptors from the ER to the *trans* Golgi. Cleavage and
634 inactivation of the ER luminal HSP70 chaperone BiP by SubAB (Paton et al., 2006) may
635 interfere with correct folding of newly synthesised insulin receptors, leading to their retention
636 in the ER by the quality control machinery of the ER (Bass et al., 1998) and, to some extent,
637 targeting of unfolded proreceptors to ERAD machinery for degradation. The effects of
638 thapsigargin on protein folding in the ER are less well understood, but depletion of the ER
639 luminal Ca^{2+} store by thapsigargin (Thastrup et al., 1990) may inhibit several molecular
640 chaperones of the ER, because many of these bind Ca^{2+} ions with high capacities (Macer and
641 Koch, 1988; Fliegel et al., 1989; Wada et al., 1991). Indirect effects resulting from depletion
642 of proteins functioning in vesicular trafficking and sorting may also account for some of the
643 effects on insulin receptor trafficking, and may, for example, explain the increased half-life of
644 the insulin receptor at the plasma membrane in ER-stressed 3T3-F442A cells (Figure 8, A-B).
645 Insulin resistance can be a consequence of decreased insulin receptor levels, inhibition of
646 transduction of the insulin signal downstream of the insulin receptor (sometimes referred to as
647 'post-receptor events'), or a combination of the two (Olefsky and Kolterman, 1981). The
648 experiments with the F_V2E-insulin receptor chimera (Figure 10) show that ER stress does not
649 affect insulin signalling downstream of the receptor. Our work also establishes that plasma
650 membrane levels of the receptor decrease (Figures 9, G and H). Therefore, we propose that
651 ER stress primarily causes insulin resistance by decreasing the levels of insulin receptors at
652 the cell surface. Decreases in insulin receptors affect insulin sensitivity of cells, in other
653 words, shift the response curve to insulin towards higher insulin concentrations, but only
654 decrease the response to insulin when receptors become severely depleted (see, for example,
655 Figure 14, B and C, curves labelled '0' and '1' in B) (Olefsky and Kolterman, 1981).
656 Elevated insulin concentrations can compensate for decreased insulin sensitivity, because
657 many cell types possess 'spare' receptors, which allows them to mount maximal responses to
658 insulin even when only a small fraction of receptors have bound to insulin, possibly as low as

659 a few percent (Kono and Barham, 1971; Olefsky, 1975; Le Marchand-Brustel et al., 1978;
660 Hofmann et al., 1980; Frank et al., 1981). A decrease in insulin receptors will diminish the
661 response to insulin at one insulin concentration, but because insulin, the insulin receptor, and
662 insulin-insulin receptor complexes are in a dynamic equilibrium, increases in the insulin
663 concentration will compensate for the decrease in insulin receptor concentration, and allow
664 for formation of a sufficient number of insulin-insulin receptor complexes to elicit a maximal
665 response to insulin. By contrast, a decrease in the response to insulin at all insulin
666 concentrations is often indicative of inhibition of signal transduction downstream of the
667 insulin receptor (Olefsky and Kolterman, 1981). Hence, when high insulin concentrations are
668 employed, as is often done in *in vitro* studies, this is expected to primarily reveal post-
669 receptor events on insulin signalling because these affect insulin signalling independent of
670 insulin concentration, and the high insulin concentration is thought to compensate for
671 decreases in insulin sensitivity.

672 This, however, changes when insulin receptor levels decrease to such an extent that the
673 concentration of insulin-insulin receptor complexes approaches the value of K_E, the
674 concentration of the hormone, or more precisely hormone-receptor complexes, at which the
675 response to the hormone is half-maximal. At this point, the response to insulin will decrease
676 over the whole insulin concentration range (Figure 14, B and C), and complete compensation
677 by increasing insulin concentrations may, depending on the magnitude of the decrease in
678 insulin receptor levels, no longer be possible. It then also becomes difficult, if not impossible,
679 to distinguish between an effect on insulin sensitivity (due to decreased receptor levels) and
680 post-receptor events, even if dose-response curves are recorded or high insulin concentrations
681 are employed. Therefore, while previous studies have largely interpreted effects of ER stress
682 for > 12 h as post-receptor events (Avery et al., 2010; Xu et al., 2010; Tang et al., 2011;
683 Hassan et al., 2012; Jung et al., 2013; Panzhinskiy et al., 2013), it is also possible that the
684 effects of long periods of ER stress are, at least in part, the consequence of profound
685 decreases in insulin receptors and subsequently insulin sensitivity. The F_V2E-insulin receptor

chimera described in this work may prove to be a valuable tool to distinguish more rigorously between receptor and post-receptor events in future work.

The interpretation of effects of ER stress on insulin signalling is further complicated by the gradual decrease of insulin receptors at the plasma membrane over time until receptor levels fall below the critical level, at which cells do no longer retain their complete responsiveness to insulin. The time it takes for insulin receptor levels to fall to this critical level depends on (*a*) the half-life of the receptor at the cell surface, which is affected by cell type and can be affected by ER stress (Figure 8), (*b*) the number of cell surface insulin receptors in unstressed cells, which can vary widely between cell types (Bar et al., 1976; Reed et al., 1977; Capeau et al., 1978), (*c*) the sizes of intracellular insulin receptor pools, including, for example, receptors that are transiting through the Golgi complex and receptors that are recycled at the plasma membrane at the time ER stress is induced, (*d*) the degree of completeness of inhibition of transport of newly synthesised receptors from the ER to the cell surface, and (*e*) the fraction of newly synthesised receptors that is targeted for degradation by ERAD in ER-stressed cells. For example, short periods of ER stress (< 1-2 half-lives), will not deplete receptors to levels where the response to insulin decreases measurably, while long periods (> 2 half-lives) will cause severe receptor depletion, severe loss of insulin sensitivity, and a loss in insulin responsiveness (Figure 14, B). Likewise, a ~10-fold lower plasma membrane insulin receptor population may result in measurable loss of insulin responsiveness after ER stress lasting for ~3 half-lives of the receptor at the plasma membrane, while in cells that possess ten times more receptors, ER stress has to last for several additional half-lives before similar effects on insulin responsiveness manifest (Figure 14, B and C).

ER stress is present in muscle, liver, and adipose tissue of obese individuals (Özcan et al., 2004; Özcan et al., 2006; Hosogai et al., 2007; Boden et al., 2008; Sharma et al., 2008; Sreejayan et al., 2008). Patients with impaired glucose tolerance or overt type II diabetes show a ~50% decrease in insulin receptors (Olefsky and Reaven, 1974; Goldstein et al., 1975; Olefsky, 1976; Olefsky and Reaven, 1977; Pagano et al., 1977; Robinson et al., 1979; Helderman and Raskin, 1980; Kobayashi et al., 1980; Kolterman et al., 1980; Kolterman et

al., 1981). This ~50% decrease in insulin receptors at the cell surface accounts for the decreased insulin sensitivity and abnormal glucose tolerance of patients with impaired glucose tolerance (Olefsky and Reaven, 1977; Pagano et al., 1977; Kolterman et al., 1980; Kolterman et al., 1981). ER stress may decrease the fraction of newly synthesised receptors that reach the plasma membrane or increase the transit time through the secretory pathway for all or some of the newly synthesised insulin receptors and through this may contribute to the decrease in the size of the steady-state cell surface population of receptors in obesity. Internalisation of the insulin receptor is necessary for its degradation (Desbuquois et al., 1982; Knutson et al., 1983; Wang et al., 1983; Draznin et al., 1984). A decrease in the insulin receptor population at the cell surface is expected to decrease its internalisation and degradation rates, and together with decreased synthesis rates may establish a new, smaller steady-state population of the receptor at the plasma membrane. Hyperinsulinemia in obesity may further aggravate decreases of the insulin receptor at the plasma membrane, because, insulin stimulates internalisation and degradation of its receptor (Kasuga et al., 1981; Knutson et al., 1982; Heidenreich et al., 1983; Ronnett et al., 1983; Freychet, 1984; Reed et al., 1984), and, in adipocytes, induces ER stress (Boden et al., 2014). Thus, the effects of ER stress on delivery of newly synthesised insulin receptors to the plasma membrane may contribute to decreased steady-state plasma membrane levels of the receptor in obesity.

In conclusion, we provide evidence that ER stress requires processing of insulin receptors in the secretory pathway to inhibit signal transduction in the insulin signalling pathway (Figure 14, A). The effects of ER stress on trafficking of newly synthesised insulin receptors to the cell surface may account for the decrease in insulin receptors in patients with impaired glucose tolerance and patients with overt type II diabetes, and underlie the decreased insulin sensitivity of patients with impaired glucose tolerance. Depending on the half-lives of individual plasma membrane receptors, analogous effects of ER stress on other plasma membrane receptors and transporters may exist.

MATERIALS AND METHODS

Antibodies and reagents. The mouse anti-β-actin antibody (clone 8F10-G10, cat. no. ab170325, batches GR184354-8 and GR327417-1) was purchased from Abcam (Cambridge, UK) and the rat anti-α-tubulin antibody (clone YOL1/34, cat. no. MCA78G, batch 1703) from Bio-Rad Laboratories (Hemel Hempstead, UK). Rabbit anti-phospho-T308-AKT (clone 244F9, cat. no. 4056S, batches 13 and 17), anti-phospho-S473-AKT (clone D9E, cat. no. 4060S, batches 16, 23, and 24), rabbit anti-AKT (clone C67E7, cat. no. 4691S, batches 11, 17, and 20), rabbit anti-phospho-S63-c-Jun (clone 54B3, cat. no. 2361S, batch 7), rabbit anti-c-Jun (clone 60A8, cat. no. 9165S, batch 11), rabbit anti-phospho-S51-eIF2α (cat. no. 9721S, batch 21), mouse anti-eIF2α (clone L57A5, cat. no. 2103S, batch 5), rabbit anti-insulin receptor β chain phosphorylated at Y1355 (clone 14A4, cat. no. 3026S, batch 1), rabbit anti-insulin receptor β chain (clone 4B8, cat. no. 3025S, batches 8 and 10), rabbit anti-phospho-Y891 (mouse)/Y896 (human)-IRS1 (cat. no. 3070S, batch 4), rabbit anti-IRS1 (clone D23G12, cat. no. 3407S, batch 6; clone D5T8J, cat no. 95816S, batch 1), rabbit anti-phospho-T183-phospho-Y185-JNK (clone 81E11, cat. no. 4668S, batches 9, 12 and 15), and rabbit anti-JNK (cat. no. 9252S, batches 15 and 17) antibody were purchased from Cell Signaling Technology (Danvers, MA, USA). The mouse anti-phospho-S307 (mouse)/S312 (human)-IRS1 (clone 24.6.2, cat. no. 05-1087, batch 3063387), rabbit anti-phospho-Y608 (mouse)/Y612 (human)-IRS1 (cat. no. 09-432, batch 3018885), rabbit anti-phospho-Y628 (mouse)/Y632 (human)-IRS1 (cat. no. 09-433, batch 3023592), rabbit anti-phospho-Y935 (mouse)/941 (human)-IRS1 (cat. no. 07-848-I, batch Q2766987), mouse anti-phosphotyrosine (clone 4G10® Platinum, cat. no. 05-1050X, batches 2967319 and 3256630), and the rabbit anti-TRB3 (cat. no. 07-2160, batch 2716134) antibody were purchased from Merck Millipore (Watford, UK). Anti-insulin receptor β chain antibody (cat. no. sc-711, batch G0511) was purchased from Santa Cruz Biotechnology (Santa Cruz, CA, USA) and the mouse anti-GAPDH antibody (clone GAPDH-71.1, cat. no. G8795, batches 092M4820V and 067M4785V) from Sigma-Aldrich (Gillingham, UK).

Normal rabbit IgG was purchased from Fisher Scientific (Loughborough, UK, cat. no. 10312573, batch UA276761) and Santa Cruz Biotechnology (cat. no. sc-2027, batches C2712

and D1415). SureBeads™ protein A magnetic beads were purchased from Bio-Rad Laboratories (cat. no. 1614013) and streptavidin agarose from Fisher Scientific (cat. no. 10302384, batch SJ523686). Goat anti-mouse IgG(H+L)-peroxidase (cat. no. 10330974, batch OE17149612) and goat anti-rat IgG(H+L)-peroxidase (cat. no. 11889140, batch PK209942) were purchased from Fisher Scientific, and goat anti-rabbit IgG(H+L)-peroxidase from Cell Signaling Technology (cat. no. 7074S, batches 26-28).

Sulphosuccinimidyl-6-(biotinamido)hexanoate [EZ-link-sulfo-NHS-biotin, cat. no. 11851185] was purchased from Fisher Scientific. JNK inhibitor VIII [*N*-(4-amino-5-cyano-6-ethoxypyridin-2-yl)-2-(2,5-dimethoxyphenyl)acetamide, cat. no. 420135-5MG], JNK inhibitor XVI [(*E*)-3-(4-(dimethylamino)but-2-enamido)-*N*-(3-methyl-4-((4-(pyridin-3-yl)pyrimidin-2-yl)amino)phenyl)benzamide, cat. no. 420150-10MG], and tunicamycin (cat. no. 654380) were purchased from Merck Millipore. Endoglycosidase H (EndoH) and peptide-N-glycosidase (PNGase) F were obtained from New England Biolabs (Hitchin, UK). Bovine insulin (cat. no. I0516), bovine serum albumin (BSA, cat. no. A2153), dexamethasone, 3-isobutyl-1-methylxanthine, and thapsigargin (cat. no. T9033) were purchased from Sigma-Aldrich. Subtilase cytotoxin (SubAB) and catalytically inactive $SubA_{A272}B$ were purified from *Escherichia coli* as described before (Paton et al., 2004; Talbot et al., 2005). siRNAs against murine *INSR* mRNA and *Aequora victoria* enhanced green fluorescent protein (eGFP) were purchased from Sigma-Aldrich and siRNAs against murine *TRB3* from Fisher Scientific. siRNA sequences are listed in Table 1.

Plasmids. Plasmids were maintained in *Escherichia coli* XL10-Gold cells (Agilent Technologies, Stockport, UK, cat. no. 200314). Standard protocols for plasmid constructions were used (Ausubel et al., 2017). Plasmid pmaxGFP was obtained from Lonza Cologne AG (Cologne, Germany). Plasmid pEGFP-N2-hINSR encodes a fusion of the human insulin receptor to eGFP (Bass et al., 2000) and was obtained from Addgene (Cambridge, MA, USA, Addgene ID 22286). Plasmid pcDNA5/FRT/TO-F_V2E-INSRβ was generated by cloning the 1,430 bp *Bsi*WI-*Xma*I fragment of pCLFv2IRE (Cotugno et al., 2004) into *Bsi*WI- and *Xma*I-digested pcDNA5/FRT/TO-F_V2E-C'hIRE1α (D. Cox and M. Schröder, unpubl.). Plasmid

797 pcDNA5/FRT/TO-MyrF_V2E-INSRβ was generated by cloning the 501 bp *Eco*RI-*Xma*I
798 fragment of pC_4M-F_V2E (Ariad Pharmaceuticals, Cambridge, MA, USA) into *Hin*dIII- and
799 *Xma*I-digested pcDNA5/FRT/TO-F_V2E-INSRβ after blunting the *Eco*RI and *Hin*dIII sites
800 with Klenow enzyme.

801 *Cell culture.* Wild type (WT), *ire1α*$^{-/-}$ (Lee et al., 2002), *jnk1*$^{-/-}$ *jnk2*$^{-/-}$ (Tournier et al., 2000),
802 and *traf2*$^{-/-}$ (Yeh et al., 1997) mouse embryonic fibroblasts (MEFs) were obtained from
803 Randal J. Kaufman (Sanford Burnham Medical Research Institute, La Jolla, CA), Roger
804 Davis (University of Massachusetts, Worchester, MA, USA), and Tak Mak (University of
805 Toronto, Ontario Cancer Institute, Toronto, Ontario, Canada), respectively. 3T3-F442A
806 preadipocytes (Green and Kehinde, 1976), C_2C_{12} myoblasts (Blau et al., 1985), HEK 293 cells
807 (Graham et al., 1977; Harrison et al., 1977; Graham et al., 1978), and Hep G2 cells (Knowles
808 et al., 1980) were obtained from C. Hutchison (Durham University), R. Bashir (Durham
809 University), M. Cann (Durham University), and A. Benham (Durham University),
810 respectively. Fao rat hepatoma cells (Deschatrette and Weiss, 1974) were obtained from
811 Public Health England (Salisbury, UK). The Flp-In T-Rex 293 cell line was obtained from
812 Life Technologies (Paisley, UK). All cell lines were tested for mycoplasma contamination
813 upon receipt in the laboratory with the EZ-PCR mycoplasma test kit from Geneflow (cat. no.
814 K1-0210, Lichfield, UK). Mycoplasma testing was repeated every ~3 months with all cells in
815 culture at the time. Contaminated cultures were discarded.

816 All cell lines were grown in an atmosphere of 95% (v/v) air, 5% (v/v) CO_2, and 95%
817 humidity. Fao rat hepatoma cells were grown in Roswell Park Memorial Institute (RPMI)
818 1640 medium (Moore et al., 1967) or in Coon's modification of Ham's F12 medium (Coon
819 and Weiss, 1969) containing 10% (v/v) fetal bovine serum (FBS) and 2 mM L-glutamine.
820 Hep G2 cells were cultured in minimum essential medium (MEM) (Eagle, 1959)
821 supplemented with 10% (v/v) FBS and 2 mM L-glutamine. All other cell lines were cultured
822 in Dulbecco's modified Eagle's medium (DMEM) containing 4.5 g/l D-glucose (Morton,
823 1970; Rutzky and Pumper, 1974), 10% (v/v) FBS, and 2 mM L-glutamine. The medium for
824 *ire1α*$^{-/-}$ and corresponding WT MEFs was supplemented with 110 mg/l pyruvate (Lee et al.,

2002). The medium for the Flp-In T-Rex 293 cells was supplemented with 100 μg/ml zeocin and 15 μg/ml blasticidin and the medium for Flp-In T-Rex 293 cells stably expressing the F_V2E-insulin receptor chimera with 100 μg/ml hygromycin B and 15 μg/ml blasticidin. For immunoprecipitation of IRS1, [^{35}S]-L-methionine pulse labelling experiments, and determination of the half-life of the insulin receptor at the cell surface 3T3-F442A cells were cultured in gelatinised tissue cultures dishes (Schröder and Friedl, 1997b).

siRNAs and plasmids were transfected with INTERFERin or jetPRIME transfection reagent (Polyplus Transfection, Illkirch, France) following the manufacturer's instructions, respectively. The stably transfected Flp-In T-Rex 293 cell lines expressing a fusion of the F_V2E drug-inducible dimerisation domain (Clackson et al., 1998) to the β chain of the human insulin receptor with an *N*-terminal myristoylation signal were generated by transfection of the Flp-In T-Rex 293 cell line with pOG44 (Life Technologies) and pcDNA5/FRT/TO-MyrF_V2E-INSRβ. Selection of stably transfected clones was initiated 24 h after transfection by using 50 μg/ml hygromycin B. After two days the hygromycin B concentration was increased to 100 μg/ml.

C_2C_{12} myoblasts were differentiated into myotubes and 3T3-F442A preadipocytes into adipocytes as described before (Mihai and Schröder, 2015; Brown et al., 2016). ER stress was induced with 0.1 to 1 μM thapsigargin, 0.1 to 10 μg/ml tunicamycin, or 1 μg/ml SubAB. To stimulate cells with insulin, cells were serum-starved for 18 h, followed by addition of fresh serum-free culture medium containing 10 nM or 100 nM insulin for 5 min or 15 min. Cells were serum-starved during the last 18 h of treatments with ER stressors lasting for more than 18 h. When cells were ER-stressed for shorter periods, the ER stressors were applied towards the end of the serum starvation, for example for the last 12 h of serum starvation in case of treatment with ER stressors for 12 h. Expression of the F_V2E-insulin receptor chimera was induced for 24 h with 1 μg/ml tetracycline in stably-transfected Flp-In T-Rex 293 cells. The chimera was dimerised by treating cells with 100 nM AP20187 (B/B homodimeriser, TaKaRa Bio Europe, Saint-Germain-en-Laye, France, cat. no. 635058) for the times indicated in the text.

Crystal violet staining was used as a proxy to determine the number of cells remaining in culture dishes after exposure to ER stressors. Cultures were washed with phosphate-buffered saline (PBS, 4.3 mM Na_2HPO_4, 1.47 mM KH_2PO_4, 2.7 mM KCl, 137 mM NaCl, pH 7.4) at RT and stained for 10 min with 0.2% (w/v) crystal violet in 2% (v/v) ethanol at RT. After washing with tap water to remove unbound crystal violet, the crystal violet was dissolved with 1% (w/v) SDS and the absorbance at 570 nm read in a Spectramax 190 microplate reader (Molecular Devices, San Jose, CA, USA). The activity of mitochondrial redox chains was determined using thiazolyl blue tetrazolium bromide (MTT) as described previously (Mihai and Schröder, 2015), except that the absorbance at 690 nm was subtracted from the absorbance at 590 nm. Corrected MTT absorbances were normalised to the crystal violet absorbance of corresponding, identically treated cultures, and expressed relative to the absorbance of cells exposed to 0.1% (v/v) DMSO, which was arbitrarily set to 1.0.

*RNA extraction an*d reverse transcriptase *PCRs.* RNA was extracted and reverse transcribed as previously described (Cox et al., 2011). Protocols for quantification of splicing of *XBP1* have been described previously (Cox et al., 2011; Brown et al., 2016). qPCRs were run on a Rotorgene 3000 (Qiagen, Crawley, UK) using GoTaq G2 Flexi DNA polymerase (Promega, Southampton, UK, cat. no. M7801) and analysed as described before (Brown et al., 2016). Primer sequences are listed in Table 2 or have been reported before (Brown et al., 2016). Amplification of a single PCR product was confirmed by recording the melting curves after each PCR. Amplification efficiencies for all qPCRs were ~0.75 ± 0.05. Results represent the average and standard error of three technical repeats. qPCR results were confirmed by at least one other biological replicate.

Cell lysis and Western blotting. Protein extracts for Western blotting except for extraction of IRS1 were produced as previously described (Brown et al., 2016). In brief, cells were washed three times with ice-cold PBS (pH 7.4) and lysed in RIPA buffer [50 mM Tris-HCl, pH 8.0 at 4 °C, 150 mM NaCl, 0.5% (w/v) sodium deoxycholate, 0.1% (v/v) Triton X-100, 0.1% (w/v) SDS] containing Roche complete protease inhibitors (Roche Applied Science, Burgess Hill, UK, cat. no. 11836153001) or 10 mM EDTA, 2 mM PMSF, 6 mM 4-(2-

aminoethyl)benzenesulphonyl flouride (AEBSF), 5 mM benzamidine, 10 μg/ml aprotinin, and each 1 μg/ml of antipain dihydrochloride, chymostatin, leupeptin, and pepstatin A. To inhibit protein phosphatases, PhosSTOP phosphatase inhibitors (Sigma-Aldrich, cat. no. 04 906 837 001) were added when Roche complete protease inhibitors were used. When individual protease inhibitors were used, 1 mM sodium fluoride, 10 mM sodium β-glycerophosphate, 10 mM sodium pyrophosphate, and 200 nM okadaic acid were included to inhibit protein serine and threonine phosphatases. To preserve protein serine, threonine, and tyrosine phosphorylation when individual protease inhibitors were used, cells were lysed in 50 mM HEPES-NaOH (pH 8.0 at 4 °C), 150 mM NaCl, 0.5% (w/v) sodium deoxycholate, 0.1% (v/v) Triton X-100, 0.1% (w/v) SDS, 6 mM EGTA, 1 mM sodium fluoride, 1 mM sodium vanadate, 10 mM sodium β-glycerophosphate, 10 mM sodium pyrophosphate, 2 mM PMSF, 6 mM AEBSF, 5 mM benzamidine, 10 μg/ml aprotinin, and each 1 μg/ml of antipain dihydrochloride, chymostatin, leupeptin, and pepstatin A, 200 nM okadaic acid, 200 μM 2-bromo-4-methoxyacetophenone (Arabaci et al., 1999; Arabaci et al., 2002) and 20 μM ethyl 3,4-dephostatin (Watanabe et al., 2000; Suzuki et al., 2001). Protein concentrations were determined with the DC protein assay from Bio-Rad Laboratories (cat. no. 500-0116). Samples were denatured for 5 min at 100 °C after addition of 1/6 volume of 6 x SDS-PAGE sample loading buffer [350 mM Tris·HCl (pH 6.8 at RT), 30% (v/v) glycerol, 10% (w/v) SDS, 0.5 g/l bromophenol blue, 2% (v/v) β-mercaptoethanol]. 10 - 100 μg total protein were separated by SDS-PAGE (Laemmli, 1970) and transferred onto polyvinylidene difluoride (PVDF) membranes (Amersham HyBond^{TM}-P, pore size 0.45 μm, GE Healthcare, Little Chalfont, UK, cat. no. RPN303F) by semi-dry blotting in 0.1 M Tris, 0.192 M glycine, 5% (v/v) methanol at 2 mA/cm^2 for 75 min.

Protein extracts for Western blotting for IRS1 and phosphorylated species of IRS1 were prepared from cells serum-starved with media lacking phenol red. Media were aspirated and cells lysed in 8 M urea, 2.5% (w/v) SDS, 50 mM Tris·HCl (pH 7.5 at 4 °C), 6 mM EDTA, 2 mM PMSF, 40 mM AEBSF, 5 mM benzamidine, and 10 μM E-64. Lysates were cleared by centrifugation at 627,000 g for 2 h at 4 °C. Protein concentrations were determined with

bicinchoninic acid (Smith et al., 1985). Samples were denatured for 5 min at 70 °C after addition of 1/6 volume of 6 x SDS-PAGE sample loading buffer. 50 – 200 µg protein were separated on 7.5% SDS-PAGE gels and transferred to PVDF membranes by wet transfer in 10 mM $NaHCO_3$, 3 mM $NaCO_3$, 0.025% (w/v) SDS (Dunn, 1986) at 50 V for 18 h (for a 1 mm thick gel) at 4 °C after equilibration of gels for 3 x 20 min at 4 °C in 10 mM $NaHCO_3$, 3 mM $NaCO_3$, 0.025% (w/v) SDS.

Membranes were blocked for 1 h at RT or overnight at 4 °C in 5% (w/v) skimmed milk powder in TBST [20 mM Tris-HCl (pH 7.6 at RT), 137 mM NaCl, and 0.1% (v/v) Tween-20] or in TBST + 3% (w/v) skimmed milk powder when the anti-phosphotyrosine antibody was used. The anti-phospho-T308-AKT, anti-phospho-S473-AKT, anti-AKT, anti-phospho-S63-c-Jun, anti-c-Jun, anti-phospho-S51-eIF2α, anti-eIF2α, anti-phospho-Y1355-insulin receptor β chain, anti-insulin receptor β chain (clone 4B8), anti-phospho-Y891 (mouse)/Y896 (human)-IRS1, anti-IRS1 (clones D23G12 and D5T8J), anti-phospho-T183-phospho-Y185-JNK, and anti-JNK antibodies were incubated with membranes at a 1:1,000 dilution in TBST + 5% (w/v) BSA over night at 4°C with constant rotation. For the rabbit anti-IRS1 antibody, clone D23G12 was used to develop Western blots of cell lysates, while clone D5T8J was used to develop Western blots of immunoprecipitates of IRS1. The anti-phospho-Y608 (mouse)/Y612 (human)-IRS1 and anti-phospho-Y628 (mouse)/Y632 (human)-IRS1 antibodies were incubated with membranes at a 1:4,000 dilution in TBST + 5% (w/v) skimmed milk power for 2 h at RT. The anti-phospho-Y935 (mouse)/941 (human)-IRS1 antibody was incubated with membranes at a 1:1,000 dilution in TBST + 5% (w/v) skimmed milk powder for 2-4 at RT or overnight at 4 °C. The anti phospho-S307 (mouse)/S312 (human)-IRS1 antibody was incubated with membranes at a 1:1,000 dilution in TBST + 5% (w/v) skimmed milk powder overnight at 4 °C, and the anti-phosphotyrosine antibody at a 1:1,000 dilution in TBST + 3% (w/v) skimmed milk powder for 4 h at RT. The polyclonal anti-INSR β chain antibody was used at a 1:200 dilution and the anti-TRB3 antibody at a concentration of 0.1 µg/ml in TBST + 5% (w/v) skimmed milk powder overnight at 4 °C. The anti-β-actin antibody was used at a dilution of 1:10,000 – 1:20,000 in TBST + 5% (w/v)

skimmed milk powder for 2 h at RT, the anti-GAPDH antibody at a dilution of 1:10,000 – 1:30,000 in TBST + 5% (w/v) skimmed milk powder for 2 h at RT or overnight at 4 °C, and the anti-α-tubulin antibody at a dilution of 1:1,000 – 1:2,000 in TBST + 5% (w/v) skimmed milk powder for 2 h at RT. Membranes were washed four times with TBST for 5 min at RT and then probed with goat anti-mouse IgG(H+L)-peroxidase at a dilution of 1:5,000 in TBST + 5% (w/v) skimmed milk power for 2 h at RT to detect the anti-phospho-S307 (mouse)/S312 (human)-IRS1 antibody and at a dilution of 1:10,000 in TBST + 5% (w/v) skimmed milk powder for 2 h at RT to detect all other murine antibodies. Goat anti-rabbit IgG(H+L)-peroxidase was used at a dilution of 1:2,000 in TBST + 5% (w/v) skimmed milk powder for 2 h at RT, and goat anti-rat IgG(H+L)-peroxidase at a dilution of 1:5,000 in TBST + 5% (w/v) skimmed milk powder for 2 h at RT. Membranes were washed four times for 5 min at RT and then developed with Thermo Scientific™ Pierce™ ECL Western Blotting Substrate (Fisher Scientific, cat. no. 10455145), Thermo Scientific™ Pierce™ ECL 2 Western Blotting Substrate (Fisher Scientific, cat. no. 11517371) or by enhanced chemiluminescence as described before (Schröder and Friedl, 1997a). Blots were exposed to Thermo Scientific™ CL-X Posure™ film (Fisher Scientific, cat. no. 10696384) or Thermo Scientific™ CL-X Posure™ film pre-flashed with a Sensitize pre-flash unit (GE Healthcare, Little Chalfont, UK, cat. no. RPN 2051) following the manufacturer's instructions to capture weak signals. Exposure times were adjusted based on previous exposures to obtain exposures in the linear range of the film. Films were scanned on a CanoScan LiDE 600F scanner (Canon Europa, Amstelveen, The Netherlands) or a MFC-5320 DW all-in-one printer (Brother Industries, Manchester, UK) and saved as tif files. Bands were quantified with CLIQS 1.1 (Totallab, Newcastle upon Tyne, United Kingdom). Intensities for phosphorylated proteins were normalised to the intensity of the unphosphorylated species of the protein. Changes in protein abundance are expressed relative to the loading control, β-actin, GAPDH, or α-tubulin. Variation of normaliser samples was preserved for statistical analyses by normalising all samples within one experiment to all samples with similar intensities or by normalising all samples of one experimental repeat to the normaliser samples of all repeats for this type of

965 experiment and using the average of these normalisations for graphing and statistical
966 analyses.

967 To reprobe blots for detection of nonphosphorylated proteins and loading controls,
968 membranes were stripped using Thermo Scientific™ Restore™ Western Blot Stripping
969 Buffer (Fisher Scientific, cat. no. 10057103) or as described before (Armstrong et al., 2017),
970 except that the pH of the100 mM glycine·HCl, 0.1% (v/v) Tween 20 solution was dropped to
971 1.5 and the incubation temperature with this buffer raised to 65 °C. Membranes were then
972 blocked with 5% (w/v) skimmed milk powder in TBST as described above.

973 *Immunoprecipitation of IRS1.* Protein extracts were prepared as described under "Cell lysis
974 and Western blotting" for extraction of IRS1. 2 mg of total protein were diluted with 50 mM
975 Tris·HCl (pH 7.5 at 4 °C), 1% (v/v) Triton X-100, 10 mM EDTA, 0.1% (w/v) BSA to a final
976 SDS concentration of 0.1% (w/v). All immunoprecipitations in one experiment were adjusted
977 to the same final volume and a SDS concentration of 0.1% (w/v). Lysates were precleared
978 with 10 µl SureBeads™ protein A magnetic beads at 4 °C with constant, slow rotation of the
979 tubes. Samples were centrifuged at 500 g and 4 °C for 10 s, magnetic beads collected in
980 magnetic racks, and supernates centrifuged at 100,000 g, 4°C for 30 min and transferred to
981 new tubes. After addition of 2 µl of anti-IRS1 antibody (clone D23G12), samples were
982 incubated at 4 °C overnight with constant, slow rotation. Samples were then centrifuged at
983 100,000 g, 4°C for 30 min, supernates transferred to new tubes, and immune complexes
984 collected by addition of 30 µl SureBeads™ protein A magnetic beads for 2 h at 4 °C with
985 constant, slow rotation. Samples were centrifuged at 500 g and 4 °C for 10 s and
986 immunoprecipitates collected in magnetic racks. Immunoprecipitates were washed three times
987 with 50 mM Tris·HCl (pH 7.5 at 4 °C), 1% (v/v) Triton X-100, 10 mM EDTA, 0.1% (w/v)
988 BSA, and once with 0.1% (w/v) BSA. The last wash solution was completely aspirated, the
989 beads resupended in 58.3 mM Tris·HCl (pH 6.8 at RT), 10% (w/v) SDS, 8 M urea, 2.5% (v/v)
990 β-mercaptoethanol, 0.083 g/l bromophenol blue, and denatured at 80 °C for 5 min. Denatured
991 samples were allowed to cool to RT for 5 min, centrifuged at 17,000 g and RT for 5 min, and
992 separated on 7.5% SDS-PAGE gels. Proteins were transferred onto PVDF membranes and

993 membranes blotted with anti-phosphotyrosine and anti-IRS1 (clone D5T8J) antibodies as
994 described under “Cell lysis and Western blotting”.
995 *[^{35}S]-L-methionine/[^{35}S]-L-cysteine pulse labelling and immunoprecipitation of the insulin*
996 *receptor*. 70-80% confluent cultures were treated with 0.1 µM thapsigargin, 0.1 µg/ml
997 tunicamycin or 0.1% (v/v) DMSO for 22.5 h. Cultures were washed twice with methionine
998 and cysteine free culture medium pre-warmed to 37 °C and incubated with methionine and
999 cysteine free culture medium containing 2% (v/v) dialysed FBS in the continued presence of
1000 0.1% (v/v) DMSO, 0.1 µM thapsigargin or 0.1 µg/ml tunicamycin for 20 min at 37 °C. The
1001 medium was then replaced with fresh methionine and cysteine free culture medium
1002 containing 2% (v/v) dialysed FBS and DMSO, thapsigargin, or tunicamycin, and [^{35}S]-L-
1003 methionine/[^{35}S]-L-cysteine. 3T3-F442A cells were labelled with 250 µCi of 70% [^{35}S]-L-
1004 methionine, 25% [^{35}S]-L-cysteine (1000 Ci/mmol, Hartmann Analytic, Braunschweig,
1005 Germany, cat. no. SCIS-103) and Hep G2 cells with 125 µCi of 70% [^{35}S]-L-methionine, 25%
1006 [^{35}S]-L-cysteine (1000 Ci/mmol) per 10 cm dish for 1 or 8 h. Dishes were placed on ice, the
1007 medium aspirated and cultures washed three times with ice-cold PBS (pH 7.4), and lysed in
1008 125 µl of ice-cold 50 mM HEPES-NaOH (pH 7.5 at 4 °C), 150 mM NaCl, 0.5% (w/v) sodium
1009 deoxycholate, 0.1% (v/v) Triton X-100, 0.1% (w/v) SDS, 10 mM EDTA, 2 mM PMSF, 6 mM
1010 AEBSF, 5 mM benzamidine, 10 µg/ml aprotinin, and each 1 µg/ml of antipain
1011 dihydrochloride, chymostatin, leupeptin, and pepstatin A/10 cm dish. Lysates were cleared by
1012 centrifugation at 16,100 g, 4 °C for 30 min, and the protein concentration of lysates
1013 determined with the Bio-Rad Laboratories DC protein assay. For each immunoprecipitation
1014 2.4 mg of total cell protein were diluted to a final concentration of 4.8 mg/ml with ice-cold 50
1015 mM HEPES-NaOH (pH 7.5 at 4 °C), 150 mM NaCl, 10 mM EDTA, 0.5% (w/v) sodium
1016 deoxycholate, 0.1% (v/v) Triton X-100, 0.1% (w/v) SDS. 3T3-F442A cell lysates were
1017 precleared by incubation with 6.24 µl 100 ng/µl of normal rabbit IgG and 60 µl of
1018 SureBeads™ protein A magnetic beads for 2 h at 10 °C with overhead rotation. For Hep G2
1019 cell lysates, 3.12 µl 100 ng/µl of normal rabbit IgG and 30 µl of SureBeads™ protein A
1020 magnetic beads were used in the preclearing step. SureBeads™ protein A magnetic beads

were collected in magnetic racks, supernates centrifuged at 16,100 g, 4 °C for 15 min, and supernates transferred to new tubes. 6 µl of 52 ng/µl anti-insulin receptor β chain antibody (clone 4B8) or 3.12 µl 100 ng/µl normal rabbit IgG were added and samples incubated overnight at 10 °C with overhead rotation. Samples were centrifuged at 16,100 g, 4 °C for 15 min, supernates transferred to new tubes, and 30 µl SureBeads™ protein A magnetic beads added to collect immune complexes while incubating samples for 2 h at 10 °C with overhead rotation. Immune complexes were collected in magnetic racks. For immunoprecipitation of the insulin receptor from 3T3-F442A cell lysates, immunoprecipitates were washed three times with ice-cold 50 mM HEPES-NaOH (pH 7.5 at 4 °C), 500 mM NaCl, 10 mM EDTA, 0.5% (w/v) sodium deoxycholate, 1% (v/v) Triton X-100, 0.1% (w/v) SDS, 1 M urea, and once with ice-cold water. For immunoprecipitation of the insulin receptor from Hep G2 cell lysates, immunoprecipitates were washed three times with ice-cold 50 mM HEPES-NaOH (pH 7.5 at 4 °C), 2 M NaCl, 10 mM EDTA, 0.5% (w/v) sodium deoxycholate, 0.1% (v/v) Triton X-100, 0.1% (w/v) SDS, and once with ice-cold water. The water was completed aspirated, immunoprecipitates resuspended in 58.3 mM Tris·HCl (pH 6.8 at RT), 5% (v/v) glycerol, 10% (w/v) SDS, 2.5% (v/v) β-mercaptoethanol, 0.083 g/l bromophenol blue, and denatured at 100 °C for 5 min. Denatured samples were allowed to cool to RT for 5 min, centrifuged at 17,000 g, RT for 15 min, and separated on 7.5% SDS-PAGE gels, in which the SDS concentration had been raised to 1.25 g/l in both the stacking and separating gels. Gels were washed three times with water for 15 min at RT and dried for autoradiography with filter paper packing on a GelAir Drying System (Bio-Rad Laboratories, cat. no. 1651772) following the manufacturer's instructions (Krishnan and Nguyen, 1990). Gels were exposed to Kodak storage phosphor SD230 screens for 12 – 16 d and scanned on a Typhoon 9400 system (GE Healthcare). The abundance of ^{35}S-labelled α-β proreceptors was expressed relative to one randomly selected sample treated with 0.1% (v/v) DMSO.

Measurement of protein synthesis rates by [^{35}S]-L-methionine/[^{35}S]-L-cysteine pulse labelling. Cells were treated with 0.1% (v/v) DMSO, 0.1 µM thapsigargin, or 0.1 µg/ml tunicamycin and labelled with 70% [^{35}S]-L-methionine, 25% [^{35}S]-L-cysteine and protein

lysates prepared as described for "[^{35}S]-L-methionine/[^{35}S]-L-cysteine labelling and immunoprecipitation of the insulin receptor", except that cells were labelled in 6 well plates with 0.35 µCi of 70% [^{35}S]-L-methionine, 25% [^{35}S]-L-cysteine (1000 Ci/mol) per cavity for 30 min, and that lysates were prepared with 50 µl of lysis buffer per cavity. 50 µg of total protein were denatured after addition of 1/6 volume of 6 x SDS-PAGE sample loading buffer and heating to 100 °C for 5 min and resolved on 12% SDS-PAGE gels. Gels were stained with 0.1% (w/v) Coomassie Brilliant Blue R-250 in 50% (v/v) methanol, 10% (v/v) acetic acid for 30 min at RT, destained in 8% (v/v) acetic acid, 7% (v/v) methanol at RT, washed three times with water for 15 min at RT, and dried for autoradiography with filter paper packing as described above. Gels were exposed to Fujifilm BAS-IP multipurpose standard (MS) storage phosphor screens for 4 d or 16 d and scanned on a Typhoon 9400 system (GE Healthcare) to record the ^{35}S autoradiography signal and on a MFC-5320 DW all-in-one printer to record images of the Coomassie Brilliant Blue R-250-stained gels. Protein synthesis rates were expressed relative to the average of all cultures for one cell line treated with 0.1% (v/v) DMSO.

To measure [^{35}S]-L-methionine/[^{35}S]-L-cysteine incorporation rates by scintillation counting of TCA precipitates, 50 µg of protein lysate were added to 100 µl 1 mg/ml BSA on ice, followed by 1 ml of ice-cold 10% (w/v) TCA. Samples were incubated on ice for 30 min. TCA precipitates were collected on GF/C glass fibre filters (GE Healthcare, cat. no. 1822-025) prewetted with ice-cold 10% (w/v) TCA. The TCA precipitates were washed twice with ice-cold 10% (w/v) TCA, twice with ethanol, and allowed to dry at RT. Precipitated radioactivity was measured by scintillation counting in a Tri-Carb 2200 CA Liquid Scintillation Analyzer (Canberra Packard, Pangbourne, UK) in 20 ml plastic scintillation vials with 10 ml Ecoscint A (National Diagnostics, Hessle, UK). Counts per minute were converted into disintegrations per minute by using a prerecorded ^{35}S quench curve for the transformed spectral index of the external standard constructed by adding increasing amounts of chloroform to vials each containing $1 \cdot 10^3$ Bq of 70% [^{35}S]-L-methionine, 25% [^{35}S]-L-cysteine (1000 Ci/mol) in a total volume of 10 ml Ecoscint A/chloroform mixtures.

Measurement of the half-life of the insulin receptor at the cell surface. 70-80% confluent cultures were washed three times with ice-cold PBS (pH 8.0; 10 mM Na_2HPO_4, 2.0 mM KH_2PO_4, 2.7 mM KCl, 137 mM NaCl), labelled for 5 min at 4 °C in PBS (pH 8.0), 1 g/l D-glucose, 100 mg/l $CaCl_2$, 100 mg/l $MgCl_2$, 36 mg/l sodium pyruvate, 2 mM sulphosuccinimidyl-6-(biotinamido)hexanoate, washed three times with PBS (pH 8.0), 100 mM glycine at RT, three times with PBS (pH 7.4) at RT, replenished with culture medium containing 0.1% (v/v) DMSO, 0.3 µM thapsigargin, 1 µg/ml tunicamycin, or 1 µg/ml SubAB prewarmed to 37 °C, and incubated at 37 °C, 5% (v/v) CO_2, and 95% relative humidity for up to 72 h. To prepare protein lysates, cultures were placed on ice, washed three times with ice-cold PBS (pH 7.4), and lysed in RIPA buffer containing 10 mM EDTA, 2 mM PMSF, 6 mM AEBSF, 5 mM benzamidine, 10 µg/ml aprotinin, and each 1 µg/ml of antipain, chymostatin, leupeptin, and pepstatin A. Protein concentrations were determined with the Bio-Rad Laboratories DC protein assay. Biotinylated proteins were collected with 10 µl streptavidin-agarose beads from 100 µg total protein for 3T3-F442A cells, 200 µg total protein for C_2C_{12} cells, and 50 µg total protein for Hep G2 cells for 1 h at 4 °C. The streptavidin-agarose beads were washed once with ice-cold 10 mM HEPES (pH 7.5 at 4 °C), 1% (v/v) Triton X-100, 10 mM EDTA, twice with ice-cold 10 mM HEPES (pH 7.5 at 4 °C), 1% (v/v) Triton X-100, 10 mM EDTA, 6 M urea, and once with ice-cold water. The water was completed aspirated and beads resuspended in 15 µl of 6 x SDS-PAGE sample loading buffer. After denaturation at 100 °C for 5 min, purified proteins were resolved on 10% SDS-PAGE gels, transferred by semi-dry blotting onto PVDF membranes, developed with anti-insulin receptor β chain (clone 4B8) and anti-GAPDH antibodies, and chemiluminescence signals quantified as described under “Cell lysis and Western blotting”. To determine the half-life of the insulin receptor at the cell surface, the intensity of biotinylated insulin receptors purified on streptavidin-agarose beads immediately after labelling of cells with sulphosuccinimidyl-6-(biotinamido)hexanoate (‘0 h time point’) was arbitrarily set to 1.0. Levels of biotinylated insulin receptors purified 6 h, 12 h, 24 h, 36 h, 48 h, and 72 h after labelling of cells with sulphosuccinimidyl-6-(biotinamido)hexanoate were expressed relative to the level of biotinylated insulin receptors

purified at the 0 h time point. Half-lives were calculated from the slopes of linear decay curves of the natural logarithm of the relative abundance of biotinylated insulin receptors over time. For each condition, half-lives were determined in at least three independent experiments. Runs tests (Wald and Wolfowitz, 1940) did not reveal significant deviations form a linear relationship between the natural logarithm of the relative abundance of biotinylated insulin receptors and the time after the labelling reaction. Pilot experiments established that labelling of surface exposed insulin receptors is maximal and that biotinylation pull-down reactions are quantitative under the conditions described above (data not shown).

Endo H and PNGase F digests. 8 µg of protein were denatured in 0.5% (w/v) SDS, 40 mM DTT at 100°C for 10 min. Samples were then incubated with 1000 U of Endo H in 50 mM sodium citrate, pH 5.5 (at 25 °C) at 37°C for 2 h. For PNGase F digests denatured samples were incubated with 1000 U of PNGase F in 50 mM sodium phosphate pH 7.5 (at 25 °C), 1% (v/v) NP-40 at 37 °C for 2 h.

Fluorescence microscopy. Images of GFP-tagged insulin receptors expressed in HEK 293 cells were taken on a Zeiss ApoTome microscope (Carl Zeiss, Cambridge, UK) equipped with a Zeiss 63x Plan-APOCHROMAT Oil PH3 objective with a numerical aperture of 1.4 18 h after induction of ER stress with 1 µg/ml tunicamycin or 1 µg/ml SubAB. The cell membrane was visualised by staining cells for 5 min at RT with 5 µg/ml CellMask Deep Red (Life Technologies). GFP fluorescence was observed using a band pass (BP) 450-490 filter (Carl Zeiss, FITC/GFP, filter set 9, cat. no. 488009-000) and a long pass (LP) 515 filter. CellMask Deep red fluorescence was observed using a BP546/12 filter (Carl Zeiss, Rhodamine, filter set 15, cat. no. 488015-0000) and a LP 590 filter. To quantify colocalisation of the GFP-tagged insulin receptors and CellMask Deep Red signals, individual cells were defined as regions of interest (ROI) in Image J 1.47 (Schneider et al., 2012), and background-corrected for the intracellular fluorescence of CellMask Deep Red using the Background Subtraction from the ROI plug-in. The Pearson correlation coefficient between the INSR-GFP and CellMask Deep Red Fluorescence was determined in individual cells using the Colocalization Test plug-in

and Costes' image randomization (Costes et al., 2004) and a point spread function (PSF) width of 0.453 μm as a quantitative measure of colocalization of both fluorescence signals (Manders et al., 1992; Manders et al., 1993).

Statistical calculations. Experimental data are presented as means and standard errors. For composite parameters, errors were propagated using the law of error propagation for random, independent errors (Ku, 1966). Data were analysed for normality using the D'Agostino-Pearson omnibus normality test (D'Agostino and Pearson, 1973) or Shapiro-Wilk test (Shapiro and Wilk, 1965), equality of variances (homoscedasticity) using the Brown-Forsythe test (Brown and Forsythe, 1974), and, for additivity of means, treatment effects, and errors using Tukey's test (Tukey, 1949b; Little and Hills, 1972) before ordinary one- or two-way analysis of variance (ANOVA). Heteroscedastic data were transformed before ANOVA (Little and Hills, 1972) or examined by Welch's test (Welch, 1947) and a Games-Howell post hoc test (Games and Howell, 1976) or Dunnett's T3 multiple comparisons test (Dunnett, 1980). Kruskal-Wallis one-way ANOVA on ranks (Kruskal and Wallis, 1952) with Dunn's post-hoc test (Dunn, 1964) was used to analyse data that are not normally distributed or heteroscedastic. Transformed data were reexamined for normality, equality of variances, and additivity. In all analyses, a familywise p value of < 0.05 was considered statistically significant. Brown-Forsythe tests for equality of variances, Tukey's test for additivity, and runs tests (Wald and Wolfowitz, 1940) were performed in Microsoft Excel 2010 or Microsoft 365 Excel (Microsoft Corporation, Redmond, WA, USA) using the Real Statistics plug-in (http://www.real-statistics.com/). All other statistical calculations, linear and non-linear regressions were performed in GraphPad Prism 6.0.7 or 8.4.3 (GraphPad Software, La Jolla, CA, USA).

ACKNOWLEDGEMENTS

This work was supported by the European Community's 7th Framework Programme (FP7/2007-2013) under grant agreement no. 201608, a PhD studentship from Diabetes UK [BDA 09/0003949], and a PhD studentship from Parkinson's UK (H-1004). We thank R.

Davis (University of Massachusetts), R. J. Kaufman (Sanford Burnham Medical Research Institute), T. Mak (University of Toronto), A. Benham (Durham University), R. Bashir (Durham University), M. Cann (Durham University), and C. Hutchison (Durham University) for providing cell lines. We thank A. Auricchio (Telethon Institute of Genetics and Medicine, Naples, Italy) for plasmid pCLFv2IRE and Arial Pharmaceuticals for providing plasmid $pC_4M\text{-}F_V2E$.

CONFLICT OF INTEREST

The authors declare that they have no conflicts of interest with the contents of this article.

AUTHOR CONTRIBUTIONS

MS conceived and coordinated the study and wrote the paper. MB, SD, NS, ADM, JNW, and MS designed and performed the experiments. RD performed experiments. AWP and JCP prepared SubAB and $SubA_{A272}B$. MB, SD, NS, ADM, and MS analysed the results and prepared the figures. All authors approved the final version of the manuscript.

REFERENCES

Aguirre V, Uchida T, Yenush L, Davis R, and White MF (2000). The c-Jun NH_2-terminal kinase promotes insulin resistance during association with insulin receptor substrate-1 and phosphorylation of Ser^{307}. J Biol Chem *275*, 9047-9054.

Aguirre V, Werner ED, Giraud J, Lee YH, Shoelson SE, and White MF (2002). Phosphorylation of Ser307 in insulin receptor substrate-1 blocks interactions with the insulin receptor and inhibits insulin action. J Biol Chem *277*, 1531-1537.

Alessi DR, Andjelkovic M, Caudwell B, Cron P, Morrice N, Cohen P, and Hemmings BA (1996). Mechanism of activation of protein kinase B by insulin and IGF-1. EMBO J *15*, 6541-6551.

Angel P, Hattori K, Smeal T, and Karin M (1988). The jun proto-oncogene is positively autoregulated by its product, Jun/AP-1. Cell *55*, 875-885.

1186 Arabaci G, Guo X-C, Beebe KD, Coggeshall KM, and Pei D (1999). α-Haloacetophenone
1187 derivatives as photoreversible covalent inhibitors of protein tyrosine phosphatases. J Am
1188 Chem Soc *121*, 5085-5086.
1189 Arabaci G, Yi T, Fu H, Porter ME, Beebe KD, and Pei D (2002). α-Bromoacetophenone
1190 derivatives as neutral protein tyrosine phosphatase inhibitors: Structure-activity relationship.
1191 Bioorg Med Chem Lett *12*, 3047-3050.
1192 Armstrong MC, Šestak S, Ali AA, Sagini HAM, Brown M, Baty K, Treumann A, and
1193 Schröder M (2017). Bypass of activation loop phosphorylation by aspartate 836 in activation
1194 of the endoribonuclease activity of Ire1. Mol Cell Biol *37*, e00655-00616.
1195 Ausubel F, Brent R, Kingston RE, Moore DD, Seidman JG, and Struhl K. (2017). Current
1196 Protocols in Molecular Biology. John Wiley & Sons: New York.
1197 Avery J, Etzion S, Debosch BJ, Jin X, Lupu TS, Beitinjaneh B, Grand J, Kovacs A,
1198 Sambandam N, and Muslin AJ (2010). TRB3 function in cardiac endoplasmic reticulum
1199 stress. Circ Res *106*, 1516-1523.
1200 Backer JM, Myers MG, Jr., Shoelson SE, Chin DJ, Sun XJ, Miralpeix M, Hu P, Margolis B,
1201 Skolnik EY, Schlessinger J, and White MF (1992). Phosphatidylinositol 3'-kinase is activated
1202 by association with IRS-1 during insulin stimulation. EMBO J *11*, 3469-3479.
1203 Baldwin GS, Burgess AW, and Kemp BE (1982). Phosphorylation of a synthetic gastrin
1204 peptide by the tyrosine kinase of A431 cell membranes. Biochem Biophys Res Commun *109*,
1205 656-663.
1206 Baldwin GS, Knesel J, and Monckton JM (1983). Phosphorylation of gastrin-17 by epidermal
1207 growth factor-stimulated tyrosine kinase. Nature *301*, 435-437.
1208 Bar RS, Gorden P, Roth J, Kahn CR, and De Meyts P (1976). Fluctuations in the affinity and
1209 concentration of insulin receptors on circulating monocytes of obese patients: effects of
1210 starvation, refeeding, and dieting. J Clin Invest *58*, 1123-1135.
1211 Bass J, Chiu G, Argon Y, and Steiner DF (1998). Folding of insulin receptor monomers is
1212 facilitated by the molecular chaperones calnexin and calreticulin and impaired by rapid
1213 dimerization. J Cell Biol *141*, 637-646.

1214 Bass J, Kurose T, Pashmforoush M, and Steiner DF (1996). Fusion of insulin receptor
1215 ectodomains to immunoglobulin constant domains reproduces high-affinity insulin binding *in*
1216 *vitro*. J Biol Chem *271*, 19367-19375.
1217 Bass J, Turck C, Rouard M, and Steiner DF (2000). Furin-mediated processing in the early
1218 secretory pathway: sequential cleavage and degradation of misfolded insulin receptors. Proc
1219 Natl Acad Sci U S A *97*, 11905-11909.
1220 Bernales S, McDonald KL, and Walter P (2006). Autophagy counterbalances endoplasmic
1221 reticulum expansion during the unfolded protein response. PLoS Biol *4*, 2311-2324.
1222 Blau HM, Pavlath GK, Hardeman EC, Chiu CP, Silberstein L, Webster SG, Miller SC, and
1223 Webster C (1985). Plasticity of the differentiated state. Science *230*, 758-766.
1224 Boden G, Cheung P, Salehi S, Homko C, Loveland-Jones C, Jayarajan S, Stein TP, Williams
1225 KJ, Liu ML, Barrero CA, and Merali S (2014). Insulin regulates the unfolded protein
1226 response (UPR) in human adipose tissue. Diabetes *63*, 912-922.
1227 Boden G, Duan X, Homko C, Molina EJ, Song W, Perez O, Cheung P, and Merali S (2008).
1228 Increase in endoplasmic reticulum (ER) stress related proteins and genes in adipose tissue of
1229 obese, insulin resistant individuals. Diabetes *57*, 2438-2444.
1230 Boyd FT, Jr., and Raizada MK (1983). Effects of insulin and tunicamycin on neuronal insulin
1231 receptors in culture. Am J Physiol *245*, C283-287.
1232 Bravo DA, Gleason JB, Sanchez RI, Roth RA, and Fuller RS (1994). Accurate and efficient
1233 cleavage of the human insulin proreceptor by the human proprotein-processing protease furin.
1234 Characterization and kinetic parameters using the purified, secreted soluble protease
1235 expressed by a recombinant baculovirus. J Biol Chem *269*, 25830-25837.
1236 Brown M, Strudwick N, Suwara M, Sutcliffe LK, Mihai AD, Ali AA, Watson JN, and
1237 Schröder M (2016). An initial phase of JNK activation inhibits cell death early in the
1238 endoplasmic reticulum stress response. J Cell Sci *129*, 2317-2328.
1239 Brown MB, and Forsythe AB (1974). Robust tests for the equality of variances. J Am Stat
1240 Assoc *69*, 364-367.

1241 Calfon M, Zeng H, Urano F, Till JH, Hubbard SR, Harding HP, Clark SG, and Ron D (2002).
1242 IRE1 couples endoplasmic reticulum load to secretory capacity by processing the *XBP-1*
1243 mRNA. Nature *415*, 92-96.
1244 Capeau J, Lascols O, Flaig-Staedel C, Blivet MJ, Beck JP, and Picard J (1985). Degradation
1245 of insulin receptors by hepatoma cells: Insulin-induced down-regulation results from an
1246 increase in the rate of basal receptor degradation. Biochimie *67*, 1133-1141.
1247 Capeau J, Picard J, and Caron M (1978). Insulin receptors in Zajdela rat ascites hepatoma
1248 cells and their sensitivity to certain enzymes and lectins. Cancer Res *38*, 3930-3937.
1249 Casagrande R, Stern P, Diehn M, Shamu C, Osario M, Zúñiga M, Brown PO, and Ploegh H
1250 (2000). Degradation of proteins from the ER of S. cerevisiae requires an intact unfolded
1251 protein response pathway. Mol Cell *5*, 729-735.
1252 Chiang W-C, Messah C, and Lin JH (2012). IRE1 directs proteasomal and lysosomal
1253 degradation of misfolded rhodopsin. Mol Biol Cell *23*, 758-770.
1254 Clackson T, Yang W, Rozamus LW, Hatada M, Amara JF, Rollins CT, Stevenson LF, Magari
1255 SR, Wood SA, Courage NL, Lu X, Cerasoli F, Jr., Gilman M, and Holt DA (1998).
1256 Redesigning an FKBP-ligand interface to generate chemical dimerizers with novel specificity.
1257 Proc Natl Acad Sci U S A *95*, 10437-10442.
1258 Cleasby ME, Reinten TA, Cooney GJ, James DE, and Kraegen EW (2007). Functional
1259 studies of Akt isoform specificity in skeletal muscle *in vivo*; maintained insulin sensitivity
1260 despite reduced insulin receptor substrate-1 expression. Mol Endocrinol *21*, 215-228.
1261 Coon HG, and Weiss MC (1969). A quantitative comparison of formation of spontaneous and
1262 virus-produced viable hybrids. Proc Natl Acad Sci U S A *62*, 852-859.
1263 Costes SV, Daelemans D, Cho EH, Dobbin Z, Pavlakis G, and Lockett S (2004). Automatic
1264 and quantitative measurement of protein-protein colocalization in live cells. Biophys J *86*,
1265 3993-4003.
1266 Cotugno G, Pollock R, Formisano P, Linher K, Beguinot F, and Auricchio A (2004).
1267 Pharmacological regulation of the insulin receptor signaling pathway mimics insulin action in
1268 cells transduced with viral vectors. Hum Gene Ther *15*, 1101-1108.

1269 Cox DJ, Strudwick N, Ali AA, Paton AW, Paton JC, and Schröder M (2011). Measuring
1270 signaling by the unfolded protein response. Methods Enzymol *491*, 261-292.
1271 Crettaz M, and Kahn CR (1984). Insulin receptor regulation and desensitization in rat
1272 hepatoma cells. Concomitant changes in receptor number and in binding affinity. Diabetes *33*,
1273 477-485.
1274 Cryer PE, and Polonsky KS. (1998). Glucose homeostasis and hypoglycemia. In: Williams
1275 Textbook of Endocrinology, eds. J.D. Wilson, D.W. Foster, H.M. Kronenberg, and P.R.
1276 Larsen, Philadelphia: W. B. Saunders Company, 939-972.
1277 D'Agostino R, and Pearson ES (1973). Tests for departure from normality. Empirical results
1278 for the distributions of b_2 and $\sqrt{b_1}$. Biometrika *60*, 613-622.
1279 Desbuquois B, Lopez S, and Burlet H (1982). Ligand-induced translocation of insulin
1280 receptors in intact rat liver. J Biol Chem *257*, 10852-10860.
1281 Deschatrette J, and Weiss MC (1974). Characterization of differentiated and dedifferentiated
1282 clones from a rat hepatoma. Biochimie *56*, 1603-1611.
1283 Draznin B, Trowbridge M, and Ferguson L (1984). Quantitative studies of the rate of insulin
1284 internalization in isolated rat hepatocytes. Biochem J *218*, 307-312.
1285 Du K, Herzig S, Kulkarni RN, and Montminy M (2003). TRB3: A *tribbles* homolog that
1286 inhibits Akt/PKB activation by insulin in liver. Science *300*, 1574-1577.
1287 Dunn OJ (1964). Multiple comparisons using rank sums. Technometrics *6*, 241-252.
1288 Dunn SD (1986). Effects of the modification of transfer buffer composition and the
1289 renaturation of proteins in gels on the recognition of proteins on Western blots by monoclonal
1290 antibodies. Anal Biochem *157*, 144-153.
1291 Dunnett CW (1955). A multiple comparison procedure for comparing several treatments with
1292 a control. J Am Stat Assoc *50*, 1096-1121.
1293 Dunnett CW (1964). New tables for multiple comparisons with control. Biometrics *20*, 482-
1294 491.
1295 Dunnett CW (1980). Pairwise multiple comparisons in the unequal variance case. J Am Stat
1296 Assoc *75*, 796-800.

1297 Eagle H (1959). Amino acid metabolism in mammalian cell cultures. Science *130*, 432-437.

1298 Emanuelli B, Eberle D, Suzuki R, and Kahn CR (2008). Overexpression of the dual-
1299 specificity phosphatase MKP-4/DUSP-9 protects against stress-induced insulin resistance.
1300 Proc Natl Acad Sci U S A *105*, 3545-3550.

1301 Ercolani L, Brown TJ, and Ginsberg BH (1984). Tunicamycin blocks the emergence and
1302 maintenance of insulin receptors on mitogen-activated human T lymphocytes. Metabolism *33*,
1303 309-316.

1304 Esposito DL, Li Y, Cama A, and Quon MJ (2001). Tyr^{612} and Tyr^{632} in human insulin
1305 receptor substrate-1 are important for full activation of insulin-stimulated phosphatidylinositol
1306 3-kinase activity and translocation of GLUT4 in adipose cells. Endocrinology *142*, 2833-
1307 2840.

1308 Fewell SW, Travers KJ, Weissman JS, and Brodsky JL (2001). The action of molecular
1309 chaperones in the early secretory pathway. Annu Rev Genet *35*, 149-191.

1310 Fleming Y, Armstrong CG, Morrice N, Paterson A, Goedert M, and Cohen P (2000).
1311 Synergistic activation of stress-activated protein kinase 1/c-Jun N-terminal kinase
1312 (SAPK1/JNK) isoforms by mitogen-activated protein kinase kinase 4 (MKK4) and MKK7.
1313 Biochem J *352*, 145-154.

1314 Fliegel L, Burns K, MacLennan DH, Reithmeier RA, and Michalak M (1989). Molecular
1315 cloning of the high affinity calcium-binding protein (calreticulin) of skeletal muscle
1316 sarcoplasmic reticulum. J Biol Chem *264*, 21522-21528.

1317 Frank HJ, Davidson MB, and Serbin PA (1981). Insulin binding and action in isolated rat
1318 hepatocytes: evidence for spare receptors. Metabolism *30*, 1159-1164.

1319 Franke TF, Yang SI, Chan TO, Datta K, Kazlauskas A, Morrison DK, Kaplan DR, and
1320 Tsichlis PN (1995). The protein kinase encoded by the Akt proto-oncogene is a target of the
1321 PDGF-activated phosphatidylinositol 3-kinase. Cell *81*, 727-736.

1322 Freychet P (1984). [Insulin resistance. Physiopathological and biochemical aspects]. Ann
1323 Endocrinol (Paris) *45*, 107-114.

Friedlander R, Jarosch E, Urban J, Volkwein C, and Sommer T (2000). A regulatory link between ER-associated protein degradation and the unfolded-protein response. Nat Cell Biol *2*, 379-384.

Gaddam D, Stevens N, and Hollien J (2013). Comparison of mRNA localization and regulation during endoplasmic reticulum stress in *Drosophila* cells. Mol Biol Cell *24*, 14-20.

Games PA, and Howell JF (1976). Pairwise multiple comparison procedures with unequal N's and/or variances: A Monte Carlo study. J Educ Stat *1*, 113-125.

Gammeltoft S, and Gliemann J (1973). Binding and degradation of ^{125}I-labelled insulin by isolated rat fat cells. Biochim Biophys Acta *320*, 16-32.

Goldstein BJ, and Kahn CR (1988). Initial processing of the insulin receptor precursor *in vivo* and *in vitro*. J Biol Chem *263*, 12809-12812.

Goldstein S, Blecher M, Binder R, Perrino PV, and Recant L (1975). Hormone receptors, 5. Binding of glucagon and insulin to human circulating mononuclear cells in diabetes mellitus. Endocr Res Commun *2*, 367-376.

Graham FL, Harrison T, and Williams J (1978). Defective transforming capacity of adenovirus type 5 host-range mutants. Virology *86*, 10-21.

Graham FL, Smiley J, Russell WC, and Nairn R (1977). Characteristics of a human cell line transformed by DNA from human adenovirus type 5. J Gen Virol *36*, 59-74.

Grako KA, Olefsky JM, and McClain DA (1992). Tyrosine kinase-defective insulin receptors undergo decreased endocytosis but do not affect internalization of normal endogenous insulin receptors. Endocrinology *130*, 3441-3452.

Green H, and Kehinde O (1976). Spontaneous heritable changes leading to increased adipose conversion in 3T3 cells. Cell *7*, 105-113.

Guertin DA, Stevens DM, Thoreen CC, Burds AA, Kalaany NY, Moffat J, Brown M, Fitzgerald KJ, and Sabatini DM (2006). Ablation in mice of the mTORC components *raptor*, *rictor*, or *mLST8* reveals that mTORC2 is required for signaling to Akt-FOXO and PKCα, but not S6K1. Dev Cell *11*, 859-871.

1351 Harding HP, Novoa I, Zhang Y, Zeng H, Wek R, Schapira M, and Ron D (2000). Regulated
1352 translation initiation controls stress-induced gene expression in mammalian cells. Mol Cell *6*,
1353 1099-1108.
1354 Harding HP, Zhang Y, and Ron D (1999). Protein translation and folding are coupled by an
1355 endoplasmic-reticulum-resident kinase. Nature *397*, 271-274.
1356 Harrison T, Graham F, and Williams J (1977). Host-range mutants of adenovirus type 5
1357 defective for growth in HeLa cells. Virology *77*, 319-329.
1358 Hassan RH, Hainault I, Vilquin J-T, Samama C, Lasnier F, Ferré P, Foufelle F, and Hajduch
1359 E (2012). Endoplasmic reticulum stress does not mediate palmitate-induced insulin resistance
1360 in mouse and human muscle cells. Diabetologia *55*, 204-214.
1361 Hebert DN, and Molinari M (2007). In and out of the ER: protein folding, quality control,
1362 degradation, and related human diseases. Physiol Rev *87*, 1377-1408.
1363 Heidenreich KA, Berhanu P, Brandenburg D, and Olefsky JM (1983). Degradation of insulin
1364 receptors in rat adipocytes. Diabetes *32*, 1001-1009.
1365 Heidenreich KA, and Brandenburg D (1986). Oligosaccharide heterogeneity of insulin
1366 receptors. Comparison of N-linked glycosylation of insulin receptors in adipocytes and brain.
1367 Endocrinology *118*, 1835-1842.
1368 Helderman JH, and Raskin P (1980). The T lymphocyte insulin receptor in diabetes and
1369 obesity: An intrinsic binding defect. Diabetes *29*, 551-557.
1370 Hers I, Bell CJ, Poole AW, Jiang D, Denton RM, Schaefer E, and Tavaré JM (2002).
1371 Reciprocal feedback regulation of insulin receptor and insulin receptor substrate tyrosine
1372 phosphorylation by phosphoinositide 3-kinase in primary adipocytes. Biochem J *368*, 875-
1373 884.
1374 Hiratani K, Haruta T, Tani A, Kawahara J, Usui I, and Kobayashi M (2005). Roles of mTOR
1375 and JNK in serine phosphorylation, translocation, and degradation of IRS-1. Biochem
1376 Biophys Res Commun *335*, 836-842.

Hoehn KL, Hohnen-Behrens C, Cederberg A, Wu LE, Turner N, Yuasa T, Ebina Y, and James DE (2008). IRS1-independent defects define major nodes of insulin resistance. Cell Metab *7*, 421-433.

Hofmann C, Marsh JW, Miller B, and Steiner DF (1980). Cultured hepatoma cells as a model system for studying insulin processing and biologic responsiveness. Diabetes *29*, 865-874.

Hollien J, Lin JH, Li H, Stevens N, Walter P, and Weissman JS (2009). Regulated Ire1-dependent decay of messenger RNAs in mammalian cells. J Cell Biol *186*, 323-331.

Hollien J, and Weissman JS (2006). Decay of endoplasmic reticulum-localized mRNAs during the unfolded protein response. Science *313*, 104-107.

Hornbeck PV, Zhang B, Murray B, Kornhauser JM, Latham V, and Skrzypek E (2015). PhosphoSitePlus, 2014: mutations, PTMs and recalibrations. Nucleic Acids Res *43*, D512-520.

Hosogai N, Fukuhara A, Oshima K, Miyata Y, Tanaka S, Segawa K, Furukawa S, Tochino Y, Komuro R, Matsuda M, and Shimomura I (2007). Adipose tissue hypoxia in obesity and its impact on adipocytokine dysregulation. Diabetes *56*, 901-911.

Hubbard SC, and Ivatt RJ (1981). Synthesis and processing of asparagine-linked oligosaccharides. Annu Rev Biochem *50*, 555-583.

Hunter T (1982). Synthetic peptide substrates for a tyrosine protein kinase. J Biol Chem *257*, 4843-4848.

Hwang JB, and Frost SC (1999). Effect of alternative glycosylation on insulin receptor processing. J Biol Chem *274*, 22813-22820.

Imanikia S, Özbey NP, Krueger C, Casanueva MO, and Taylor RC (2019). Neuronal XBP-1 activates intestinal lysosomes to improve proteostasis in *C. elegans*. Curr Biol *29*, 2322-2338 e2327.

Jacinto E, Facchinetti V, Liu D, Soto N, Wei S, Jung SY, Huang Q, Qin J, and Su B (2006). SIN1/MIP1 maintains rictor-mTOR complex integrity and regulates Akt phosphorylation and substrate specificity. Cell *127*, 125-137.

1404 Jang YY, Kim NK, Kim MK, Lee HY, Kim SJ, Kim HS, Seo HY, Lee IK, and Park KG
1405 (2010). The effect of tribbles-related protein 3 on ER stress-suppressed insulin gene
1406 expression in INS-1 cells. Korean Diabetes J *34*, 312-319.
1407 Jung DY, Chalasani U, Pan N, Friedline RH, Prosdocimo DA, Nam M, Azuma Y, Maganti R,
1408 Yu K, Velagapudi A, O'Sullivan-Murphy B, Sartoretto JL, Jain MK, Cooper MP, Urano F,
1409 Kim JK, and Gray S (2013). KLF15 is a molecular link between endoplasmic reticulum stress
1410 and insulin resistance. PLoS One *8*, e77851.
1411 Kadle R, Fellows RE, and Raizada MK (1984). The effects of insulin and tunicamycin on
1412 insulin receptors of cultured fibroblasts. Exp Cell Res *151*, 533-541.
1413 Kasuga M, Kahn CR, Hedo JA, Van Obberghen E, and Yamada KM (1981). Insulin-induced
1414 receptor loss in cultured human lymphocytes is due to accelerated receptor degradation. Proc
1415 Natl Acad Sci U S A *78*, 6917-6921.
1416 Keefer LM, and De Meyts P (1981). Glycosylation of cell surface receptors: tunicamycin
1417 treatment decreases insulin and growth hormone binding to different levels in cultured
1418 lymphocytes. Biochem Biophys Res Commun *101*, 22-29.
1419 Knowles BB, Howe CC, and Aden DP (1980). Human hepatocellular carcinoma cell lines
1420 secrete the major plasma proteins and hepatitis B surface antigen. Science *209*, 497-499.
1421 Knutson VP, Ronnett GV, and Lane MD (1982). Control of insulin receptor level in 3T3
1422 cells: effect of insulin-induced down-regulation and dexamethasone-induced up-regulation on
1423 rate of receptor inactivation. Proc Natl Acad Sci U S A *79*, 2822-2826.
1424 Knutson VP, Ronnett GV, and Lane MD (1983). Rapid, reversible internalization of cell
1425 surface insulin receptors. Correlation with insulin-induced down-regulation. J Biol Chem *258*,
1426 12139-12142.
1427 Kobayashi M, Ohgaku S, Iwasaki M, Harano Y, Maegawa H, and Shigeta Y (1980).
1428 Evaluation of the method of insulin binding studies in human erythrocytes. Endocrinol Jpn
1429 *27*, 337-342.
1430 Koh HJ, Arnolds DE, Fujii N, Tran TT, Rogers MJ, Jessen N, Li Y, Liew CW, Ho RC,
1431 Hirshman MF, Kulkarni RN, Kahn CR, and Goodyear LJ (2006). Skeletal muscle-selective

knockout of LKB1 increases insulin sensitivity, improves glucose homeostasis, and decreases TRB3. Mol Cell Biol *26*, 8217-8227.

Koh HJ, Toyoda T, Didesch MM, Lee MY, Sleeman MW, Kulkarni RN, Musi N, Hirshman MF, and Goodyear LJ (2013). Tribbles 3 mediates endoplasmic reticulum stress-induced insulin resistance in skeletal muscle. Nat Commun *4*, 1871.

Kolterman OG, Gray RS, Griffin J, Burstein P, Insel J, Scarlett JA, and Olefsky JM (1981). Receptor and postreceptor defects contribute to the insulin resistance in noninsulin-dependent diabetes mellitus. J Clin Invest *68*, 957-969.

Kolterman OG, Insel J, Saekow M, and Olefsky JM (1980). Mechanisms of insulin resistance in human obesity: evidence for receptor and postreceptor defects. J Clin Invest *65*, 1272-1284.

Kono T, and Barham FW (1971). The relationship between the insulin-binding capacity of fat cells and the cellular response to insulin. Studies with intact and trypsin-treated fat cells. J Biol Chem *246*, 6210-6216.

Kornfeld R, and Kornfeld S (1985). Assembly of asparagine-linked oligosaccharides. Annu Rev Biochem *54*, 631-664.

Krishnan M, and Nguyen HT (1990). Drying acrylamide slab gels for fluorography without using gel drier and vacuum pump. Anal Biochem *187*, 51-53.

Krupp M, and Lane MD (1981). On the mechanism of ligand-induced down-regulation of insulin receptor level in the liver cell. J Biol Chem *256*, 1689-1694.

Kruskal WH, and Wallis WA (1952). Use of ranks in one-criterion variance analysis. J Am Stat Assoc *47*, 583-621.

Ku HH (1966). Notes on the use of propagation of error formulas. J Res Nat Bureau Standards Sect C - Eng Instrumentat *70*, 263-273.

Kuo SC, and Lampen O (1976). Tunicamycin inhibition of [^{3}H] glucosamine incorporation into yeast glycoproteins: binding of tunicamycin and interaction with phospholipids. Arch Biochem Biophys *172*, 574-581.

1459 Kurzban GP, Bayer EA, Wilchek M, and Horowitz PM (1991). The quaternary structure of
1460 streptavidin in urea. J Biol Chem *266*, 14470-14477.
1461 Laemmli UK (1970). Cleavage of structural proteins during the assembly of the head of
1462 bacteriophage T4. Nature *227*, 680-685.
1463 Lawler S, Fleming Y, Goedert M, and Cohen P (1998). Synergistic activation of
1464 SAPK1/JNK1 by two MAP kinase kinases in vitro. Curr Biol *8*, 1387-1390.
1465 Le Marchand-Brustel Y, Jeanrenaud B, and Freychet P (1978). Insulin binding and effects in
1466 isolated soleus muscle of lean and obese mice. Am J Physiol *234*, E348-358.
1467 Lee K, Tirasophon W, Shen X, Michalak M, Prywes R, Okada T, Yoshida H, Mori K, and
1468 Kaufman RJ (2002). IRE1-mediated unconventional mRNA splicing and S2P-mediated ATF6
1469 cleavage merge to regulate XBP1 in signaling the unfolded protein response. Genes Dev *16*,
1470 452-466.
1471 Lee YH, Giraud J, Davis RJ, and White MF (2003). c-Jun N-terminal kinase (JNK) mediates
1472 feedback inhibition of the insulin signaling cascade. J Biol Chem *278*, 2896-2902.
1473 Lehle L, and Tanner W (1976). The specific site of tunicamycin inhibition in the formation of
1474 dolichol-bound *N*-acetylglucosamine derivatives. FEBS Lett *71*, 167-170.
1475 Little TM, and Hills FJ. (1972). Statistical Methods in Agricultural Research. University of
1476 California Agricultural Extension: Davis.
1477 Macer DR, and Koch GL (1988). Identification of a set of calcium-binding proteins in
1478 reticuloplasm, the luminal content of the endoplasmic reticulum. J Cell Sci *91*, 61-70.
1479 Maley F, Trimble RB, Tarentino AL, and Plummer TH, Jr. (1989). Characterization of
1480 glycoproteins and their associated oligosaccharides through the use of endoglycosidases. Anal
1481 Biochem *180*, 195-204.
1482 Manders EMM, Stap J, Brakenhoff GJ, van Driel R, and Aten JA (1992). Dynamics of three-
1483 dimensional replication patterns during the S-phase, analysed by double labelling of DNA and
1484 confocal microscopy. J Cell Sci *103*, 857-862.
1485 Manders EMM, Verbeek FJ, and Aten JA (1993). Measurement of co-localization of objects
1486 in dual-colour confocal images. J Microsc *169*, 375-382.

1487 Mao K, Kobayashi S, Jaffer ZM, Huang Y, Volden P, Chernoff J, and Liang Q (2008).
1488 Regulation of Akt/PKB activity by P21-activated kinase in cardiomyocytes. J Mol Cell
1489 Cardiol *44*, 429-434.
1490 Maurer-Stroh S, Eisenhaber B, and Eisenhaber F (2002a). N-terminal N-myristoylation of
1491 proteins: prediction of substrate proteins from amino acid sequence. J Mol Biol *317*, 541-557.
1492 Maurer-Stroh S, Eisenhaber B, and Eisenhaber F (2002b). N-terminal N-myristoylation of
1493 proteins: refinement of the sequence motif and its taxon-specific differences. J Mol Biol *317*,
1494 523-540.
1495 McDonald PC, Oloumi A, Mills J, Dobreva I, Maidan M, Gray V, Wederell ED, Bally MB,
1496 Foster LJ, and Dedhar S (2008). Rictor and integrin-linked kinase interact and regulate Akt
1497 phosphorylation and cancer cell survival. Cancer Res *68*, 1618-1624.
1498 Meusser B, Hirsch C, Jarosch E, and Sommer T (2005). ERAD: the long road to destruction.
1499 Nat Cell Biol *7*, 766-772.
1500 Mihai AD, and Schröder M (2015). Glucose starvation and hypoxia, but not the saturated
1501 fatty acid palmitic acid or cholesterol, activate the unfolded protein response in 3T3-F442A
1502 and 3T3-L1 adipocytes. Adipocyte *4*, 188-202.
1503 Moore GE, Gerner RE, and Franklin HA (1967). Culture of normal human leukocytes. J Am
1504 Med Assoc *199*, 519-524.
1505 Morton HJ (1970). A survey of commercially available tissue culture media. In Vitro *6*, 89-
1506 108.
1507 Myers MG, Jr., Wang LM, Sun XJ, Zhang Y, Yenush L, Schlessinger J, Pierce JH, and White
1508 MF (1994). Role of IRS-1-GRB-2 complexes in insulin signaling. Mol Cell Biol *14*, 3577-
1509 3587.
1510 Neil JC, Ghysdael J, Vogt PK, and Smart JE (1981). Homologous tyrosine phosphorylation
1511 sites in transformation-specific gene products of distinct avian sarcoma viruses. Nature *291*,
1512 675-677.

1513 Nguyen MTA, Satoh H, Favelyukis S, Babendure JL, Imamura T, Sbodio JI, Zalevsky J,
1514 Dahiyat BI, Chi NW, and Olefsky JM (2005). JNK and tumor necrosis factor-α mediate free
1515 fatty acid-induced insulin resistance in 3T3-L1 adipocytes. J Biol Chem *280*, 35361-35371.
1516 Ohoka N, Yoshii S, Hattori T, Onozaki K, and Hayashi H (2005). *TRB3*, a novel ER stress-
1517 inducible gene, is induced via ATF4-CHOP pathway and is involved in cell death. EMBO J
1518 *24*, 1243-1255.
1519 Olefsky JM (1975). Effect of dexamethasone on insulin binding, glucose transport, and
1520 glucose oxidation of isolated rat adipocytes. J Clin Invest *56*, 1499-1508.
1521 Olefsky JM (1976). Decreased insulin binding to adipocytes and circulating monocytes from
1522 obese subjects. J Clin Invest *57*, 1165-1172.
1523 Olefsky JM, and Kolterman OG (1981). Mechanisms of insulin resistance in obesity and
1524 noninsulin-dependent (type II) diabetes. Am J Med *70*, 151-168.
1525 Olefsky JM, and Reaven GM (1974). Decreased insulin binding to lymphocytes from diabetic
1526 subjects. J Clin Invest *54*, 1323-1328.
1527 Olefsky JM, and Reaven GM (1977). Insulin binding in diabetes. Relationships with plasma
1528 insulin levels and insulin sensitivity. Diabetes *26*, 680-688.
1529 Örd D, and Örd T (2003). Mouse NIPK interacts with ATF4 and affects its transcriptional
1530 activity. Exp Cell Res *286*, 308-320.
1531 Özcan U, Cao Q, Yilmaz E, Lee A-H, Iwakoshi NN, Özdelen E, Tuncman G, Görgün C,
1532 Glimcher LH, and Hotamisligil GS (2004). Endoplasmic reticulum stress links obesity,
1533 insulin action, and type 2 diabetes. Science *306*, 457-461.
1534 Özcan U, Yilmaz E, Özcan L, Furuhashi M, Vaillancourt E, Smith RO, Görgün CZ, and
1535 Hotamisligil GS (2006). Chemical chaperones reduce ER stress and restore glucose
1536 homeostasis in a mouse model of type 2 diabetes. Science *313*, 1137-1140.
1537 Pagano G, Cassader M, and Lenti G (1977). Insulin receptors in adipocytes of non-diabetic
1538 and diabetic subjects. Preliminary report. Acta Diabetol Lat *14*, 164-169.

1539 Panzhinskiy E, Hua Y, Culver B, Ren J, and Nair S (2013). Endoplasmic reticulum stress
1540 upregulates protein tyrosine phosphatase 1B and impairs glucose uptake in cultured
1541 myotubes. Diabetologia *56*, 598-607.
1542 Paton AW, Beddoe T, Thorpe CM, Whisstock JC, Wilce MC, Rossjohn J, Talbot UM, and
1543 Paton JC (2006). AB5 subtilase cytotoxin inactivates the endoplasmic reticulum chaperone
1544 BiP. Nature *443*, 548-552.
1545 Paton AW, Srimanote P, Talbot UM, Wang H, and Paton JC (2004). A new family of potent
1546 AB_5 cytotoxins produced by Shiga toxigenic *Escherichia coli*. J Exp Med *200*, 35-46.
1547 Patschinsky T, Hunter T, Esch FS, Cooper JA, and Sefton BM (1982). Analysis of the
1548 sequence of amino acids surrounding sites of tyrosine phosphorylation. Proc Natl Acad Sci U
1549 S A *79*, 973-977.
1550 Pike LJ, Gallis B, Casnellie JE, Bornstein P, and Krebs EG (1982). Epidermal growth factor
1551 stimulates the phosphorylation of synthetic tyrosine-containing peptides by A431 cell
1552 membranes. Proc Natl Acad Sci U S A *79*, 1443-1447.
1553 Reed BC, Glasted K, and Miller B (1984). Direct comparison of the rates of internalization
1554 and degradation of covalent receptor-insulin complexes in 3T3-L1 adipocytes. Internalization
1555 of occupied receptors is not the rate-limiting step in receptor-hormone complex degradation. J
1556 Biol Chem *259*, 8134-8143.
1557 Reed BC, Kaufmann SH, Mackall JC, Student AK, and Lane MD (1977). Alterations in
1558 insulin binding accompanying differentiation of 3T3-L1 preadipocytes. Proc Natl Acad Sci U
1559 S A *74*, 4876-4880.
1560 Reed BC, and Lane MD (1980). Insulin receptor synthesis and turnover in differentiating
1561 3T3-L1 preadipocytes. Proc Natl Acad Sci U S A *77*, 285-289.
1562 Reed BC, Ronnett GV, Clements PR, and Lane MD (1981a). Regulation of insulin receptor
1563 metabolism. Differentiation-induced alteration of receptor synthesis and degradation. J Biol
1564 Chem *256*, 3917-3925.

Reed BC, Ronnett GV, and Lane MD (1981b). Role of glycosylation and protein synthesis in insulin receptor metabolism by 3T3-L1 mouse adipocytes. Proc Natl Acad Sci U S A *78*, 2908-2912.

Robertson BJ, Moehring JM, and Moehring TJ (1993). Defective processing of the insulin receptor in an endoprotease-deficient Chinese hamster cell strain is corrected by expression of mouse furin. J Biol Chem *268*, 24274-24277.

Robinson TJ, Archer JA, Gambhir KK, Hollis VW, Jr., Carter L, and Bradley C (1979). Erythrocytes: a new cell type for the evaluation of insulin receptor defects in diabetic humans. Science *205*, 200-202.

Rocchi S, Tartare-Deckert S, Mothe I, and Van Obberghen E (1995). Identification by mutation of the tyrosine residues in the insulin receptor substrate-1 affecting association with the tyrosine phosphatase 2C and phosphatidylinositol 3-kinase. Endocrinology *136*, 5291-5297.

Ron E, Shenkman M, Groisman B, Izenshtein Y, Leitman J, and Lederkremer GZ (2011). Bypass of glycan-dependent glycoprotein delivery to ERAD by upregulated EDEM1. Mol Biol Cell *22*, 3945-3954.

Ronnett GV, Knutson VP, Kohanski RA, Simpson TL, and Lane MD (1984). Role of glycosylation in the processing of newly translated insulin proreceptor in 3T3-L1 adipocytes. J Biol Chem *259*, 4566-4575.

Ronnett GV, and Lane MD (1981). Post-translational glycosylation-induced activation of aglycoinsulin receptor accumulated during tunicamycin treatment. J Biol Chem *256*, 4704-4707.

Ronnett GV, Tennekoon G, Knutson VP, and Lane MD (1983). Kinetics of insulin receptor transit to and removal from the plasma membrane. J Biol Chem *258*, 283-290.

Rosen OM, Chia GH, Fung C, and Rubin CS (1979). Tunicamycin-mediated depletion of insulin receptors in 3T3-L1 adipocytes. J Cell Physiol *99*, 37-42.

Rutzky LP, and Pumper RW (1974). Supplement to a survey of commercially available tissue culture media (1970). In Vitro *9*, 468-469.

1593 Saltiel AR, and Kahn CR (2001). Insulin signalling and the regulation of glucose and lipid
1594 metabolism. Nature *414*, 799-806.
1595 Sarbassov DD, Guertin DA, Ali SM, and Sabatini DM (2005). Phosphorylation and
1596 regulation of Akt/PKB by the rictor-mTOR complex. Science *307*, 1098-1101.
1597 Savoie S, Rindress D, Posner BI, and Bergeron JJ (1986). Tunicamycin sensitivity of
1598 prolactin, insulin and epidermal growth factor receptors in rat liver plasmalemma. Mol Cell
1599 Endocrinol *45*, 241-246.
1600 Schneider CA, Rasband WS, and Eliceiri KW (2012). NIH Image to ImageJ: 25 years of
1601 image analysis. Nat Methods *9*, 671-675.
1602 Schröder M, and Friedl P (1997a). Overexpression of recombinant human antithrombin III in
1603 Chinese hamster ovary cells results in malformation and decreased secretion of the
1604 recombinant protein. Biotechnol Bioeng *53*, 547-559.
1605 Schröder M, and Friedl P (1997b). A protein-free solution as replacement for serum in
1606 trypsinization protocols for anchorage-dependent cells. Methods Cell Sci *19*, 137-147.
1607 Schröder M, and Kaufman RJ (2005). The mammalian unfolded protein response. Annu Rev
1608 Biochem *74*, 739-789.
1609 Shapiro SS, and Wilk MB (1965). An analysis of variance test for normality (complete
1610 samples). Biometrika *52*, 591-611.
1611 Sharma NK, Das SK, Mondal AK, Hackney OG, Chu WS, Kern PA, Rasouli N, Spencer HJ,
1612 Yao-Borengasser A, and Elbein SC (2008). Endoplasmic reticulum stress markers are
1613 associated with obesity in non-diabetic subjects. J Clin Endocrinol Metab *93*, 4532-4541.
1614 Shen X, Ellis RE, Lee K, Liu C-Y, Yang K, Solomon A, Yoshida H, Morimoto R, Kurnit
1615 DM, Mori K, and Kaufman RJ (2001). Complementary signaling pathways regulate the
1616 unfolded protein response and are required for *C. elegans* development. Cell *107*, 893-903.
1617 Shi Y, An J, Liang J, Hayes SE, Sandusky GE, Stramm LE, and Yang NN (1999).
1618 Characterization of a mutant pancreatic eIF-2α kinase, PEK, and co-localization with
1619 somatostatin in islet delta cells. J Biol Chem *274*, 5723-5730.

1620 Shi Y, Vattem KM, Sood R, An J, Liang J, Stramm L, and Wek RC (1998). Identification and
1621 characterization of pancreatic eukaryotic initiation factor 2 α-subunit kinase, PEK, involved
1622 in translational control. Mol Cell Biol *18*, 7499-7509.
1623 Shirakami A, Toyonaga T, Tsuruzoe K, Shirotani T, Matsumoto K, Yoshizato K, Kawashima
1624 J, Hirashima Y, Miyamura N, Kahn CR, and Araki E (2002). Heterozygous knockout of the
1625 IRS-1 gene in mice enhances obesity-linked insulin resistance: A possible model for the
1626 development of type 2 diabetes. J Endocrinol *174*, 309-319.
1627 Shoelson SE, Chatterjee S, Chaudhuri M, and White MF (1992). YMXM motifs of IRS-1
1628 define substrate specificity of the insulin receptor kinase. Proc Natl Acad Sci U S A *89*, 2027-
1629 2031.
1630 Šidák Z (1967). Rectangular confidence regions for the means of multivariate normal
1631 distributions. J Am Stat Assoc *62*, 626-633.
1632 Smart JE, Oppermann H, Czernilofsky AP, Purchio AF, Erikson RL, and Bishop JM (1981).
1633 Characterization of sites for tyrosine phosphorylation in the transforming protein of Rous
1634 sarcoma virus (pp60$^{v\text{-}src}$) and its normal cellular homologue (pp60$^{c\text{-}src}$). Proc Natl Acad Sci U
1635 S A *78*, 6013-6017.
1636 Smith PK, Krohn RI, Hermanson GT, Mallia AK, Gartner FH, Provenzano MD, Fujimoto
1637 EK, Goeke NM, Olson BJ, and Klenk DC (1985). Measurement of protein using
1638 bicinchoninic acid. Anal Biochem *150*, 76-85.
1639 Sreejayan N, Dong F, Kandadi MR, Yang X, and Ren J (2008). Chromium alleviates glucose
1640 intolerance, insulin resistance, and hepatic ER stress in obese mice. Obesity (Silver Spring,
1641 Md.) *16*, 1331-1337.
1642 Sun XJ, Crimmins DL, Myers MG, Jr., Miralpeix M, and White MF (1993). Pleiotropic
1643 insulin signals are engaged by multisite phosphorylation of IRS-1. Mol Cell Biol *13*, 7418-
1644 7428.
1645 Sun XJ, Rothenberg P, Kahn CR, Backer JM, Araki E, Wilden PA, Cahill DA, Goldstein BJ,
1646 and White MF (1991). Structure of the insulin receptor substrate IRS-1 defines a unique
1647 signal transduction protein. Nature *352*, 73-77.

1648 Suzuki T, Hiroki A, Watanabe T, Yamashita T, Takei I, and Umezawa K (2001). Potentiation
1649 of insulin-related signal transduction by a novel protein-tyrosine phosphatase inhibitor, Et-
1650 3,4-dephostatin, on cultured 3T3-L1 adipocytes. J Biol Chem *276*, 27511-27518.
1651 Szczepankiewicz BG, Kosogof C, Nelson LT, Liu G, Liu B, Zhao H, Serby MD, Xin Z, Liu
1652 M, Gum RJ, Haasch DL, Wang S, Clampit JE, Johnson EF, Lubben TH, Stashko MA,
1653 Olejniczak ET, Sun C, Dorwin SA, Haskins K, Abad-Zapatero C, Fry EH, Hutchins CW,
1654 Sham HL, Rondinone CM, and Trevillyan JM (2006). Aminopyridine-based c-Jun N-terminal
1655 kinase inhibitors with cellular activity and minimal cross-kinase activity. J Med Chem *49*,
1656 3563-3580.
1657 Talbot UM, Paton JC, and Paton AW (2005). Protective immunization of mice with an active-
1658 site mutant of subtilase cytotoxin of Shiga toxin-producing *Escherichia coli*. Infect Immun
1659 *73*, 4432-4436.
1660 Tang X, Shen H, Chen J, Wang X, Zhang Y, Chen LL, Rukachaisirikul V, Jiang H-l, and
1661 Shen X (2011). Activating transcription factor 6 protects insulin receptor from ER stress-
1662 stimulated desensitization via p42/44 ERK pathway. Acta Pharmacol Sin *32*, 1138-1147.
1663 Termine DJ, Moremen KW, and Sifers RN (2009). The mammalian UPR boosts glycoprotein
1664 ERAD by suppressing the proteolytic downregulation of ER mannosidase I. J Cell Sci *122*,
1665 976-984.
1666 Thastrup O, Cullen PJ, Drøbak BK, Hanley MR, and Dawson AP (1990). Thapsigargin, a
1667 tumor promoter, discharges intracellular Ca^{2+} stores by specific inhibition of the endoplasmic
1668 reticulum Ca^{2+}-ATPase. Proc Natl Acad Sci U S A *87*, 2466-2470.
1669 Tirasophon W, Lee K, Callaghan B, Welihinda A, and Kaufman RJ (2000). The
1670 endoribonuclease activity of mammalian IRE1 autoregulates its mRNA and is required for the
1671 unfolded protein response. Genes Dev *14*, 2725-2736.
1672 Tirasophon W, Welihinda AA, and Kaufman RJ (1998). A stress response pathway from the
1673 endoplasmic reticulum to the nucleus requires a novel bifunctional protein
1674 kinase/endoribonuclease (Ire1p) in mammalian cells. Genes Dev *12*, 1812-1824.

1675 Tournier C, Hess P, Yang DD, Xu J, Turner TK, Nimnual A, Bar-Sagi D, Jones SN, Flavell
1676 RA, and Davis RJ (2000). Requirement of JNK for stress-induced activation of the
1677 cytochrome c-mediated death pathway. Science *288*, 870-874.
1678 Tukey JW (1949a). Comparing individual means in the analysis of variance. Biometrics *5*,
1679 99-114.
1680 Tukey JW (1949b). One degree of freedom for non-additivity. Biometrics *5*, 232-242.
1681 Unger RH, and Foster DW. (1998). Diabetes mellitus. In: Williams Textbook of
1682 Endocrinology, eds. J.D. Wilson, D.W. Foster, H.M. Kronenberg, and P.R. Larsen,
1683 Philadelphia: W. B. Saunders Company, 973-1060.
1684 Urano F, Wang X, Bertolotti A, Zhang Y, Chung P, Harding HP, and Ron D (2000). Coupling
1685 of stress in the ER to activation of JNK protein kinases by transmembrane protein kinase
1686 IRE1. Science *287*, 664-666.
1687 Valverde AM, Mur C, Pons S, Alvarez AM, White MF, Kahn CR, and Benito M (2001).
1688 Association of insulin receptor substrate 1 (IRS-1) y895 with Grb-2 mediates the insulin
1689 signaling involved in IRS-1-deficient brown adipocyte mitogenesis. Mol Cell Biol *21*, 2269-
1690 2280.
1691 Wada I, Rindress D, Cameron PH, Ou WJ, Doherty II JJ, Louvard D, Bell AW, Dignard D,
1692 Thomas DY, and Bergeron JJ (1991). SSRα and associated calnexin are major calcium
1693 binding proteins of the endoplasmic reticulum membrane. J Biol Chem *266*, 19599-19610.
1694 Wald A, and Wolfowitz J (1940). On a test whether two samples are from the same
1695 population. Ann Math Stat *11*, 147-162.
1696 Walter P, and Lingappa VR (1986). Mechanism of protein translocation across the
1697 endoplasmic reticulum membrane. Annu Rev Cell Biol *2*, 499-516.
1698 Walter P, and Ron D (2011). The unfolded protein response: from stress pathway to
1699 homeostatic regulation. Science *334*, 1081-1086.
1700 Wang CC, Sonne O, Hedo JA, Cushman SW, and Simpson IA (1983). Insulin-induced
1701 internalization of the insulin receptor in the isolated rat adipose cell. Detection of the

internalized 138-kilodalton receptor subunit using a photoaffinity ^{125}I-insulin. J Biol Chem *258*, 5129-5134.

Watanabe T, Suzuki T, Umezawa Y, Takeushi T, Otsuka M, and Umezawa K (2000). Structure-activity relationship and rational design of 3,4-dephostatin derivatives as protein tyrosine phosphatase inhibitors. Tetrahedron *56*, 741-752.

Welch BL (1947). The generalisation of student's problems when several different population variances are involved. Biometrika *34*, 28-35.

Werner ED, Lee J, Hansen L, Yuan M, and Shoelson SE (2004). Insulin resistance due to phosphorylation of insulin receptor substrate-1 at serine 302. J Biol Chem *279*, 35298-35305.

Whitehead JP, Molero JC, Clark S, Martin S, Meneilly G, and James DE (2001). The role of Ca^{2+} in insulin-stimulated glucose transport in 3T3-L1 cells. J Biol Chem *276*, 27816-27824.

Wu J, Rutkowski DT, Dubois M, Swathirajan J, Saunders T, Wang J, Song B, Yau GD-Y, and Kaufman RJ (2007). ATF6α optimizes long-term endoplasmic reticulum function to protect cells from chronic stress. Dev Cell *13*, 351-364.

Xu B, Bird VG, and Miller WT (1995). Substrate specificities of the insulin and insulin-like growth factor 1 receptor tyrosine kinase catalytic domains. J Biol Chem *270*, 29825-29830.

Xu L, Spinas GA, and Niessen M (2010). ER stress in adipocytes inhibits insulin signaling, represses lipolysis, and alters the secretion of adipokines without inhibiting glucose transport. Horm Metab Res *42*, 643-651.

Yamamoto K, Sato T, Matsui T, Sato M, Okada T, Yoshida H, Harada A, and Mori K (2007). Transcriptional induction of mammalian ER quality control proteins is mediated by single or combined action of ATF6α and XBP1. Dev Cell *13*, 365-376.

Yang W, Rozamus LW, Narula S, Rollins CT, Yuan R, Andrade LJ, Ram MK, Phillips TB, van Schravendijk MR, Dalgarno D, Clackson T, and Holt DA (2000). Investigating protein-ligand interactions with a mutant FKBP possessing a designed specificity pocket. J Med Chem *43*, 1135-1142.

1728 Ye J, Rawson RB, Komuro R, Chen X, Dave UP, Prywes R, Brown MS, and Goldstein JL
1729 (2000). ER stress induces cleavage of membrane-bound ATF6 by the same proteases that
1730 process SREBPs. Mol Cell *6*, 1355-1364.
1731 Yeh W-C, Shahinian A, Speiser D, Kraunus J, Billia F, Wakeham A, de la Pompa JL, Ferrick
1732 D, Hum B, Iscove N, Ohashi P, Rothe M, Goeddel DV, and Mak TW (1997). Early lethality,
1733 functional NF-κB activation, and increased sensitivity to TNF-induced cell death in TRAF2-
1734 deficient mice. Immunity *7*, 715-725.
1735 Yoshida H, Matsui T, Yamamoto A, Okada T, and Mori K (2001a). XBP1 mRNA is induced
1736 by ATF6 and spliced by IRE1 in response to ER stress to produce a highly active
1737 transcription factor. Cell *107*, 881-891.
1738 Yoshida H, Okada T, Haze K, Yanagi H, Yura T, Negishi M, and Mori K (2000). ATF6
1739 activated by proteolysis binds in the presence of NF-Y (CBF) directly to the *cis*-acting
1740 element responsible for the mammalian unfolded protein response. Mol Cell Biol *20*, 6755-
1741 6767.
1742 Yoshida H, Okada T, Haze K, Yanagi H, Yura T, Negishi M, and Mori K (2001b).
1743 Endoplasmic reticulum stress-induced formation of transcription factor complex ERSF
1744 including NF-Y (CBF) and activating transcription factors 6α and 6β that activates the
1745 mammalian unfolded protein response. Mol Cell Biol *21*, 1239-1248.
1746 Zhang T, Inesta-Vaquera F, Niepel M, Zhang J, Ficarro SB, Machleidt T, Xie T, Marto JA,
1747 Kim N, Sim T, Laughlin JD, Park H, LoGrasso PV, Patricelli M, Nomanbhoy TK, Sorger PK,
1748 Alessi DR, and Gray NS (2012). Discovery of potent and selective covalent inhibitors of
1749 JNK. Chem Biol *19*, 140-154.
1750 Zhou L, Zhang J, Fang Q, Liu M, Liu X, Jia W, Dong LQ, and Liu F (2009). Autophagy-
1751 mediated insulin receptor down-regulation contributes to endoplasmic reticulum stress-
1752 induced insulin resistance. Mol Pharmacol *76*, 596-603.
1753

TABLES

Table 1. siRNAs.

Species	Gene	#	Sequence, sense strand	Sequence, antisense strand
Mus musculus	*INSR*	1	GAGAUCUCCUGGGAUUCAUdTdT	AUGAAUCCCAGGAGAUCUCdTdT
M. musculus	*INSR*	2	CCUUAUCAAGGCCUGUCUAdTdT	UAGACAGGCCUUGAUAAGGdTdT
M. musculus	*INSR*	3	GAAACUCUGCUUGUCUGAAdTdT	UUCAGACAAGCAGAGUUUCdTdT
M. musculus	*TRB3*	1	GGCAGAAGCUGUGUGGAGdTdT	CUCCACACAGGCUUCUGCdTdT
M. musculus	*TRB3*	2	GGACAAUCCCUUUCACAAAdTdT	UUUGUGAAAGGGAUUGUCCdTdT
Aequora victoria	eGFP		GCAAGCUGACCCUGAAGUUCAU	GAACUUCAGGGUCAGCUUGCCG

Table 2. Oligodeoxynucleotides.

Name	Purpose	Sequence
H8962	*TRB3* real time PCR, forward	TTTGGAACGAGAGCAAGGCA
H8963	*TRB3* real time PCR, reverse	CCACATGCTGGTGGGTAGG
H9044	*INSR* real time PCR, forward	CTTCTCTTCCGTGTCTATGG
H0945	*INSR* real time PCR, reverse	GACCATCTCGAAGATAACCA

FIGURE LEGENDS

Figure 1. Acute ER stress does not inhibit phosphorylation of AKT on T308 or S473 in C_2C_{12} myotubes stimulated with 100 nM insulin for 15 min. (A) C_2C_{12} myotubes were serum-starved for 18 h and treated with the indicated concentrations of thapsigargin (Tg), tunicamycin (Tm), 1 μg/ml SubAB, or 1 μg/ml catalytically inactive $SubA_{A272}B$ during the last 1-8 h of serum starvation and then stimulated with 100 nM insulin for 15 min where indicated. Cell lysates were analysed by Western blotting. Quantification of phosphorylation of AKT on (B) T308 and (C) S473. Bars represent standard errors (n = 5 for S473 phosphorylation of AKT at 8 h in unstressed, insulin-stimulated cells, n = 6 for all other unstressed, insulin-stimulated samples, and n = 3 for all other treatments). p values for comparison of ER-stressed samples and samples not stimulated with 100 nM insulin to samples stimulated with 100 nM insulin were calculated by ordinary two-way ANOVA with Dunnett's multiple comparisons test (Dunnett, 1955, 1964). (D) Detection of *XBP1* splicing by reverse transcriptase PCR. PCR products derived from unspliced (u) and spliced (s) *XBP1* mRNA are indicated by arrows. β-Actin (*ACTB*) was used as a loading control. (E-F) Induction of *TRB3* in C_2C_{12} cells by ER stress. C_2C_{12} cells were treated with 300 nM thapsigargin, 1 μg/ml tunicamycin, SubAB (labelled 'WT'), or $SubA_{A272}B$ (labelled 'mt.') for (E) 4 h and (F) 8 h. *TRB3* mRNA levels were determined by reverse transcriptase-qPCR and standardised to the loading control *ACTB*. Bars represent standard errors (n = 2 for the samples treated with thapsigargin or tunicamycin for 8 h, n = 3 for all other samples). p values for comparison of treated samples to the untreated sample ('-') were calculated by ordinary two-way ANOVA with Dunnett's multiple comparisons test taking data shown in Fig. 10F into account. Abbreviations: *ns* – not significant, * or # - $p < 0.05$, ** or ## - $p < 0.01$, *** or ### - $p < 0.001$, and ****or #### - $p < 0.0001$.

Figure 2. Acute ER stress does not inhibit phosphorylation of AKT on S473 stimulated with 10 nM insulin for 15 min. (A) 3T3-F442A cells, (B) C_2C_{12} myotubes, and (C) Hep G2 cells were serum-starved for 18 h and treated with 0.3 μM thapsigargin, 1 μg/ml tunicamycin, 1

μg/ml SubAB, or 1 μg/ml catalytically inactive $SubA_{A272}B$ during the last 30 min of serum starvation and then stimulated with 10 nM insulin for 15 min where indicated. Cell lysates were analysed by Western blotting. Bars represent standard errors (n = 3). p values for comparison of ER-stressed samples and samples not stimulated with 10 nM insulin to samples stimulated with 10 nM insulin were calculated by ordinary two-way ANOVA with Dunnett's multiple comparisons test.

Figure 3. Acute ER stress does not inhibit insulin-stimulated phosphorylation of IRS1 at four specific tyrosine phosphorylation sites in C_2C_{12} myotubes. Tyrosine phosphorylation at (A) Y608, (B) Y628, (C) Y891, and (D) Y935 was analysed by Western blotting. C_2C_{12} myotubes were serum-starved for 18 h before exposure to 1 μM thapsigargin for 10, 20, or 30 min (left side of figure panels) or to 0.1, 1.0, or 10 μg/ml tunicamycin for 30 min (right side of figure panels), followed by stimulation with the indicated concentrations of insulin for 5 min in the continued presence of thapsigargin or tunicamycin. Bars represent standard errors (n = 3). p values for comparison of effects of thapsigargin or tunicamycin within one insulin concentration and for comparison of effects of different insulin concentrations were calculated by ordinary two-way ANOVA with Tukey's multiple comparisons test (Tukey, 1949a). Abbreviation: α-Tub – α-tubulin.

Figure 4. Acute ER stress does not inhibit insulin-stimulated tyrosine phosphorylation of IRS1. Serum-starved cells were exposed to (A) 1 μM thapsigargin or (B) 10 μg/ml tunicamycin for 30 min, followed by stimulation with the indicated concentrations of insulin for 5 min in the continued presence of thapsigargin or tunicamycin. After immunoprecipitation of IRS1, Western blots were probed with an anti-phosphotyrosine ('pY') and an anti-IRS1 antibody. Bars represent standard errors (n = 3 for thapsigargin-treated C_2C_{12} myotubes, n = 4 for thapsigargin-treated 3T3-F442A cells and tunicamycin-treated Hep G2 cells, n = 5 for tunicamycin-treated 3T3-F442A cells and thapsigargin-treated Hep G2 cells, and n = 6 for tunicamycin-treated C_2C_{12} myotubes). p values for comparison of effects of thapsigargin or tunicamycin within one insulin concentration and for comparison of effects

of different insulin concentrations were calculated by ordinary two-way ANOVA with Tukey's multiple comparisons test. For 3T3-F442A cells and Hep G2 cells treated with tunicamycin data were square root transformed before statistical analyses.

Figure 5. ER stress does not elicit IRS1 S307/S312 phosphorylation. (A, B) Serum-starved 3T3-F442A cells, (C, D) C_2C_{12} myotubes, and (E, F) Hep G2 cells were treated with 1 μM thapsigargin or 5 μg/ml anisomycin (ANI) for the indicated times. (A, C, and E) Cell lysates were analysed by Western blotting. (B, D, and F) Quantification of the Western blots shown in panels A, C, and E. Bars represent standard errors (n = 3). p values for comparison of every sample to every other sample were calculated by ordinary one-way ANOVA with Tukey's multiple comparisons test. Anisomycin-treated samples are positive controls in the phospho-S307/S312-IRS1 Western blots.

Figure 6. Depletion of insulin receptors coincides and correlates with decreased AKT S473 phosphorylation in ER-stressed C_2C_{12} myoblasts and suffices to decrease AKT S473 phosphorylation. (A) Serum-starved C_2C_{12} cells were treated with the indicated concentrations of thapsigargin, tunicamycin, 1 μg/ml SubAB or 1 μg/ml $SubA_{A272}B$ for 12 - 24 h before stimulation with 100 nM insulin for 15 min. Cell lysates were analysed by Western blotting for pS473-AKT, total AKT, the insulin receptor (INSR), and GAPDH. Bands representing the α-β proreceptor, the unglycosylated α-β proreceptor, and the β chain of the mature insulin receptor are labelled α-β, α-β – N, and β, respectively. (B) Quantification of the phosphorylation of AKT on S473 ('pS473-AKT') and of the relative abundance of β chains of the insulin receptor ('β chain'). Bars represent standard errors (AKT phosphorylation at S473: n = 6 for cells stimulated with 100 nM insulin at the 12 h time points, n = 7 and n = 9 for the 18 and 24 h time points, for all other samples n = 3 for the 12 h time point, n = 4 for the 18 h time point and n = 5 for the 24 h time point; relative abundance of β chains: n = 9 for cells stimulated with 100 nM insulin at the 12 h time point, n = 10 for the 18 h time point, and n = 12 for the 24 h time point, 12 h: n = 5 for the unstimulated cells and the insulin-stimulated cells treated with 0.1 mM thapsigargin, n = 3 for the cells treated with $SubA_{A272}B$, and n = 4

for all other samples, 18 h: n = 6 for the unstimulated cells, n = 3 for cells treated with $SubA_{A272}B$, and n = 5 for all other samples, 24 h: n = 6 for all samples). Phosphorylation of AKT at S473 and the relative abundance of β chains are expressed relative to unstressed cells that were stimulated with 100 nM insulin for 15 min. p values for comparison of ER-stressed to unstressed samples were calculated using ordinary two-way ANOVA with Dunnett's multiple comparisons test on the original data for AKT phosphorylation at S473 and square root-transformed data for the relative abundance of β chains. (C) Correlation of insulin-stimulated AKT phosphorylation with insulin receptor β chains (r^2 = 0.80, two-tailed p < 0.0001 for a significantly non-zero slope, and p > 0.05 for deviation from linearity calculated by a runs test, n = 27). Dotted lines represent the 95% confidence interval of the linear regression line. The relative phosphorylation of AKT at S473 shown in panel (B) was plotted against the relative abundance of β chains shown in panel (B). (D) Steady-state *INSR* mRNA levels in C_2C_{12} cells transfected with 50 nM of the indicated siRNAs for 24, 48, or 72 h. Bars represent standard errors (n = 3). p values for comparison of cells transfected with the three *INSR* siRNAs to the cells transfected with the eGFP siRNA were calculated with an ordinary two-way ANOVA with Tukey's multiple comparisons test. Differences in *INSR* mRNA levels between different *INSR* siRNAs within individual time points or between different time points for individual siRNAs are not significant. (E) siRNA-mediated knock-down of expression of the insulin receptor inhibits insulin-stimulated phosphorylation of AKT. Serum-starved C_2C_{12} cells were stimulated with insulin 48 h after transfection of 50 nM of the indicated siRNAs. Two unspecific bands are marked with an asterisk ('*').

Figure 7. Inhibition of insulin receptor synthesis at the transcriptional or translational level cannot fully account for decreased insulin-stimulated AKT S473 phosphorylation. (A) *INSR* mRNA levels measured by reverse transcriptase-qPCR in C_2C_{12} cells treated with 300 nM thapsigargin, 1 μg/ml tunicamycin, or 1 μg/ml SubAB for 24 h. Bars represent standard errors (n = 3). p values for comparison of ER-stressed samples to unstressed samples were calculated using ordinary one-way ANOVA with Dunnett's multiple comparisons test. (B-D) Protein synthesis rates in (B) 3T3-F442A (n = 8), (C) C_2C_{12} (n = 8), and (D) Hep G2 cells (n

= 4) treated with 0.1 μM thapsigargin or 0.1 μg/ml tunicamycin for 24 h measured by incorporation of [^{35}S]-L-methionine into protein. Protein synthesis rates were determined as TCA-precipitable counts standardised to total protein. Bars represent standard errors. *p* values were calculated by ordinary one-way ANOVA with Tukey's multiple comparisons test. (E) Protein synthesis rates in cells treated for 24 h with 0.1 μM thapsigargin or 0.1 μg/ml tunicamycin measured by storage phosphor analysis of [^{35}S]-L-methionine incorporation into protein. For each cell line the storage phosphor image of the SDS-PAGE gel is shown to the left, and an image of the Coomassie Brilliant Blue R250-stained gel is shown to the right. Quantification of [^{35}S]-L-methionine incorporation into protein, expressed as the volume of the ^{35}S storage phosphor signal relative to the Coomassie Brilliant Blue R250 staining intensity is shown in the bar graphs below the gel images. Bars represent standard errors (*n* = 8). *p* values were calculated by ordinary one-way ANOVA with Tukey's multiple comparisons test. (F) Phosphorylation of eIF2α at S51 in 3T3-F442A cells (*n* = 13 for 0.5 h and *n* = 12 for 24 h), C_2C_{12} cells (*n* = 21), and Hep G2 cells (*n* = 13 for 0.5 h and *n* = 8 for 24 h) exposed for 0.5 or 24 h to 0.1 μg/ml tunicamycin or 0.1 μM thapsigargin. The treatment with 0.1 μM thapsigargin for 0.5 h is a positive control for the pS51-eIF2α Western blots. Bars represent standard errors. For 3T3-F442A cells, *p* values were calculated by Welch's ANOVA with Dunnett's T3 multiple comparisons test. For C_2C_{12} and Hep G2 cells, *p* were calculated by a Kruskal-Wallis test with Dunn's multiple comparisons test. (G) Immunoprecipitation of the insulin receptor after a 1 h label with [^{35}S]-L-methionine in 3T3-F442A cells. Thapsigargin was used at 0.1 μM and tunicamycin at 0.1 μg/ml. Abbreviations: Mock – immunoprecipitation with non-immune IgG. 1st – immunoprecipitation of the insulin receptor after an 8 h labelling period. 2nd – immunoprecipitation of insulin receptors remaining in the supernate of the 1st immunoprecipitation. #1, #2, and #3 indicate three biological repeats. (H) Quantification of newly synthesised α-β proreceptors in 3T3-F442A cells (left) and Hep G2 cells (right). Bars represent standard errors (*n* = 3). *p* values were calculated by ordinary one-way ANOVA with Tukey's multiple comparisons test.

Figure 8. ER stress does not increase turnover of insulin receptors at the cell surface. (A, C, and E) Pull-down of cell surface proteins with streptavidin-agarose after biotinylation with the cell-impermeable biotinylation reagent sulphosuccinimidyl-6-(biotinamido)hexanoate from (A) 3T3-F442A, (C) C_2C_{12}, and (E) Hep G2 cells. Cell extracts were prepared 0 – 72 h after labelling of cell surface proteins. Biotinylated proteins were isolated with streptavidin-agarose, separated by SDS-PAGE, and Western-blotted for the insulin receptor and GAPDH. '-' refers to a pull-down reaction with unlabelled cell lysates. The arrows indicate that the supernate of the pull-down reaction with the labelled 0 h sample was subjected to a second pull-down with streptavidin-agarose. The lanes labelled 'Input' serve as a positive control for the GAPDH Western blots on precipitates of the streptavidin-agarose pull down reactions and themselves were not subjected to pull-down with streptavidin-agarose. The rows labelled 'Input' show Western blots for GAPDH on equal amounts of input protein for the streptavidin-agarose pull-down assays. The graphs show plots of the natural logarithm of the abundance of biotinylated insulin receptors over time, the line of linear regression (uninterrupted line), and the 95% confidence interval of the line of linear regression (dotted lines). (B, D, and F) Comparison of the half-life, $t_{1/2}$, of the insulin receptor at the cell surface of (B) 3T3-F442A (n = 3), (D) C_2C_{12} (n = 3), and (F) Hep G2 (untreated n= 7, 0.3 μM thapsigargin n = 8, and 1 μg/ml tunicamycin and SubAB n = 5) cells. Half-lives were calculated from the slopes of linear regression lines obtained from plots of the natural logarithm of the abundance of biotinylated insulin receptors over time. Bars represent standard errors. p values were calculated by ordinary one-way ANOVA with Tukey's multiple comparisons test.

Figure 9. Unprocessed α-β proreceptors accumulate in the ER of ER-stressed cells. (A) Quantification of the relative abundance of α-β precursors of the insulin receptor in C_2C_{12} cells exposed to the indicated concentrations of thapsigargin, tunicamycin, 1 μg/ml SubAB, or $SubA_{A272}B$ for 24 h. Bars represent standard errors (n = 12 for unstressed, insulin-stimulated cells, n = 5 for the samples treated with 0.3 μM thapsigargin and $SubA_{A272}B$, and n = 6 for all other samples). p values for comparison of ER-stressed samples and samples not stimulated

with 100 nM insulin to the sample stimulated with 100 nM insulin were calculated using ordinary two-way ANOVA with Dunnett's multiple comparisons test including data for 12 h (n = 8 for unstressed, insulin-stimulated cells, n = 4 for all other samples) and 18 h (n = 10 for unstressed, insulin-stimulated cells, n = 5 for all other samples) time points. (B) Endo H digest of cell lysates prepared from C_2C_{12} cells exposed to 1 μg/ml SubAB, 0.3 μM thapsigargin, or 1 μg/ml tunicamycin. (C) Quantification of the relative abundance of β chains and α-β proreceptors from panel B. (D) The mature β chain of the insulin receptor carries Endo H sensitive *N*-linked oligosaccharides. Endo H and PNGase F digests of unstressed C_2C_{12} cells were immunoblotted for the β chain of the insulin receptor. '#' indicates an unspecific band. (E) Steady-state insulin receptor levels in untreated HEK 293 cells or HEK 293 cells treated for 18 h with 0.1 μg/ml tunicamycin, 1 μg/ml SubAB or $SubA_{A272}B$. (F) MTT activity of untreated HEK 293 cells and HEK 293 exposed for 18 h to 300 nM thapsigargin, 1 μg/ml tunicamycin, or 1 μg/ml SubAB. Bars represent standard errors (n = 3). p values for comparison of treated samples to the untreated sample were calculated by ordinary one-way ANOVA with Dunnett's multiple comparisons test. (G) Localisation of GFP-tagged insulin receptors in transiently transfected HEK 293 cells after 18 h treatment with 1 μg/ml tunicamycin or 1 μg/ml SubAB. Scale bar - 10 μm. (H) Average Pearson's correlation coefficient r_{obs} between the GFP-tagged insulin receptor and CellMask Deep Red fluorescence determined from eleven randomly chosen cells. Bars represent standard errors (n = 10 for tunicamycin-treated samples and n = 11 for all other samples). p values for comparison of the treated to the untreated samples were calculated with an ordinary two-way ANOVA using Tukey's multiple comparisons test on arcsine-transformed data. The Pearson correlation coefficients for the randomised images are -0.13 ± 0.08, -0.13 ± 0.07, and -0.33 ± 0.07 for the untreated, tunicamycin-, and SubAB-treated cells and are significantly different (p < 0.001, calculated with a two-way ANOVA using Šidák's correction for multiple comparisons (Šidák, 1967) on arcsine-transformed data) from the corresponding Pearson correlation coefficients for the non-randomised images.

Figure 10. Bypass of the ER in insulin receptor synthesis abrogates ER stress-induced insulin resistance. (A) Schematic of the WT insulin receptor, the myristoylated F_V2E-insulin receptor chimera, and activation of the chimera by AP20187. Black boxes represent the signal peptide sequence and transmembrane domain of the insulin preproreceptor, striped boxes the protein tyrosine kinase domain of the insulin receptor, and checkered boxes individual F_V domains. Disulphide bonds that link α to β chains and two insulin receptor monomers are shown as grey lines. Abbreviations: M, Myr – myristoylation signal. (B) Autophosphorylation of the F_V2E-insulin receptor chimera in stably transfected Flp-In T-Rex 293 cells. Expression of the chimera was induced for 27 h with 1 μg/ml tetracycline, followed by dimerisation of the chimera with 100 nM AP20187 for 1 or 4 h. (C) C_2C_{12} cells were transiently transfected with pmaxGFP or pcDNA5/FRT/TO-MyrF_V2E-INSR. 24 h after transfection, ER stress was induced for 24 h with 0.1 μM thapsigargin, 0.1 μg/ml tunicamycin, or 1 μg/ml SubAB followed by dimerisation of the receptor chimera with 100 nM AP20187 for 4 h. '#' indicates an unspecific band. Quantification of (D) S473 AKT phosphorylation and (E) the relative abundance of α-β proreceptors in panel C. Bars represent standard errors (n = 3-4). p values for comparison of the treated to the untreated samples were calculated by ordinary one-way ANOVA using Dunnett's multiple comparisons test. (F) Induction of *TRB3* in C_2C_{12} cells by ER stress. C_2C_{12} cells were treated with 300 nM thapsigargin, 1 μg/ml tunicamycin, SubAB, or SubA_{A272}B for 24 h. *TRB3* mRNA levels were determined by reverse transcriptase-qPCR and standardised to the loading control *ACTB*. Bars represent standard errors (n = 3). p values for comparison of treated samples to the untreated sample ("-") were calculated by ordinary two-way ANOVA with Dunnett's multiple comparisons test taking data shown in Figures 1E and 1F into account.

Figure 11. JNKs are not required for insulin resistance in ER-stressed cells. (A) Activation of JNK in Hep G2 cells exposed to different concentrations of thapsigargin, but not tunicamycin or SubAB, for 18 – 36 h. The arrows indicate the p46 and p54 isoforms of JNKs, the three lines phosphorylated species of p38, p42, and p44 MAP kinases. Bars represent standard errors (n = 3). p values for comparison of treated samples to the untreated sample ('-') were

calculated by ordinary two-way ANOVA with Tukey's multiple comparisons test. (B) JNKi VIII and XVI inhibit phosphorylation of c-Jun at S63 in Hep G2 cells exposed to the indicated concentrations of thapsigargin for 36 h. Hep G2 cells were treated with 8 μM JNKi VIII or XVI for 0.5 h before exposure to thapsigargin in the presence of 8 μM JNKi VIII or XVI or no JNK inhibitor ('-') for 36 h. The bar graphs show S63 phosphorylation of c-Jun standardised to c-Jun levels, and c-Jun levels standardised the GAPDH levels. Bars represent standard errors (n = 3). p values were calculated by ordinary two-way ANOVA with Tukey's multiple comparisons test on square root or arctangent-transformed data, respectively. (C-E) JNKi VIII and XVI do not reverse inhibition of insulin-stimulated phosphorylation of AKT at S473 by thapsigargin in Hep G2 cells. Hep G2 cells were treated for 0.5 h with 8 μM JNKi VIII or XVI, followed by exposure to the indicated concentrations of thapsigargin in the presence of 8 μM JNKi VIII or XVI or no JNK inhibitor ('-') for 36 h. Cells were serum-starved in the last 18 h of thapsigargin treatment and then stimulated with 10 nM or 100 nM insulin for 15 min in the continued presence of thapsigargin and JNK inhibitors, were applicable. (C) Western blots for pS473-AKT, AKT, and GAPDH. (D) Quantification of the Western blots in panel (C). Bars represent standard errors (n = 3). p values were calculated by ordinary two-way ANOVA with Dunnett's multiple comparisons test. (E) Reanalysis of the data in panel D after normalisation of data for each condition of JNK inhibition to the insulin-stimulated sample not exposed to thapsigargin for the corresponding condition. p values were calculated by ordinary two-way ANOVA with Dunnett's multiple comparisons test. (F) JNKi VIII and XVI do not restore levels of insulin receptor β chains or restore processing of α- β proreceptors to levels of untreated cells. Hep G2 cells were treated with 8 μM JNKi VIII or XVI for 0.5 h before exposure to thapsigargin in the presence of 8 μM JNKi VIII or XVI or no JNK inhibitor ('-') for 36 h. Bars represent standard errors (n = 3 for β chains and n = 4 for α-β proreceptors). p values were calculated by ordinary two-way ANOVA with Tukey's multiple comparisons test.

Figure 12. JNK1 and JNK2 are not required for development of insulin resistance in ER-stressed cells. (A) Serum-starved WT and (B) *jnk1*$^{-/-}$ *jnk2*$^{-/-}$ MEFs were treated for 24 h with

the indicated concentrations of thapsigargin, tunicamycin, 1 μg/ml SubAB, or 1 μg/ml $SubA_{A272}B$ before stimulation with 100 nM insulin for 15 min. (C) Quantification of phosphorylation of AKT on S473 relative to total AKT levels in WT and *jnk1*$^{-/-}$ *jnk2*$^{-/-}$ MEFs exposed to thapsigargin, tunicamycin, and 1 μg/ml SubAB or $SubA_{A272}B$. Bars represent standard errors (n = 12 for unstressed, insulin-stimulated WT MEFs, n = 10 for unstressed, insulin-stimulated *jnk1*$^{-/-}$ *jnk2*$^{-/-}$ MEFs, n = 6 for all other samples for WT MEFs, and n = 5 for all other samples for *jnk1*$^{-/-}$ *jnk2*$^{-/-}$ MEFs). p values for comparison of the relative AKT S473 phosphorylation between WT and *jnk1*$^{-/-}$ *jnk2*$^{-/-}$ MEFs were calculated using ordinary two-way ANOVA with Šidák's correction for multiple comparisons. p values for comparison of ER-stressed samples and samples not stimulated with 100 nM insulin to samples stimulated with 100 nM insulin were calculated using ordinary two-way ANOVA with Dunnett's multiple comparisons test. (D) Activation of JNK in serum-starved WT MEFs exposed to the indicated concentrations of thapsigargin or tunicamycin, 1 μg/ml SubAB, or $SubA_{A272}B$ for 24 h before stimulation with 100 nM insulin for 15 min. (E) Quantification of the Western blots in panel D. Bars represent standard errors (n = 8 for insulin-stimulated cells, n = 4 for all other samples). p values for comparison of ER-stressed samples and samples not stimulated with 100 nM insulin to samples stimulated with 100 nM insulin were calculated using ordinary one-way ANOVA with Dunnett's multiple comparisons test. (F) JNK deficiency does not protect from the effects of ER stress on insulin receptor processing in the secretory pathway. The relative abundance of α-β proreceptors was determined by Western blotting of lysates of serum-starved WT and *jnk1*$^{-/-}$ *jnk2*$^{-/-}$ MEFs exposed for 24 h to the indicated concentrations of thapsigargin, tunicamycin, and 1 μg/ml SubAB or $SubA_{A272}B$ followed by stimulation with 100 nM insulin for 15 min where indicated. Bars represent standard errors (n = 4 for unstressed, insulin-stimulated cells, n = 2 for all other samples). p values for comparison of the relative abundance of α-β proreceptors between WT and *jnk1*$^{-/-}$ *jnk2*$^{-/-}$ MEFs were calculated by Welch's test (Welch, 1947) followed by a Games-Howell *post hoc* test (Games and Howell, 1976). p values for comparisons of treatments were calculated by ordinary two-way ANOVA with Dunnett's multiple comparisons test.

Figure 13. TRB3 is not required for development of insulin resistance in ER-stressed C_2C_{12} cells. (A) siRNA-mediated knock-down of *TRB3* at the mRNA level 48 h after transfection of C_2C_{12} cells with 50 nM of the indicated siRNAs. *TRB3* mRNA was determined by reverse transcriptase-qPCR and normalised to *ACTB*. Bars represent the standard error from three technical replicates. *p* values were calculated by ordinary one-way ANOVA with Dunnett's multiple comparisons test. (B) siRNA-mediated knock-down of TRB3 at the protein level 48 and 72 h after transfection of C_2C_{12} cells with 50 nM of the indicated siRNAs. (C) 24 h after transfection with the indicated siRNAs C_2C_{12} cells were exposed to 300 μM thapsigargin, 1 μg/ml tunicamycin or SubAB for 24 h and serum-starved during the last 18 h of exposure to ER stressors before being stimulated with 100 nM insulin for 15 min. Phosphorylation of AKT at S473 and insulin receptors were analysed by Western blotting. (D) Quantification of the relative phosphorylation of AKT at S473 in the Western blots of panel C. Bars represent standard errors (n = 5 for cells transfected with siRNAs against eGFP, n = 3 for all other samples). *p* values were calculated by ordinary two-way ANOVA with Dunnett's correction for multiple comparisons. (E) Quantification of the relative abundance of α-β proreceptors in the Western blots of panel C. Bars represent standard errors (n = 6 for cells transfected with siRNAs against eGFP, n = 3 for all other samples). *p* values were calculated by ordinary two-way ANOVA with Dunnett's multiple comparisons test to compare of samples to the insulin-stimulated, unstressed sample and Tukey's multiple comparisons test to compare different siRNAs.

Figure 14. ER stress decreases insulin sensitivity by decreasing the plasma membrane population of the insulin receptor. (A) Inhibition of insulin signalling by ER stress requires transport of newly synthesised insulin receptors from the ER to the cell surface. The signal peptide sequence targets ribosomes translating the insulin receptor mRNA to the ER, where the newly synthesised polypeptide chain folds into molecules with insulin binding activity. ER stress interferes with folding of newly synthesised insulin receptor molecules, preventing its transport to the Golgi complex. The Myr-F_V2E-insulin receptor chimera is not affected by ER stress because it is translated by cytoplasmic ribosomes and folds in the cytosol into active

molecules thus bypassing the ER. Abbreviation: TGN – *trans*-Golgi network. (B and C) Modelling of the response to insulin as a function of insulin and insulin receptor concentration. The response to insulin, R, is defined by the equation $R = R_{max} \cdot [INS \cdot INSR]/(K_E + [INS \cdot INSR])$, with K_E – concentration of insulin (INS)-insulin receptor (INSR) complexes at which $R = 0.5 \cdot R_{max}$, and R_{max} – maximal response to insulin. The concentration of insulin-insulin receptor complexes is calculated from the equilibrium INS + INSR ↔ INS·INSR considering only high affinity binding of insulin to the insulin receptor with a dissociation constant of 200 pM (Bass et al., 1996). K_E varies widely for different physiological responses to insulin (Gammeltoft and Gliemann, 1973; Hofmann et al., 1980; Crettaz and Kahn, 1984) and has been assumed to be equal to 1 pM for illustrative purposes only. Numbers represent the half-lives of the insulin receptor at the cell surface that have elapsed since ER stress was induced.

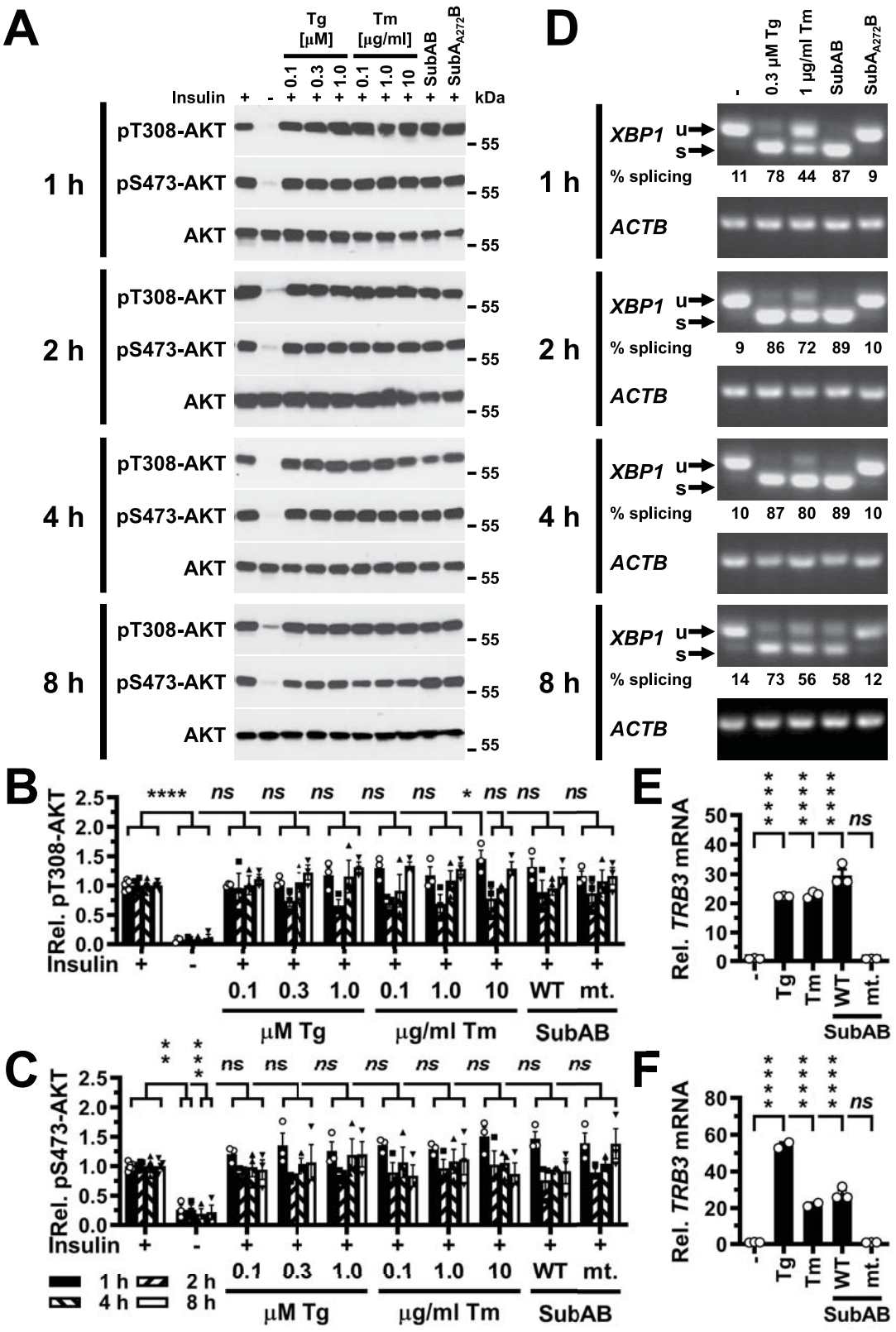
A
Tg [µM]
Tm [µg/ml]
SubAB
SubA$_{A272}$B
Insulin
kDa
1 h
2 h
4 h
8 h
pT308-AKT
pS473-AKT
AKT
55
D
0.3 µM Tg
1 µg/ml Tm
XBP1
u
s
% splicing
ACTB
B
Rel. pT308-AKT
C
Rel. pS473-AKT
µM Tg
µg/ml Tm
SubAB
WT
mt.
E
Rel. TRB3 mRNA
Tg
Tm
F
ns

Figure 1

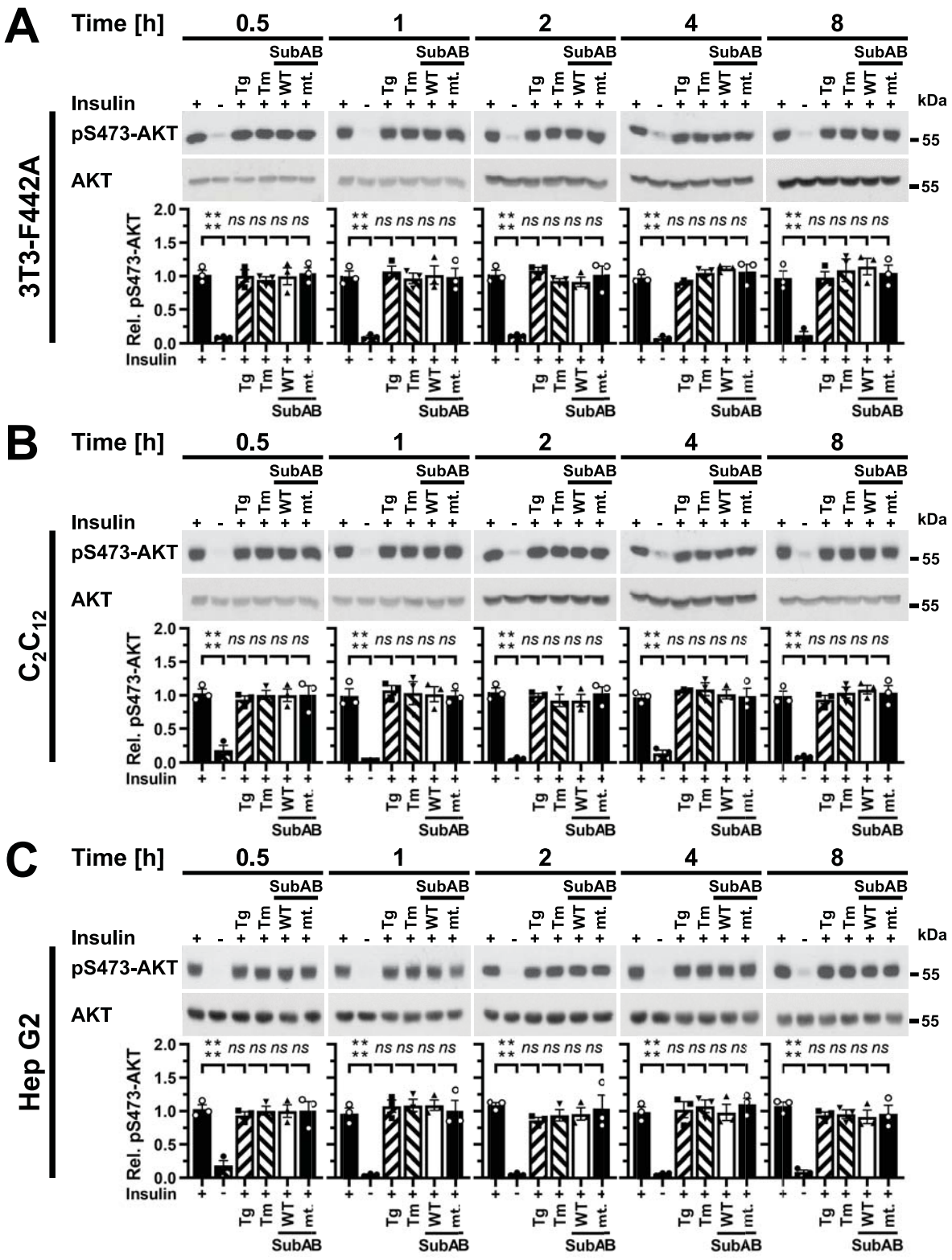
A
B
C
Time [h]
0.5
1
2
4
8
SubAB
Insulin
+ - + Tg + Tm + WT + mt.
kDa
3T3-F442A
C2C12
Hep G2
pS473-AKT
AKT
55
Rel. pS473-AKT
2.0
1.5
1.0
0.5
0.0
** ** ns ns ns ns

Figure 2

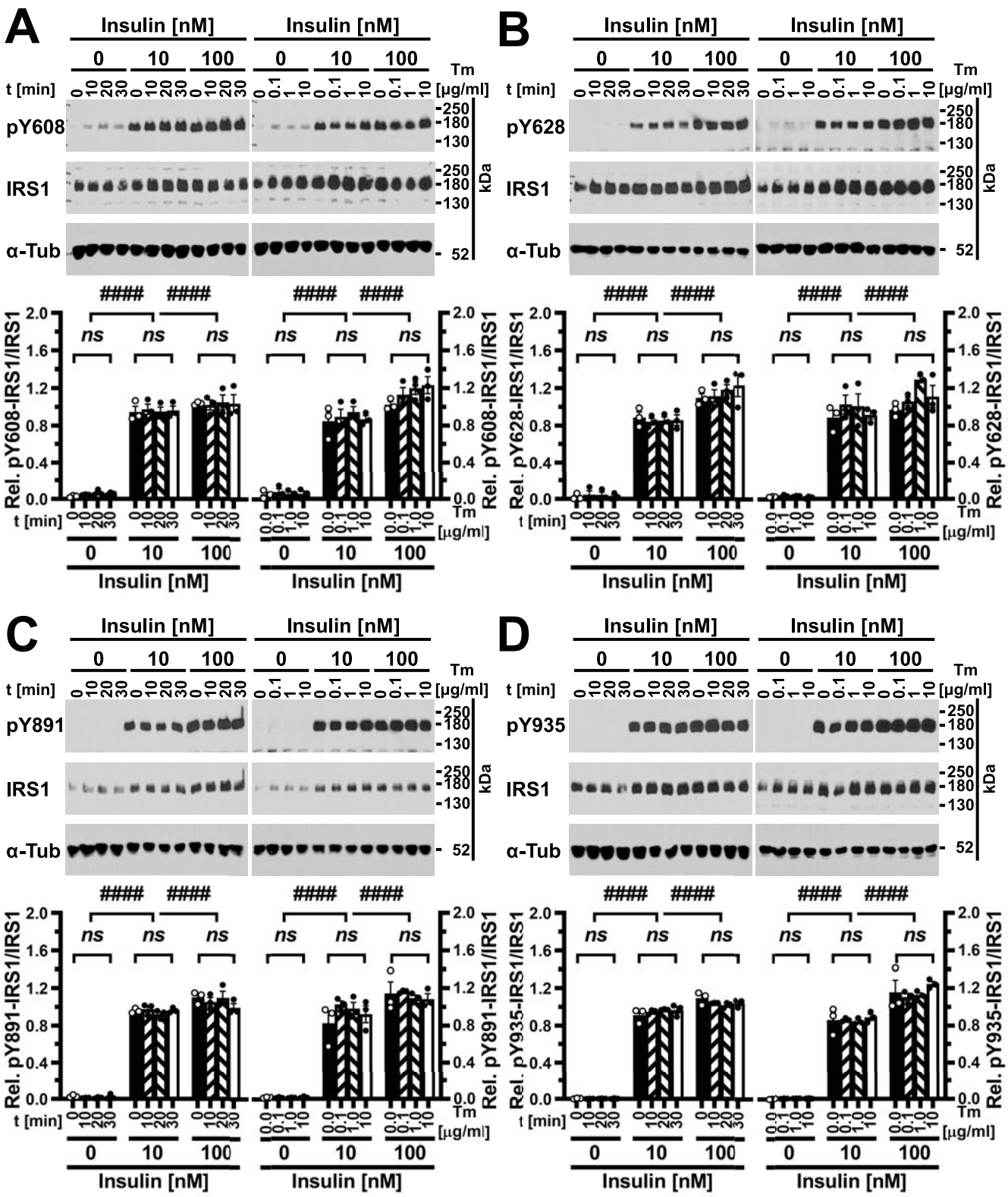
A
B
C
D
Insulin [nM]
0
10
100
t [min]
Tm
[µg/ml]
pY608
pY628
pY891
pY935
IRS1
α-Tub
kDa
250
180
130
52
Rel. pY608-IRS1/IRS1
Rel. pY628-IRS1/IRS1
Rel. pY891-IRS1/IRS1
Rel. pY935-IRS1/IRS1
####
ns

Figure 3

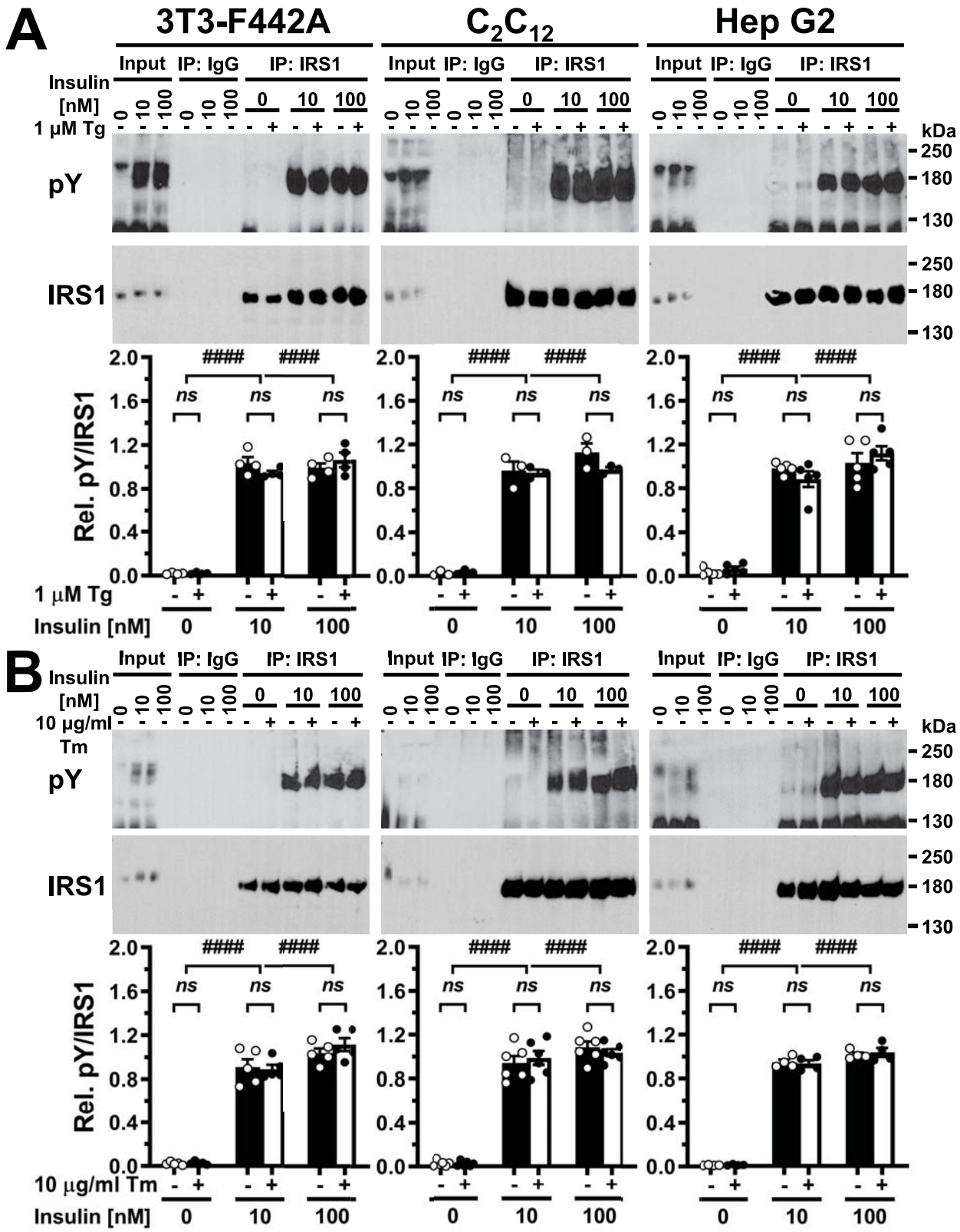
A
3T3-F442A
C2C12
Hep G2
Input
IP: IgG
IP: IRS1
Insulin [nM]
0
10
100
1 μM Tg
pY
IRS1
kDa
250
180
130
Rel. pY/IRS1
####
ns
2.0
1.6
1.2
0.8
0.4
0.0
B
10 μg/ml Tm

Figure 4

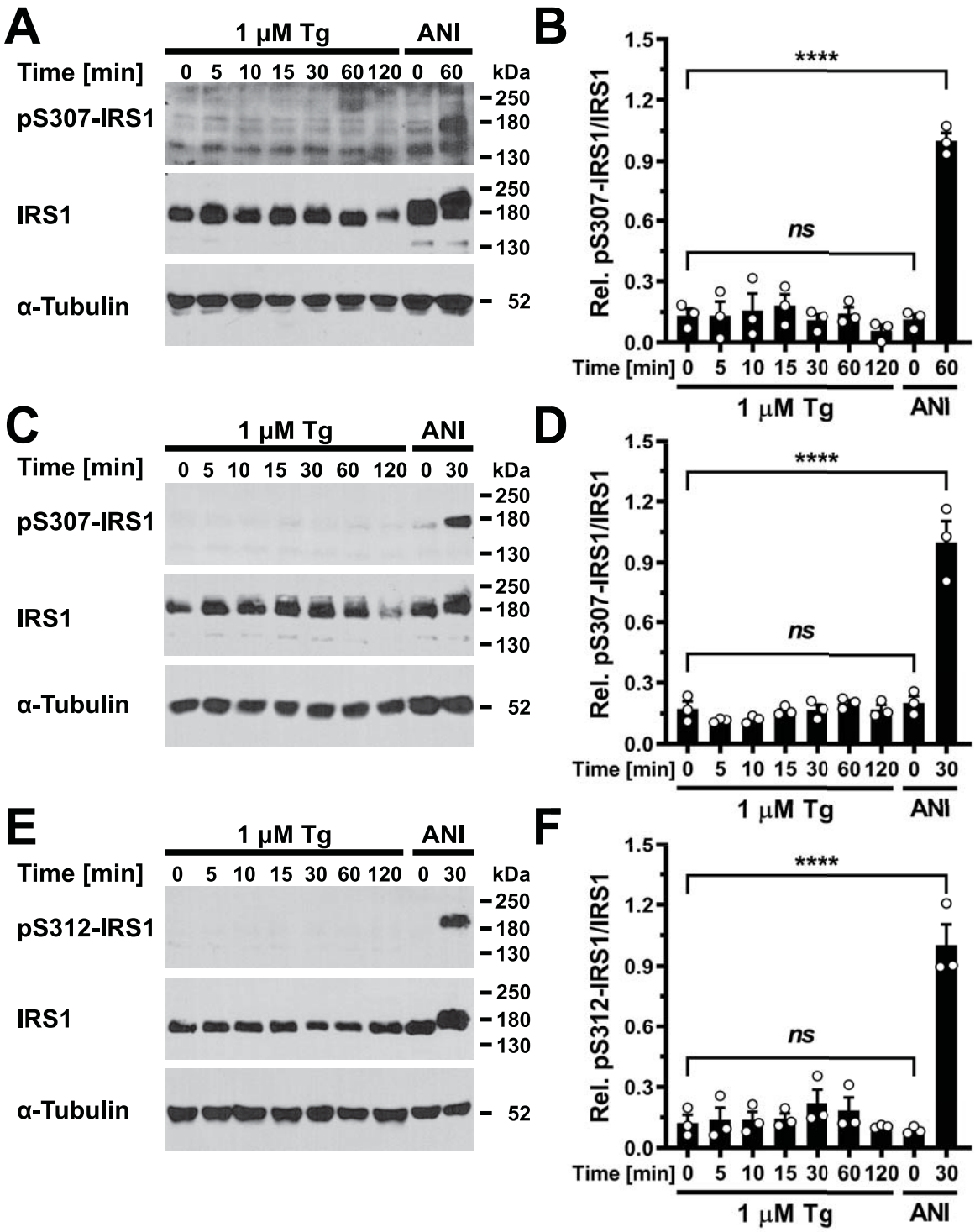
A
1 μM Tg
ANI
Time [min]
0 5 10 15 30 60 120 0 60
kDa
pS307-IRS1
IRS1
α-Tubulin
250
180
130
52
B
Rel. pS307-IRS1/IRS1
****
ns
1 μM Tg
ANI
C
0 5 10 15 30 60 120 0 30
D
E
pS312-IRS1
F
Rel. pS312-IRS1/IRS1

Figure 5

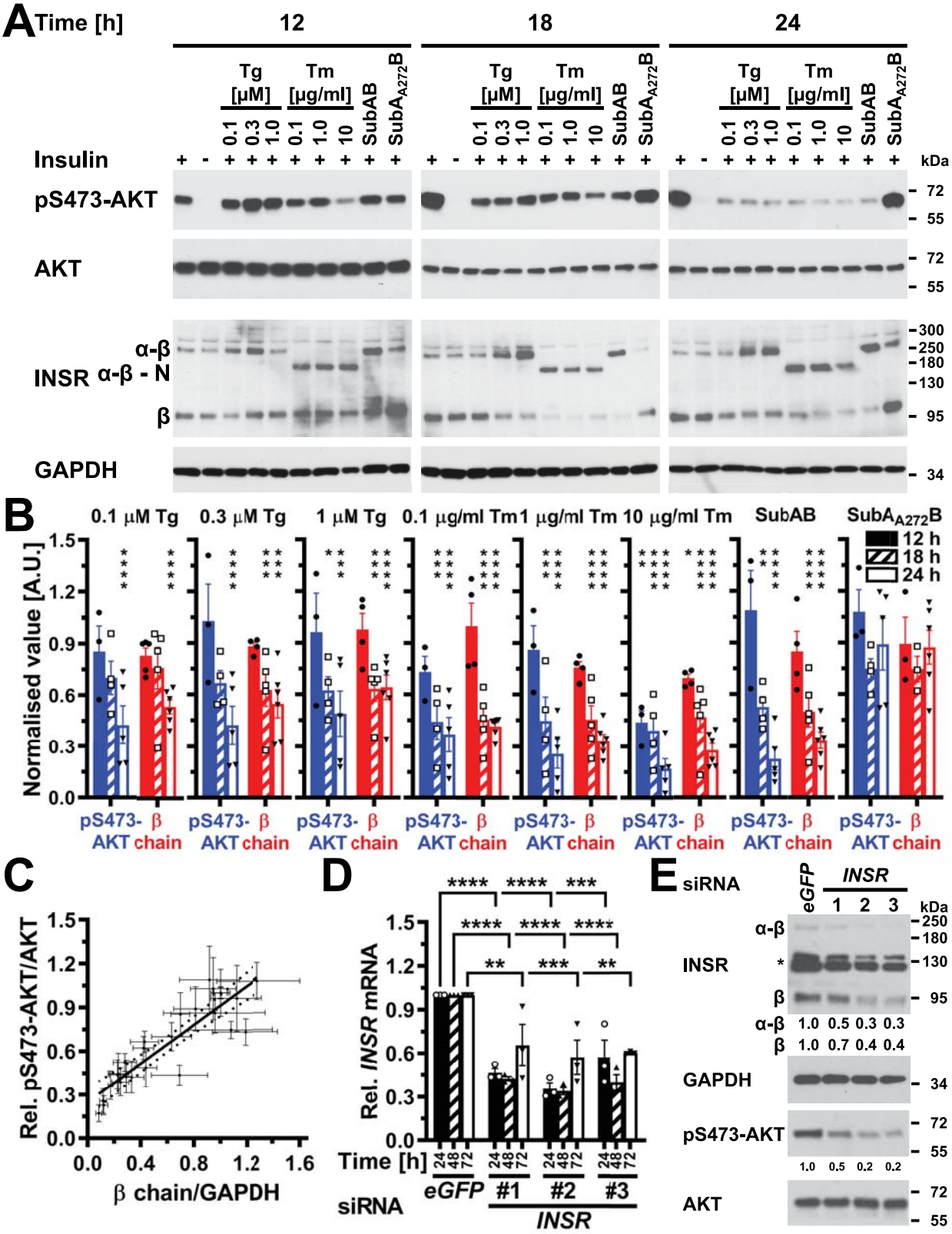
A
Time [h]
12
18
24
Tg [µM]
Tm [µg/ml]
0.1
0.3
1.0
0.1
1.0
10
SubAB
SubA272B
Insulin
kDa
pS473-AKT
AKT
INSR
α-β
α-β - N
β
GAPDH
72
55
300
250
180
130
95
34
B
0.1 µM Tg
0.3 µM Tg
1 µM Tg
0.1 µg/ml Tm
1 µg/ml Tm
10 µg/ml Tm
SubAB
SubA272B
12 h
18 h
24 h
Normalised value [A.U.]
pS473-AKT
β chain
C
Rel. pS473-AKT/AKT
β chain/GAPDH
D
Rel. INSR mRNA
Time [h]
siRNA
eGFP
#1
#2
#3
INSR
E
siRNA
eGFP
INSR
1
2
3
α-β
INSR
β
α-β 1.0 0.5 0.3 0.3
β 1.0 0.7 0.4 0.4
GAPDH
pS473-AKT
1.0 0.5 0.2 0.2
AKT

Figure 6

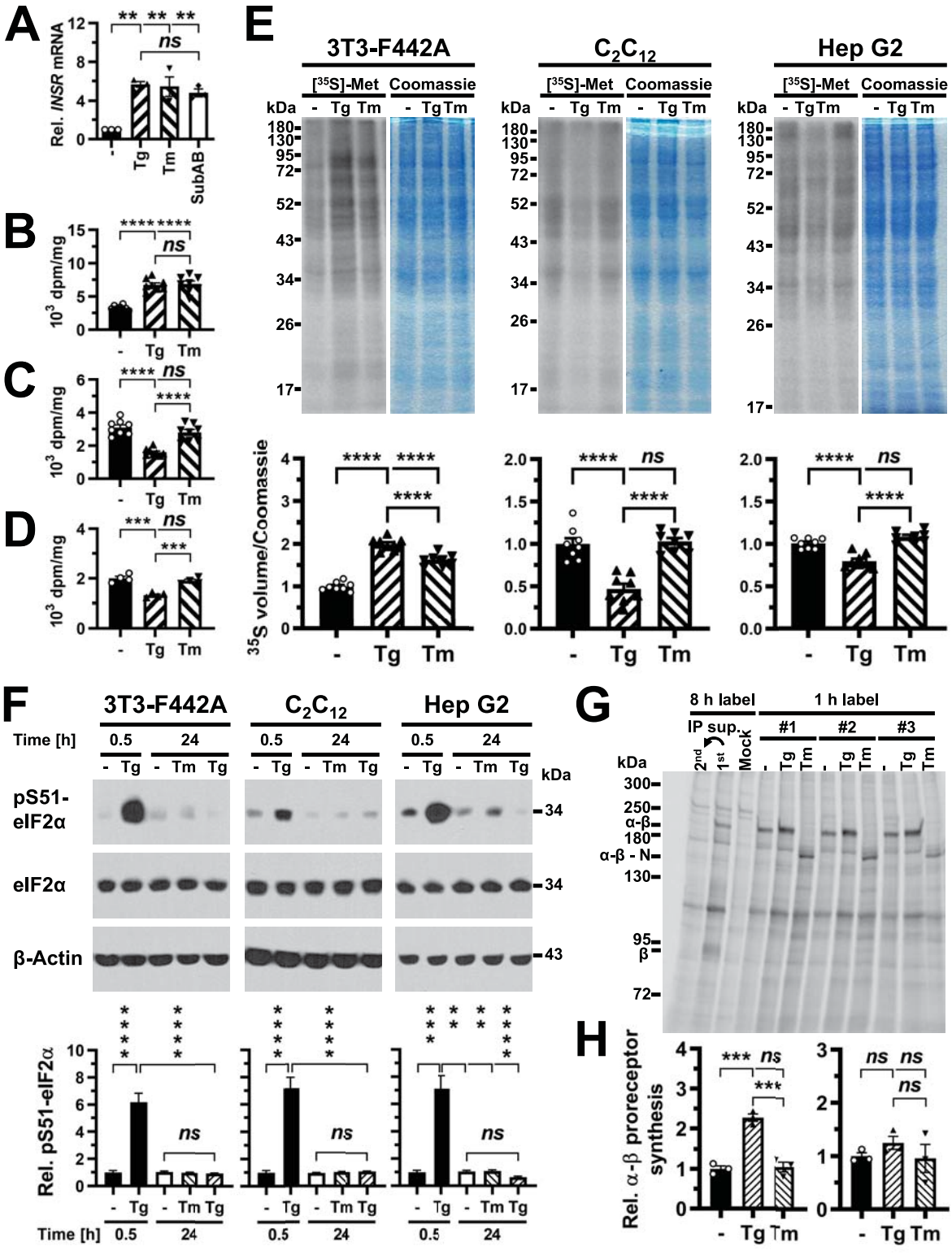
A
Rel. INSR mRNA
B
10³ dpm/mg
C
10³ dpm/mg
D
10³ dpm/mg
E
3T3-F442A
C2C12
Hep G2
[35S]-Met
Coomassie
kDa
35S volume/Coomassie
F
3T3-F442A
C2C12
Hep G2
Time [h]
pS51-eIF2α
eIF2α
β-Actin
Rel. pS51-eIF2α
G
8 h label
1 h label
IP sup.
Mock
#1
#2
#3
α-β
α-β - N
β
H
Rel. α-β proreceptor synthesis

Figure 7

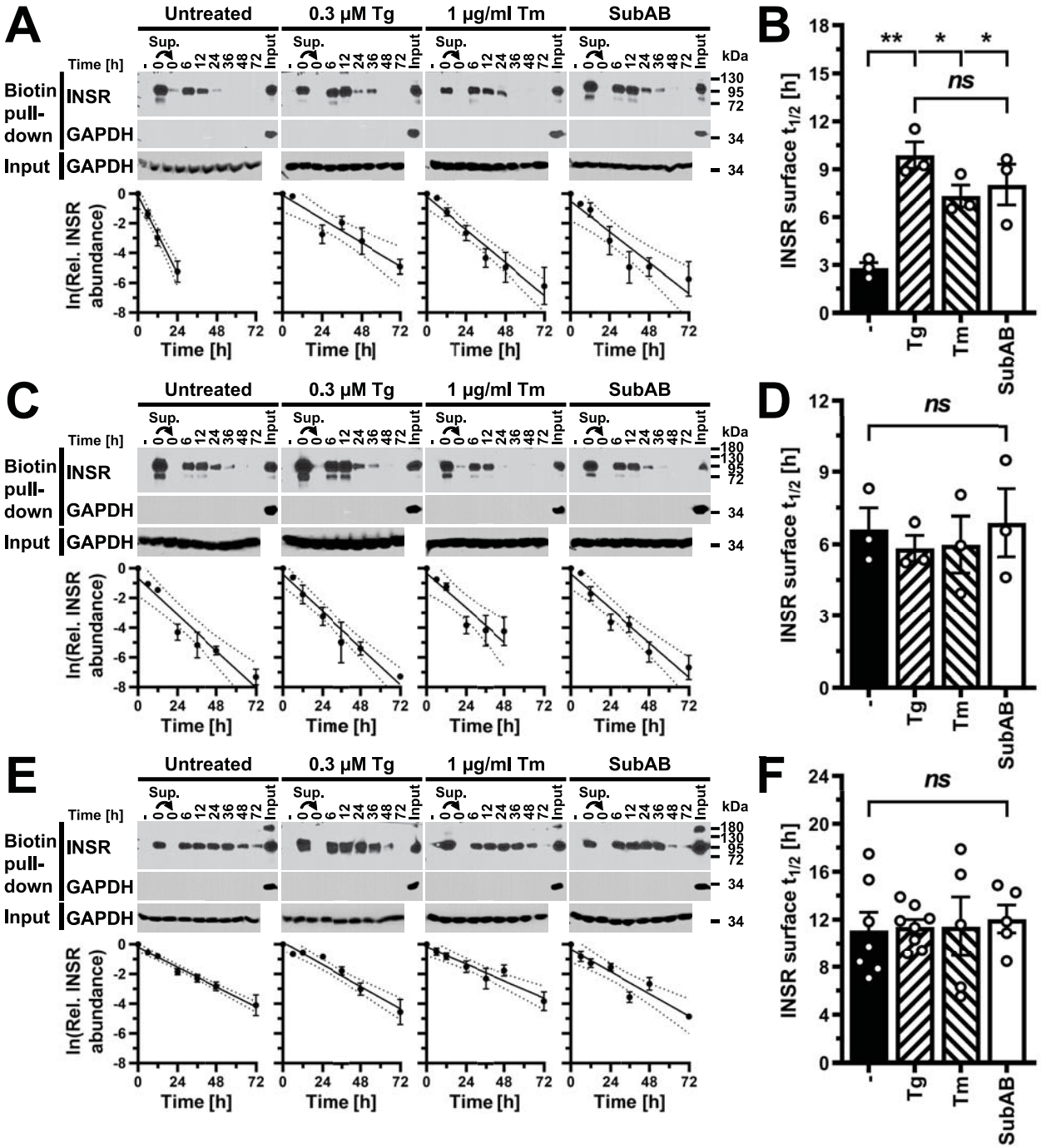
A
Untreated
0.3 µM Tg
1 µg/ml Tm
SubAB
Sup.
Input
Time [h]
kDa
Biotin pull-down
INSR
GAPDH
Input
ln(Rel. INSR abundance)
Time [h]
B
INSR surface t1/2 [h]
ns
Tg
Tm
SubAB
C
D
E
F

Figure 8

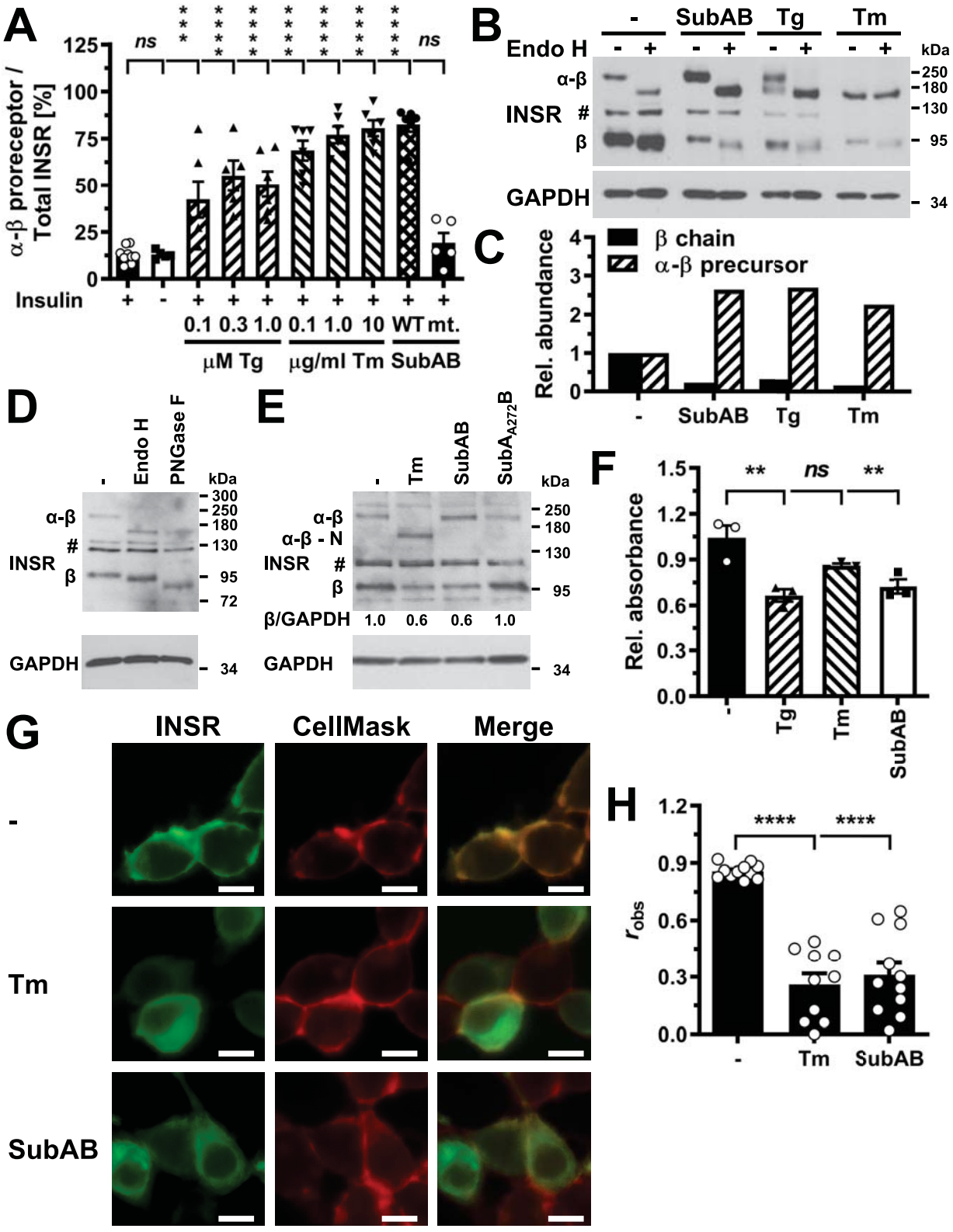
A
α-β proreceptor / Total INSR [%]
ns
****
Insulin
0.1 0.3 1.0 0.1 1.0 10 WT mt.
μM Tg
μg/ml Tm SubAB
B
Endo H
SubAB
Tg
Tm
kDa
α-β
INSR #
β
GAPDH
C
β chain
α-β precursor
Rel. abundance
D
Endo H
PNGase F
E
Tm
SubAA272B
α-β - N
β/GAPDH
1.0 0.6 0.6 1.0
F
Rel. absorbance
**
ns
G
INSR
CellMask
Merge
Tm
SubAB
H
****
robs

Figure 9

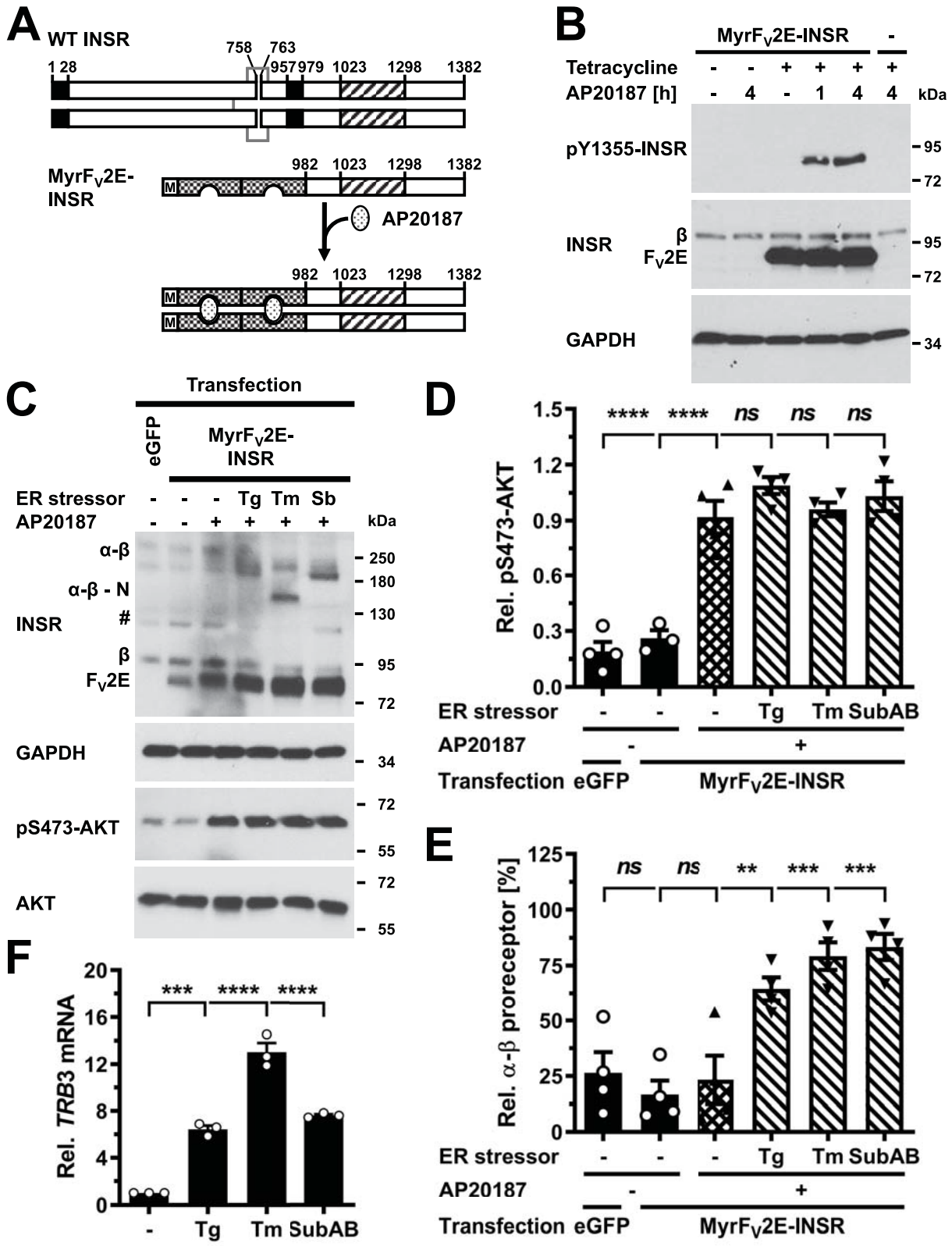
A
WT INSR
758
763
1
28
957
979
1023
1298
1382
MyrF$_V$2E-INSR
982
1023
1298
1382
M
AP20187
B
MyrF$_V$2E-INSR
-
Tetracycline
AP20187 [h]
kDa
pY1355-INSR
95
72
INSR
β
F$_V$2E
GAPDH
34
C
Transfection
eGFP
MyrF$_V$2E-INSR
ER stressor
Tg
Tm
Sb
AP20187
kDa
α-β
α-β - N
#
INSR
β
F$_V$2E
250
180
130
95
72
GAPDH
34
pS473-AKT
72
55
AKT
72
55
D
Rel. pS473-AKT
1.5
1.2
0.9
0.6
0.3
0.0
****
****
ns
ns
ns
ER stressor
Tg
Tm
SubAB
AP20187
Transfection
eGFP
MyrF$_V$2E-INSR
E
Rel. α-β proreceptor [%]
125
100
75
50
25
0
ns
ns
**
***
***
ER stressor
Tg
Tm
SubAB
AP20187
Transfection
eGFP
MyrF$_V$2E-INSR
F
Rel. TRB3 mRNA
20
16
12
8
4
0
***
****
****
-
Tg
Tm
SubAB

Figure 10

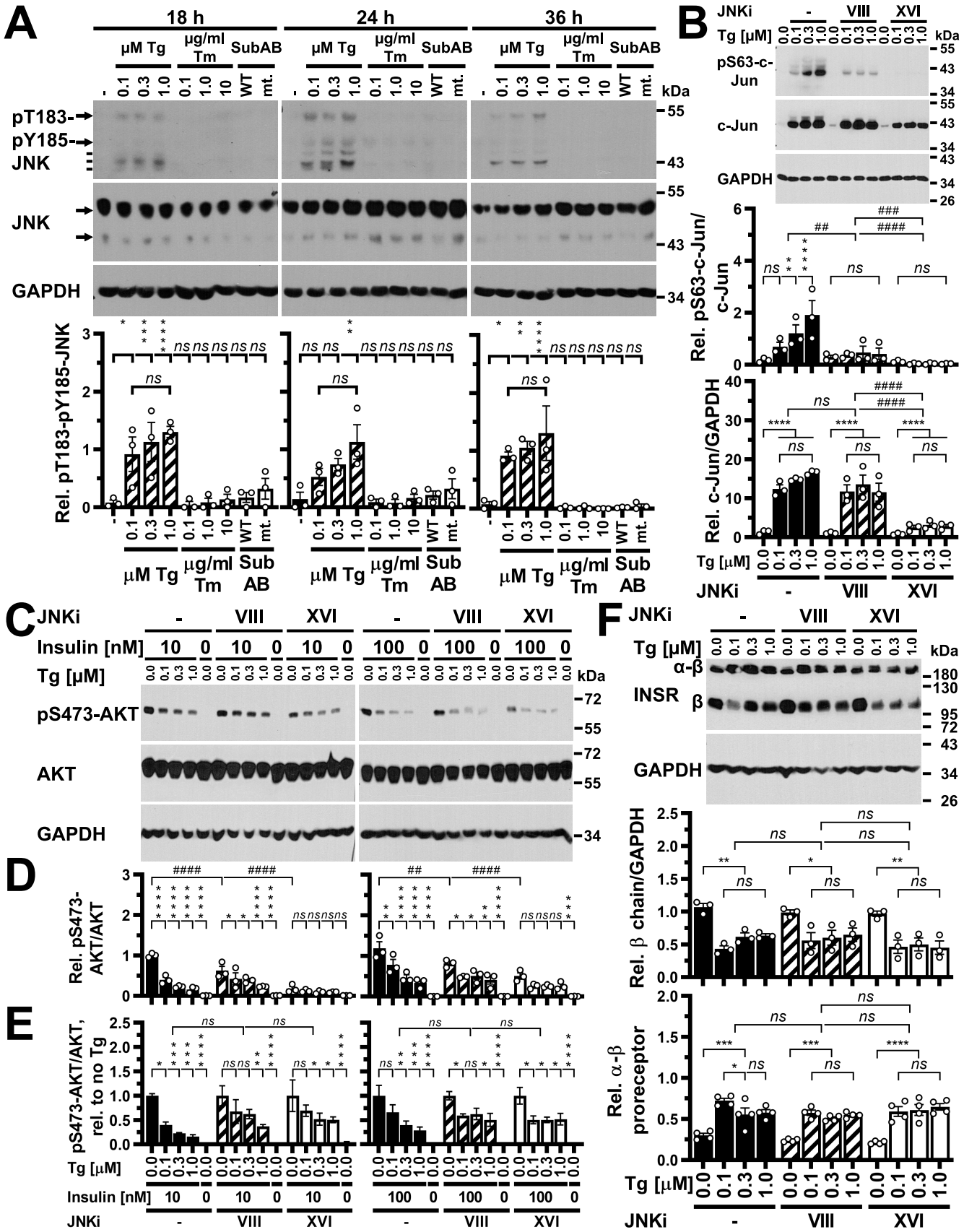
A
18 h
24 h
36 h
µM Tg
µg/ml Tm
SubAB
pT183-
pY185-
JNK
GAPDH
kDa
Rel. pT183-pY185-JNK
B
JNKi
pS63-c-Jun
c-Jun
Rel. pS63-c-Jun/c-Jun
Rel. c-Jun/GAPDH
C
Insulin [nM]
pS473-AKT
AKT
D
Rel. pS473-AKT/AKT
E
pS473-AKT/AKT, rel. to no Tg
F
α-β
INSR β
Rel. β chain/GAPDH
Rel. α-β proreceptor

Figure 11

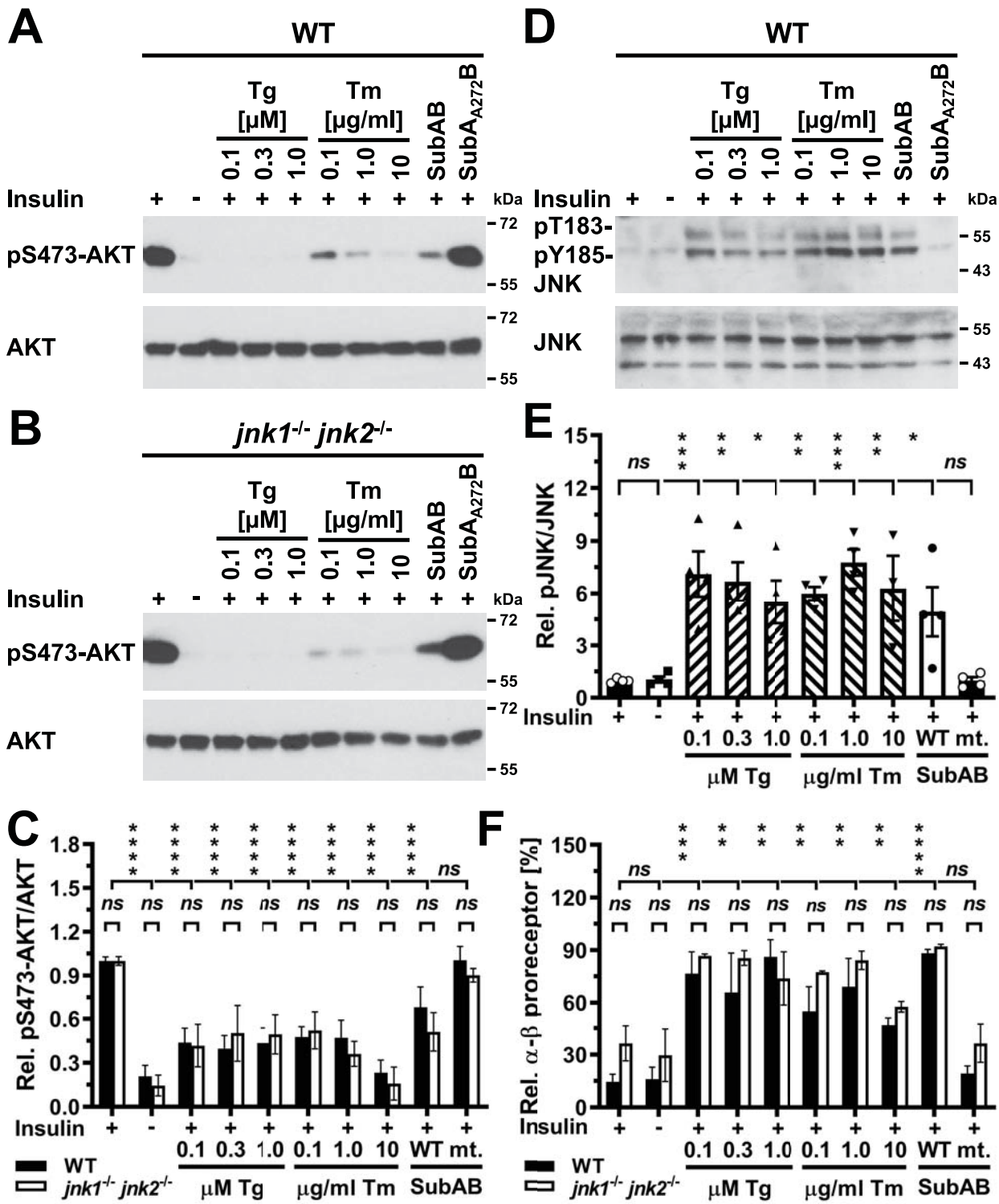
A
WT
Tg [μM]
Tm [μg/ml]
0.1 0.3 1.0 0.1 1.0 10 SubAB SubA$_{A272}$B
Insulin + - + + + + + + + +
kDa
pS473-AKT
AKT
72
55
D
WT
pT183-pY185-JNK
JNK
43
B
jnk1$^{-/-}$ jnk2$^{-/-}$
E
Rel. pJNK/JNK
ns
0.1 0.3 1.0 0.1 1.0 10 WT mt.
μM Tg
μg/ml Tm
SubAB
C
Rel. pS473-AKT/AKT
WT
jnk1$^{-/-}$ jnk2$^{-/-}$
F
Rel. α-β proreceptor [%]

Figure 12

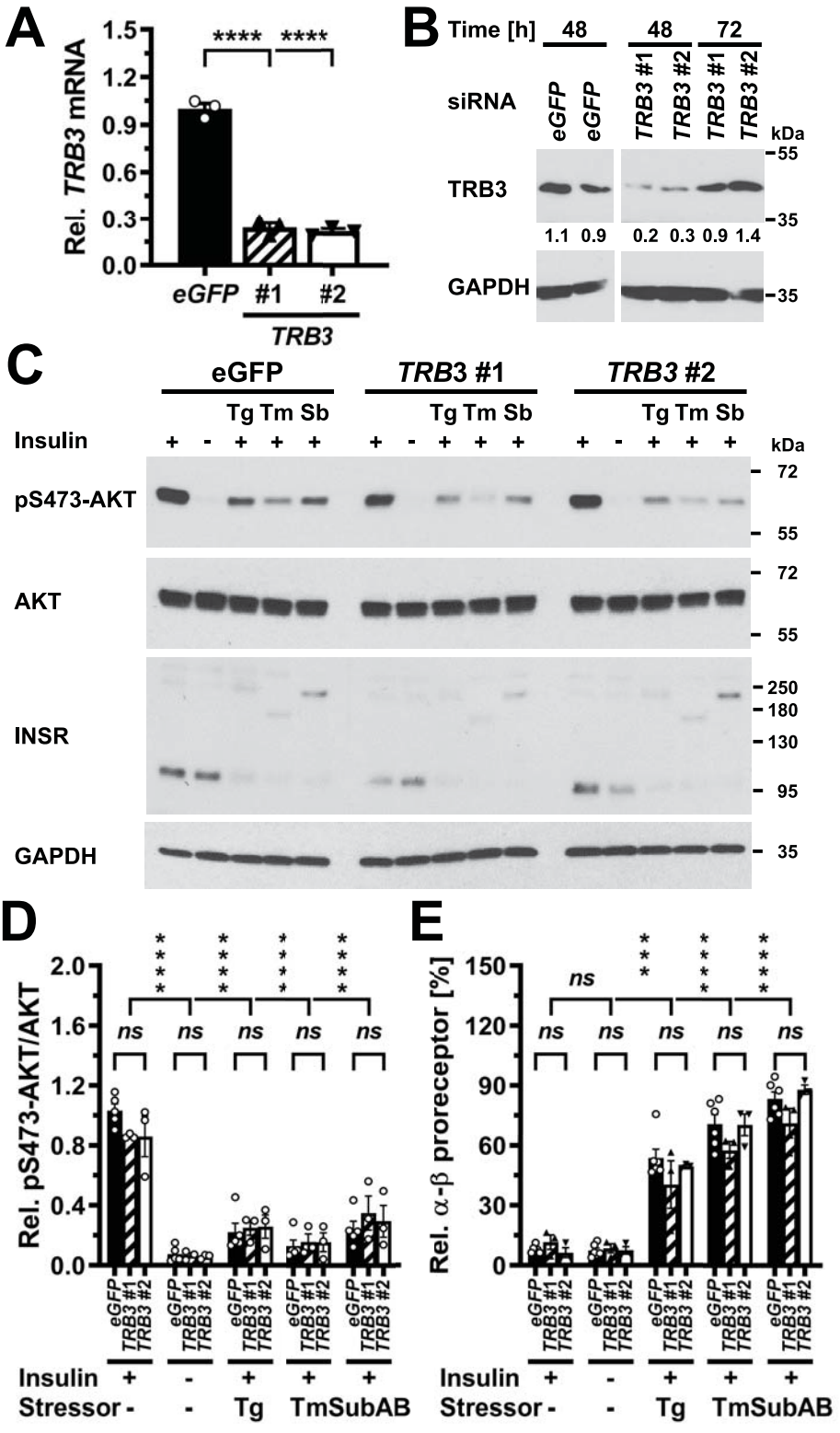
A
Rel. TRB3 mRNA
1.5
1.2
0.9
0.6
0.3
0.0
****
****
eGFP
#1
#2
TRB3
B
Time [h]
48
48
72
siRNA
eGFP
eGFP
TRB3 #1
TRB3 #2
TRB3 #1
TRB3 #2
kDa
TRB3
55
35
1.1 0.9
0.2 0.3 0.9 1.4
GAPDH
35
C
eGFP
TRB3 #1
TRB3 #2
Tg Tm Sb
Tg Tm Sb
Tg Tm Sb
Insulin
+ - + + +
+ - + + +
+ - + + +
kDa
pS473-AKT
72
55
AKT
72
55
INSR
250
180
130
95
GAPDH
35
D
Rel. pS473-AKT/AKT
2.0
1.6
1.2
0.8
0.4
0.0
****
****
****
****
ns
ns
ns
ns
ns
eGFP
TRB3 #1
TRB3 #2
Insulin + - + + +
Stressor - - Tg TmSubAB
E
Rel. α-β proreceptor [%]
150
120
90
60
30
0
ns
****
****
****
ns
ns
ns
ns
ns
eGFP
TRB3 #1
TRB3 #2
Insulin + - + + +
Stressor - - Tg TmSubAB

Figure 13

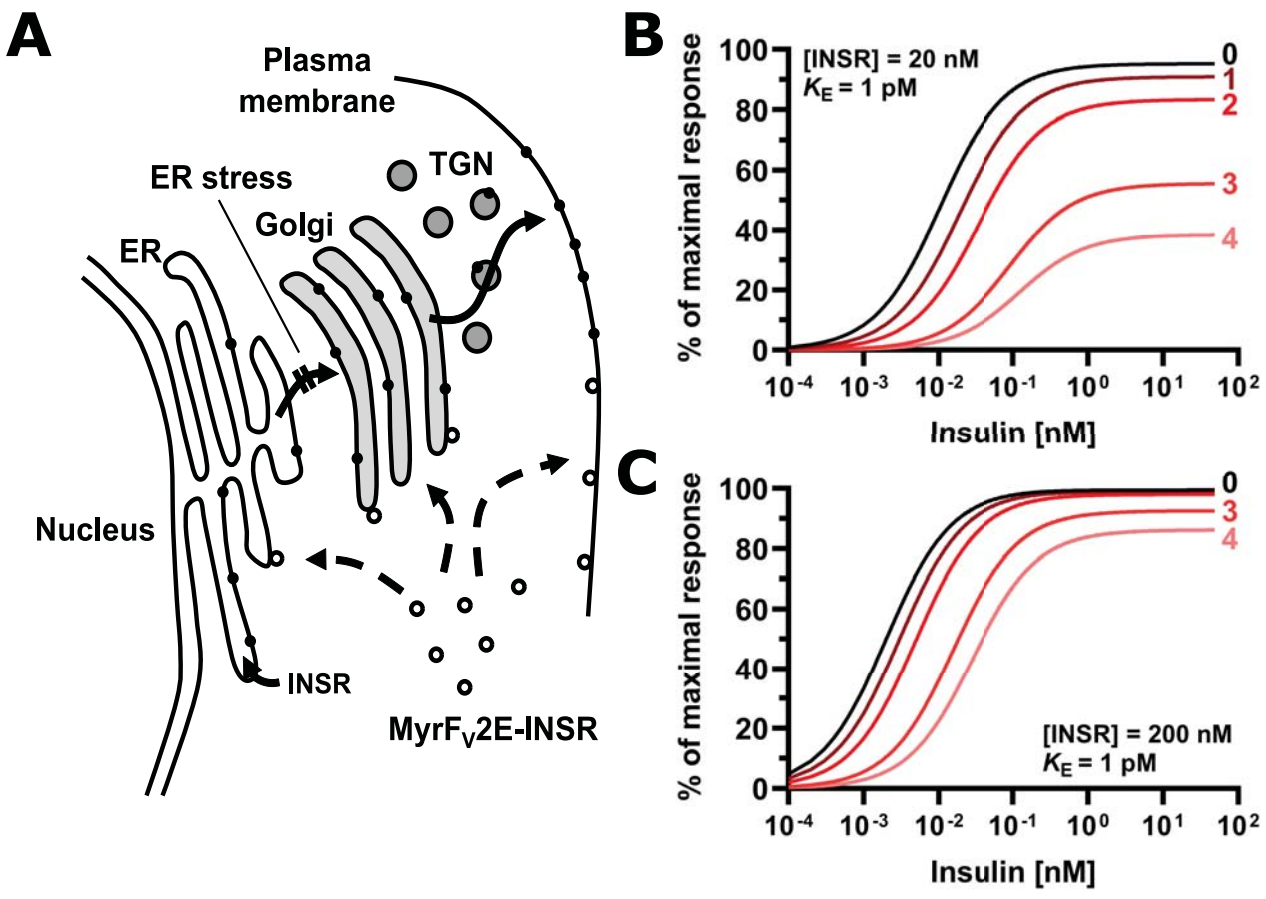
A
Plasma membrane
TGN
ER stress
Golgi
ER
Nucleus
INSR
MyrF$_V$2E-INSR
B
[INSR] = 20 nM
K_E = 1 pM
% of maximal response
Insulin [nM]
0
1
2
3
4
C
[INSR] = 200 nM
K_E = 1 pM
% of maximal response
Insulin [nM]
0
3
4

Figure 14